Temperature-Pressure Phase Diagrams of Metal Nitrogen Compounds through Density Functional Theory Computations and Thermodynamic Calculations

By

Hanof Dawas Alkhaldi

DISSERTATION

Submitted in partial fulfillment of the requirements

For the degree of Doctor of Philosophy

At The University of Texas at Arlington

December 2021

Arlington, Texas

Supervising committee:

Peter Kroll, Supervising Professor

Kwangho Nam

Robin Macaluso

Jongyun Heo

ABSTRACT

The need for novel materials for new generations of applications is growing tremendously. One of many pathways to attain new materials is the route of high pressure synthesis. A particular active area in this high–pressure research is to attain nitrogen-rich compounds. Many of these compounds discovered over the last decades have a potential use as hard material or as high–energy storage material. While it is not possible to predict a potential application for a compound before its experimental realization, it is worthy to explore beforehand what opportunities may exist. This kind of targeted development requires understanding of the synthesis process, potential structural polymorphism, and materials properties. Thus, it is necessary to support experimental endeavors with computational studies and explorations.

My research is divided into two parts. Part I outlines a pathway to compute pressure-temperature phase diagrams of N–rich compounds through a combination of available thermochemical data and quantum–chemical calculations. The approach is validated by comparing computed results to experimental data. This is done for phase boundaries appearing in three different systems: between molecular and polymeric nitrogen, between silicon nitride and silicon pernitride, and between nitrogen–rich Ti–N phases (Chapter I). In Part II the approach is applied to two systems with a rich structure diversity. We investigated the pressure-temperature phase diagram for tantalum–nitrogen (Chapter I) and for iron–nitrogen (Chapter II). The final chapter is then devoted to explore the ternary phase diagram Li–W–N at high pressure and high temperature. With the target of attaining tungsten in high oxidation state in a nitrogen compound, we first evaluate the binary W–N system, before we address ternary Li–W–N structures with their possible decomposition into binary W–N and Li–N phases. (Chapter III).

ACKNOWLEDGEMENTS

I would like first to express my deep acknowledgement to all who encouraged and supported me to complete my PhD. First and foremost, special appreciation goes to my advisor Peter Kroll, for his guidance and extreme support. I highly appreciate the great amount of time and patience that he spent to teach me and to involve me to the field of computational research. I still and will not forget in the first time he taught me how to work with computational research resources; he told me houses are not built in one day so it was great to learn from him how to develop my skills. I will be always grateful to him for his continuous encouragement to make me confident through sending me to the conferences, meetings to help me increasing my knowledge. I am so grateful for the journey that I had in Prof. Peter Kroll's group, as it gave me an opportunity to improve my skills and develop my ability as an independent researcher. Without his continuous support, I wouldn't be able to accomplish this work.

I want to express special gratitude to my dissertation committee members: Dr Kwangho Nam, Dr. Robin Macaluso and Dr. Jongyun Heo for being accommodating and for devoting their time and comments to evaluate my progress as PhD student.

Many thanks to Saudi Arabian Cultural Mission for granted me full scholarship. This honorable scholarship gave me a great opportunity to complete my graduate study and conduct my research.

Great thanks to my colleagues from the group: Ilia Ponomarev, Atreyi Dasmahapatra, Susana Aguiree-Medel, Poroshat Taheri, Shariq Haseen, Aaron West, Kendall Hendrix, Akshada Hande and Mitchell Falgoust.

Special thanks are extended to the chemistry department support staff – Jill Howard, Debbie Cooke, Stephanie Henry for help in dealing with the University-related bureaucracy.

Finally, I want to thank my father Dawas Alkhaldi for supporting and encouraging me to make decision to study abroad. His deep emotions were great reason to overcome all the difficulties I faced without him it would not be possible to achieve my dream. I also want to thank my wonderful sister Sarah, and my brothers Fahad, Mohammad, and Mefleh for their unconditional support and patience regardless the distance. Special gratitude to my sister Noura who was the first person encouraged me to get my PhD, and for standing me through my graduate study. She was always with me inspiring, advising, supporting, and keeping me strong.

Most important, with all of my deep heart I want to express my heartiest gratitude to my mother who passed away. However, she always with me in my heart, and I will keep her lessons for the rest of my life.

TABLE OF CONTENT

LIST OF FIGURES AND TABLES

LIST OF ABBREVIATIONS

HEDMs: high-energy-density materials

LEDs: Light-emitting diodes

SSL: Solid state light

CVD: Chemical vapor deposition

PVD: Physical vapour deposition

High-p,T: High pressure and high temperature

LH-DAC: Laser heated diamond anvil cell

PTM: Pressure-transmitting medium

DFT: Density Functional Theory

VASP: Vienna abs initio simulation package

PAW: Projector-augmented-wave

LDA: Local Density Approximation

GGA: Generalized Gradient Approximation

SCAN: Strongly constrained and appropriately normed

AIRSS: Ab initio random structure searching

USPEX: Universal Structure Predictor: Evolutionary Xtallography

CALYPSO: Crystal Structure Prediction via Particle Swarm Optimization

INTRODUCTION

Diatomic nitrogen ($N \equiv N$) is the most abundant molecule of Earth's atmosphere. It is highly stable and unreactive at ambient conditions due to the strong triple bond combined with its high ionization potential. The triple bond contains an average energy of ~954 kJ/mol, far more than three times that of a single bond (N–N; ~160 kJ/mol) and more than that of a double bond (N=N; 418 kJ/mol, respectively.[1] While the diatomic nitrogen is the most stable form of nitrogen at ambient conditions, modifications of nitrogen with single and double bonds are formed under high pressure.[2-4] Noteworthy is, in particular, the synthesis of "polymeric" cubic-gauche nitrogen – a structure in which each nitrogen forms single bonds with three adjacent nitrogen atoms. The transformation of this singly bonded polymeric nitrogen to the diatomic nitrogen molecule is expected to release enormous amount of energy.[5] Consequently, nitrogen and its various compounds gained research interest not only due to their unique physical properties but also for the fact that they are promising high-energy-density materials (HEDMs).[6] These HEDMs have potential applications in impulse power engineering, high-voltage and high-power electrophysics, welding materials, and impact protection of space vehicles.[7] Several binary compounds of nitrogen and other elements are relevant to industrial applications. For instance, Ta_3N_5 – synthesized at ambient pressure – is used as pigment.[8-11] Cu_3N is a semiconductor with a wide range of applications such as lithium-ion batteries, electrodes, conductive inks, and solar energy harvesting.[12-14] Iron-nitrogen compounds are relevant to planetary cores.[15-19] Furthermore, some ternary nitrogen compounds shows potential for photovoltaic, thermoelectric devices,[20] room temperature spintronic applications,[21] UV and IR detectors,[22] nuclear detection,[23] and optoelectronics including blue and green light-emitting diodes (LEDs), white light solid state light (SSL), and Blu-ray DVD players.[24] Cubic boron nitride, silicon nitride, and titanium nitride exhibit high hardness and are

used as cutting materials and coatings. Hexagonal boron nitride adopts a structure similar to graphite and is used as lubricant at high-temperature.[25] Hence, the synthesis routes of new nitrogen-rich compounds and studying their structural polymorphism and their properties are an active area of past and current research.

Synthesis of Nitrogen-compounds at ambient conditions

A straightforward approach to obtain binary nitrogen compounds is to react a pure metal with N_2 or NH_3 at high temperature. This will lead to the formation of nitride carbide compounds.[26] Thin films of hard nitrogen coatings, an example being ZrN_x films, are obtained by chemical vapor deposition (CVD) as well as by physical vapour deposition (PVD).[27] It was speculated that even c-Zr_3N_4, which adopts a cubic Th_3P_4-type structure and is considered a high pressure phase, has been produced this way as thin film.[28-29] Nitrogen-rich compounds such as Ta_3N_5, Ta_4N_5, and Nb_3N_4 are obtained by various PVD methods, reactive sputtering, and by pulsed laser deposition of Nb in N_2/H_2 mixtures, respectively.[30-32] Further transition metal–nitrogen compounds with compositions M_4N_5 (M=Nb, Ta, and Mo) and M_5N_6 (M=Nb and Ta) were produced by reaction of thin metal films with ammonia.[33-35]

Another route to synthesize nitrogen compounds are metathesis reactions between a metal halide and an alkali nitrogen source such as Li_3N or NaN_3.[36-39] Solvothermal syntheses have been used to prepare CrN, Cr_2N, MnN, Fe_2N, and Ni_3N.[29, 40-41] Nitrogen-rich phases including Zr_3N_4 and Mo_5N_6 can also be synthesized by ammonolysis of $ZrCl_4$ and MoS_2, respectively, at high temperature.[42-43] Bulk metal nitride powders of TiN, VN, CrN, Fe_2N, Fe_3N, NbN, Mo_2N, MoN, and W_2N were prepared by using urea as a nitrogen source with chloride or alkoxide based molecular precursors.[44] It is worthy to note that all the product nitrogen compounds attained of the aforementioned reactions exhibit the nitride anion N^{3-}.

Synthesis and prediction of Nitrogen-compounds at high pressure-high temperature

The high pressure chemistry of metal nitrogen compounds has advanced tremendously over the last decade. Combining experimental and computational studies facilitate the synthesis and characterization of new phases at high pressure and high temperature (high-p,T). Various forms of nitrogen complex ions have been discovered in nitrogen-rich compounds these include nitrides, diazenides, pernitrides, mixed nitride-pernitrides, compounds comprising complex polyatomic nitrogen anions, and compounds with extended anionic nitrogen chains.

Experimentally, one of the routes to synthesize new metal nitrogen compounds happens within a laser heated diamond anvil cell (LH-DAC) apparatus. The principle of LH-DAC is based on a piston-cylinder mechanism. Each diamond has flat culet. The pressure is created by pressing the sample chamber as shown in figure 1. The sample chamber contains a pure metal or, alternatively, a low-pressure polymorph of a solid-state compound, within a metallic gasket. The apparatus is loaded with excess nitrogen, which works as a pressure-transmitting medium (PTM) as well as a possible reactant. Force is applied to the outside of the piston using a screw or by deforming a metallic membrane with a high-pressure gas. The transparency of diamonds allows heating of the reaction chamber by light over a wide range of wavelengths from infrared (IR) to hard X-rays. LH-DACs provide extremely great dynamic range of pressures and temperatures. The approach is highly useful when coupled with X-ray diffraction and optical spectroscopy to provide structural studies of products.[3, 45-47]

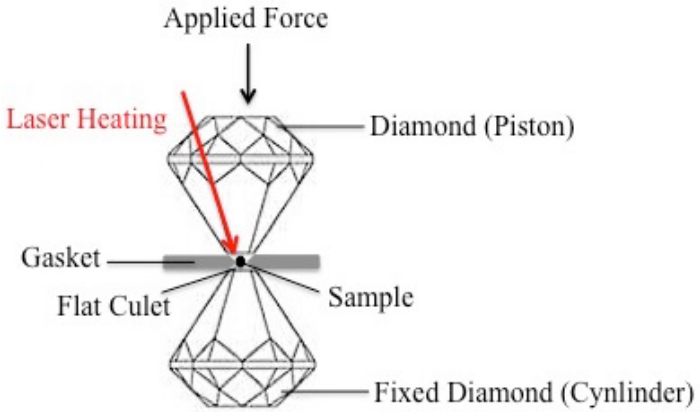

Figure 1. Schematic diagram of laser heated diamond anvil cell.

Overall, LH-DAC experiments are a state-of-the-art approach for fundamental research in high-pressure science. While the volume of the DAC is considered a disadvantage, there are further methods involving large-volume presses (LVP) available for producing significant amounts of products. These include octahedral-anvil (split-sphere) apparatus, cubic-anvil apparatus, Multiple-anvil sliding system, piston cylinder, Bridgman opposed anvil or "belt" press devices, toroidal and Paris-Edinburgh cell designs. High pressure syntheses in these devices cannot use pure nitrogen, since that will escape the reaction chamber quickly. Instead, experiments typically start with low-pressure solid-state compounds or nitrogen-containing precursors, sometimes in combination with nitrogen-rich reactants. After compression to a desired pressure, the temperature is raised to temperatures above 1500 K to initiate reactions between reactants and nitrogen.[48-49]

Quantum-chemical calculations, so-called first principles calculations, and structure prediction methods play a significant role in the search for new nitrogen and nitrogen-rich compounds. Exploration and investigation of many candidate compounds have been carried out using Density Functional Theory (DFT) techniques.[50-55] Over the years, different approximations for electron exchange and correlation have been used including the Local Density Approximation (LDA), the Generalized Gradient Approximation

(GGA), or the strongly constrained and appropriately normed (SCAN) semilocal density functional.[54-58]

A critical part in computational prediction of new high pressure phases – in augmentation to a search for new structures – is an assessment of stability of a candidate structure. Various algorithms and programs have been applied [Ab initio random structure searching (AIRSS)[59], Universal Structure Predictor: Evolutionary Xtallography (USPEX)[60], XTALOPT [61], Crystal Structure Prediction via Particle Swarm Optimization (CALYPSO)[62]] to make high-throughput calculations feasible and to increase fidelity in predictions of new structures. Overall, availability of compute power together with DFT calculations yield accurate assessments of relative enthalpies between different phases, assuming they exhibit same composition and ideal solid state structures. Phase sequences and thermodynamic stabilities between structures emerge with astounding reliability. Transition pressures usually falls within a few GPa comparing computational and experimental data. Discrepancies arise from the fact that enthalpy differences are computed at 0 K only, and that most temperature effects on enthalpy are neglected. And while there are procedures to assess the impact of vibrational entropy, presence of defects including non-stoichiometric phases are extremely difficult to address. However, frequently calculations gave rise to new experiments, which often identified previous experimental data as erroneous.

An essential obstacle in predicting new nitrogen compounds is to account for their thermodynamic stability at elevated temperatures – during the experiment and synthesis itself. This is related to the fact that nitrogen at temperatures above 1000K or 1500K is not a solid–state structure.[63-65] With nitrogen being a supercritical fluid at T>126 K and p>3.44 MPa. There is currently no quantum-chemical approach available to compute its thermodynamic properties at high temperatures and high pressures. Experimental data, however, does exist – at least at ambient and low-pressure conditions. Making use of this,

a detailed approach was developed to access and predict the chemical potential change of nitrogen at high-T high–p conditions – based on experimental data. The chemical potential change of nitrogen is the included in thermochemical calculations together with accurate quantum–chemical results to provide phase diagrams at high-temperature and high-pressure. A detailed description of the computational method can be found in part 1 chapter 1.

Landmark examples of high–pressure syntheses are new nitrides of group 14 elements, γ-Si_3N_4 and γ-Ge_3N_4, with cubic spinel structure type.[66-69] These polymorphs still exhibit isolated nitride N^{3-} anions tetrahedrally coordinated to group 14 cations. SiN_2 with a pyrite-type structure comprising the pernitride ($[N-N]^{4-}$) anion was first predicted to be more favorable than a combination of γ-Si_3N_4 and N_2 at pressures above 17 GPa.[70-71] Subsequently, SiN_2 was indeed synthesized at approximately 60 GPa through direct reaction between pure silicon in nitrogen as pressure-transmitting medium. [72] The same study reported similar pyrite-type structures of germanium and tin as well.[72] The interatomic distance of N–N in pernitrides ($[N-N]^{4-}$) is about 1.4 Å, and comparable to the F–F bond length in molecular F_2. A high-pressure structure of γ-P_3N_5, which consists of a three-dimensional network structure of linked PN_4 tetrahedra and tetragonal-pyramidal PN_5 units, was obtained at 1800 K and 11 GPa using multianvil technique.[73] Further main group elements and their nitrogen compounds were synthesizes in LH-DAC experiments. For instance, multiple new lithium nitrogen compounds have been synthesized at 0-73 GPa and 1500-2000 K. These include Li_3N and its high-pressure modification comprising isolated nitride N^{3-}. Then LiN == Li_2N_2, dilithium diazenide, with ($[N=N]^{2-}$) dimers with intramolecular distance of 1.320 Å. Furthermore LiN_2, lithium diazenide, with nitrogen dimers at a distance of 1.197 Å. This distance is close to the bond distance of a triple bond, supporting transfer of a single electron charge yielding $[N_2]^{\sim 1-}$) as is expected for one lithium atom per nitrogen pair. Last, LiN_5, lithium

pentazolate, comprising the cyclic aromatic N_5^- or pentazolate anion, which is isoelectronic to cyclopentadiene $C_5H_5^-$.[74-76] Sodium–nitrogen compounds – NaN_2 at about 4 GPa and a unique compound with composition $Na_3(N_2)_4$ at about 28 GPa – were synthesized in a LH-DAC using sodium azide with nitrogen as pressure medium.[77] Guided by theory, CsN_5 (again comprising cyclic aromatic N_5^- pentazolate anion) was obtained in a LH-DAC by compressing Cs azide in excess of nitrogen at ~65 GPa.[78] Alkaline earth metal–nitrogen compounds have been targeted as well: a high pressure cubic nitride of Ca_3N_2 and its transformation was studied at 9 and 19 GPa in a DAC.[79] Mg_3N_2 was synthesized by laser heating Mg in excess of nitrogen below 52 GPa. Further heating at high pressure led to the synthesis of MgN_4. MgN_4 has infinite nitrogen chains with N–N distances of 1.33 Å and 1.32 Å).[80-81] Recently, tetranitride tr-BeN_4, comprising very similar infinite $[N_4]^{2-}$–chains, was synthesized from pure elements at about 85 GPa and 2000 K.[82]

There are many more nitrogen compounds of main group elements awaiting their synthesis. Several beryllium nitrogen compounds were studied as potential 2D materials.[83-84] Multiple stable and metastable phases of aluminum nitrogen including Al_2N, Al_2N_3, AlN, AlN_2, Al_2N_5, Al_2N_7, AlN_4, AlN_5, and AlN_7 have been preposed.[85-86] Barium nitrogen compounds have been thoroughly screened, with Ba_3N Ba_2N, BaN, Ba_2N_3, BaN_2, Ba_3N_8, BaN_3, BaN_4, BaN_4, Ba_2N_{11}, BaN_6, and BaN_{10} predicted to occur at pressures up to 100 GPa.[87] Noteworthy, BaN_{10} (== $Ba(N_5)_2$) and MgN_{10} both comprising pentazolate anions are predicted to become stable around 12 GPa and 28 GPa, respectively.[88]

Much attention was devoted to exploring high pressure phases of transition metals nitrogen compounds. Zr_3N_4 and Hf_3N_4, both adopting cubic Th_3P_4–type structure, were synthesized at 15-18 GPa and at temperature 2500-3000 K using LH-DAC.[89-91] Computational studies of Ti–N compounds first predicted a Th_3P_4-type of Ti_3N_4 and a

pernitride TiN_2 to become favorable above 15 GPa and 26 GPa, respectively.[90-92] Experimental studies then reported synthesis of Th_3P_4-type Ti_3N_4 at 75 GPa and 2400 K, and synthesis of TiN_2 at 73 GPa and 2300 K.[93-94] In part 1 chapter 1 we will give a detailed rationale as to why both phases emerge at almost equivalent temperature pressure conditions. A large selection of Ta–N compounds has been explored by computational work.[95-100] Experiments conducted between ambient pressure and 100 GPa then yielded Ta_2N, TaN, Ta_5N_6, Ta_4N_5, Ta_2N_3, Ta_3N_5, TaN_4, and TaN_5. TaN_4 comprises isolate N_4^{4-}anions, while TaN_5 exhibits infinite branched $[N_5]^{5-}$-chains.[101-105] Similarly, multiple Nb–N compounds are predicted at ambient pressure and up to 100 GPa including Nb_2N, NbN, Nb_5N_6, Nb_2N_3, NbN_2, NbN_3, NbN_4, Nb_8N_7, Nb_4N_3, and $Nb_{32}N_{31}$.[106-107] Within group six, chromium pernitride, CrN_2, was synthesized at 70 GPa via direct reaction between Cr and molecular nitrogen. Tungsten nitrogen phases including W_3N, W_2N, W_3N_2, W_2N_3,WN, WN_2, WN_4, WN_6 , and WN_8-N_2 were investigated through first principle calculations. Subsequently, they were obtained through solid state reactions as well as in LH-DAC experiments with nitrogen as reactive medium. W_3N, W_2N,W_3N_2, W_2N_3, and WN are nitride compounds. Compounds of WN_2 and WN_4 exhibit pernitride, mix nitride-pernitride, and 1D nitrogen chains. WN_6 comprises an armchair-like hexazine cyclo-N_6^{6-} with N–N single bonds, and in WN_8-N_2 one finds a dinitrogen molecule [N≡N] besides polydiazenediyl anions $[N_4]_\infty^{2-}$). More details about synthesis of W–N compounds are provided in chapter 4.[95, 108-125] A phase transition of MoN_6 at high pressure, from a structure with space group *R-3m* (no.166)) to one with space group *Pm-3* (no.200) at 54 GPa was investigated by first principle calculations.[126] In group seven, high–pressure Mn–N compounds still await to emerge, as the currently known ε-Mn_4N, ζ-$Mn_6N_{2.58}$, and η-Mn_3N_2 are accessible at low pressure by nitration of pure Mn.[127] Investigations of Re–N compounds at high pressures got off the ground with synthesis of Re_2N and Re_3N at 13 and 16 GPa, respectively, at temperature between 1600 and 2400 K.[128] Much computational and experimental efforts were devoted to ReN_2. The claim of

MoS_2–type ReN_2 attained at 7.7 GPa and 1873 K trough the solid-state high-pressure reaction between $ReCl_5$ and Li_3N could not be supported, however.[129] Instead, a new modification ReN_2 == $Re_2(N_2)(N)_2$ comprising both pernitride $N_2^{4-}$and isolated nitride N^{3-} anions was obtained at 33 GPa and 2500 K.[130] Moreover, ReN_8-N_2, which comprises the dinitrogen molecule [N≡N] and polydiazenediyl anion $2[N_4]_\infty^{2-}$, was obtained from the elements at about 134 GPa and 2700 K in LH-DAC.[131] The Re–N phase diagram may offer more phases, since modificatons of ReN_8 are proposed to occur for pressures up to 200 GPa.[127] The osmium pernitride OsN_2, formed in LH-DAC experiment above 50 GPa and 2000 K, is currently the only Os–N compound.[132-133] Binary Fe–N compounds synthesized from ambient pressure up to 180 GPa include crystalline structures of Fe_4N, Fe_3N, Fe_2N, Fe_3N_2, FeN, FeN_2, and FeN_4.[134-142] Further computational work has been devoted to identify additional iron nitrogen polymorphs up to 300 GPa including additional FeN_6 and FeN_8.[143-146] Subsequently, both compounds FeN_2 and FeN_4 (FeN_4 has catena-poly[tetraz-1-ene-1,4-diyl] anions $[N_4]_\infty^{2-}$), were synthesized in high pressure experiments.[139-141] Within group nine, Co_2N was synthesized at about 10 GPa directly from elements in LH-DAC experiments.[142] Zincblende ZnS-type CoN emerges at 40 GPa, and a pernitride CoN_2 with marcasite-type structure at 50 GPa in LH-DAC experiments.[138, 147] Guided by theoretical predictions [148-149] RhN_2 with marcasite-type structure was attained via direct chemical reaction between pure Rh and molecular nitrogen at 43.2 GPa.[150] Alternative routes to RhN_2 using the single-source precursor $[Rh(NH_3)_6]_3Cl_4(N_3)_5$ were successful at about 39 GPa and 1600 K.[151] IrN_2 was observed above 50 GPa and 2000 K, resembling conditions reported for synthesis of PtN_2 and OsN_2.[132-133, 152] Additional Ir–N compounds IrN_4 and IrN_7 await their synthesis.[153] Two Ni–N compounds have been realized through high pressure synthesis: Ni_3N at 10 GPa [142] and the pernitride NiN_2 at 40 GPa in LH-DAC.[154] While two Cu–N compounds, the azide CuN_3 and a nitride Cu_3N, are attainable through ambient pressure synthesis, a CuN_2 comprising diazenides ($[N_2]^{2-}$) was realized through direct synthesis from the elements

above 50 GPa and 1500 K.[155-156] In short, twenty years ago no binary nitrogen compounds were known for elements such as Pt, Os, or even Ir. Today all metals in the periodic table comprise at least one nitrogen compound, and many case more nitrogen-rich M–N structures have been synthesized.

Reference:

1. Uhlein, E., *Cotton,Fa - Advanced Inorganic Chemistry*, 1967; Vol. 218, p 66-&.
2. Mailhiot, C.; Yang, L. H.; McMahan, A. K., Polymeric Nitrogen. *Physical Review B* **1992**, *46*, 14419-14435.
3. Eremets, M. I.; Gavriliuk, A. G.; Trojan, I. A.; Dzivenko, D. A.; Boehler, R., Single-Bonded Cubic Form of Nitrogen. *Nature Materials* **2004**, *3*, 558-563.
4. Laniel, D.; Geneste, G.; Weck, G.; Mezouar, M.; Loubeyre, P., Hexagonal Layered Polymeric Nitrogen Phase Synthesized near 250 Gpa. *Physical Review Letters* **2019**, *122*.
5. Greschner, M. J.; Zhang, M.; Majumdar, A.; Liu, H. Y.; Peng, F.; Tse, J. S.; Yao, Y. S., A New Allotrope of Nitrogen as High-Energy Density Material. *Journal of Physical Chemistry A* **2016**, *120*, 2920-2925.
6. Yao, Y. S.; Adeniyi, A. O., Solid Nitrogen and Nitrogen-Rich Compounds as High-Energy-Density Materials. *Physica Status Solidi B-Basic Solid State Physics* **2021**, *258*.
7. Bartlett, R. J., Exploding the Mysteries of Nitrogen. *Chemistry & Industry* **2000**, 140-143.
8. Oyama, S. T., *The Chemistry of Transition Metal Carbides and Nitrides*; Blackie Academic & Professional; Chapman & Hall: : Glasgow, Scotland, 1996.
9. Hitoki, G.; Ishikawa, A.; Takata, T.; Kondo, J. N.; Hara, M.; Domen, K., Ta3n5 as a Novel Visible Light-Driven Photocatalyst ($\gamma < 600$ nm). *Chemistry Letters* **2002**, 736-737.
10. Ishikawa, A.; Takata, T.; Kondo, J. N.; Hara, M.; Domen, K., Electrochemical Behavior of Thin Ta_3N_5 Semiconductor Film. *Journal of Physical Chemistry B* **2004**, *108*, 11049-11053.
11. Yokoyama, D.; Hashiguchi, H.; Maeda, K.; Minegishi, T.; Takata, T.; Abe, R.; Kubota, J.; Domen, K., Ta_3N_5 Photoanodes for Water Splitting Prepared by Sputtering. *Thin Solid Films* **2011**, *519*, 2087-2092.
12. Wang, J. R.; Li, F.; Liu, X. B.; Zhou, H. C.; Shao, X. F.; Qu, Y. Y.; Zhao, M. W., Cu3n and Its Analogs: A New Class of Electrodes for Lithium Ion Batteries. *Journal of Materials Chemistry A* **2017**, *5*, 8762-8768.
13. Nakamura, T.; Hayashi, H.; Hanaoka, T.; Ebina, T., Preparation of Copper Nitride (Cu_3N) Nanoparticles in Long-Chain Alcohols at 130-200 ºC and Nitridation Mechanism. *Inorganic Chemistry* **2014**, *53*, 710-715.
14. Zakutayev, A.; Caskey, C. M.; Fioretti, A. N.; Ginley, D. S.; Vidal, J.; Stevanovic, V.; Tea, E.; Lany, S., Defect Tolerant Semiconductors for Solar Energy Conversion. *Journal of Physical Chemistry Letters* **2014**, *5*, 1117-1125.
15. Adler, J. F.; Williams, Q., A High-Pressure X-Ray Diffraction Study of Iron Nitrides: Implications for Earth's Core. *Journal of Geophysical Research-Solid Earth* **2005**, *110*.
16. Roskosz, M.; Bouhifd, M. A.; Jephcoat, A. P.; Marty, B.; Mysen, B. O., Nitrogen Solubility in Molten Metal and Silicate at High Pressure and Temperature. *Geochimica Et Cosmochimica Acta* **2013**, *121*, 15-28.
17. Litasov, K. D.; Shatskiy, A. F., Composition of the Earth's Core: A Review. *Russian Geology and Geophysics* **2016**, *57*, 22-46.

18. Litasov, K. D.; Shatskiy, A.; Ponomarev, D. S.; Gavryushkin, P. N., Equations of State of Iron Nitrides Epsilon-Fe_3N_x and -Fe4ny to 30gpa and 1200k and Implication for Nitrogen in the Earth's Core. *Journal of Geophysical Research-Solid Earth* **2017**, *122*, 3574-3584.
19. Zhuang, Y. K.; Su, X. W.; Salke, N. P.; Cui, Z. X.; Hu, Q. Y.; Zhang, D. Z.; Liu, J., The Effect of Nitrogen on the Compressibility and Conductivity of Iron at High Pressure. *Geosci Front* **2021**, *12*, 983-989.
20. Lu, N.; Ferguson, I., Iii-Nitrides for Energy Production: Photovoltaic and Thermoelectric Applications. *Semiconductor Science and Technology* **2013**, *28*.
21. Liu, Z. Q.; Yi, X. Y.; Wang, J. W.; Kang, J.; Melton, A. G.; Shi, Y.; Lu, N.; Wang, J. X.; Li, J. M.; Ferguson, I., Ferromagnetism and Its Stability in N-Type Gd-Doped Gan: First-Principles Calculation. *Applied Physics Letters* **2012**, *100*.
22. Ariyawansa, G., et al., Gan/Algan Ultraviolet/Infrared Dual-Band Detector. *Applied Physics Letters* **2006**, *89*.
23. Zhou, C. L.; Melton, A. G.; Burgett, E.; Hertel, N.; Ferguson, I. T., Neutron Detection Performance of Gallium Nitride Based Semiconductors. *Scientific Reports* **2019**, *9*.
24. Haverlag, M.; Kroesen, G.; Ferguson, I., Special Issue on Advanced and Emerging Light Sources. *Journal of Physics D-Applied Physics* **2011**, *44*.
25. Xu, C.; He, D. W.; Wang, H. K.; Wang, W. D.; Tang, M. J.; Wang, P., Synthesis of Novel Superhard Materials under Ultrahigh Pressure. *Chinese Science Bulletin* **2014**, *59*, 5251-5257.
26. Ramanathan, S.; Oyama, S. T., New Catalysts for Hydroprocessing - Transition-Metal Carbides and Nitrides. *Journal of Physical Chemistry* **1995**, *99*, 16365-16372.
27. Lamni, R.; Martinez, E.; Springer, S. G.; Sanjines, R.; Schmid, P. E.; Levy, F., Optical and Electronic Properties of Magnetron Sputtered Zrnx Thin Films. *Thin Solid Films* **2004**, *447*, 316-321.
28. Chhowalla, M.; Unalan, H. E., Thin Films of Hard Cubic Zr_3N_4 Stabilized by Stress. *Nature Materials* **2005**, *4*, 317-322.
29. Sui, Y. R.; Xu, Y.; Yao, B.; Xiao, L.; Liu, B., Preparation, Characterization and Properties of N-Rich Zr-N Thin Film with Th_3P_4 Structure. *Applied Surface Science* **2009**, *255*, 6355-6358.
30. Radhakrishnan, K.; Ing, N. G.; Gopalakrishnan, R., Reactive Sputter Deposition and Characterization of Tantalum Nitride Thin Films. *Materials Science and Engineering B-Solid State Materials for Advanced Technology* **1999**, *57*, 224-227.
31. Kim, D. K.; Lee, H.; Kim, D.; Kim, Y. K., Electrical and Mechanical Properties of Tantalum Nitride Thin Films Deposited by Reactive Sputtering. *Journal of Crystal Growth* **2005**, *283*, 404-408.
32. Treece, R. E.; Horwitz, J. S.; Chrisey, D. B.; Donovan, E. P.; Qadri, S. B., Pulsed-Laser Ablation Synthesis of NbN_x ($0 \leq X \leq 1.3$) Thin-Films. *Chemistry of Materials* **1994**, *6*, 2205-2207.
33. Terao, N., New Phases of Niobium Nitride. *Journal of the Less-Common Metals* **1971**, *23*, 159-&.
34. Ganin, A. Y.; Kienle, L.; Vajenine, G. V., Synthesis and Characterisation of Hexagonal Molybdenum Nitrides. *Journal of Solid State Chemistry* **2006**, *179*, 2339-2348.

35. Tessier, F.; Assabaa, R.; Marchand, R., Mixed Valent Niobium Nitrides and Oxynitrides Resulting from Ammonolysis of Alkaline Niobates. *Journal of Alloys and Compounds* **1997**, *262*, 512-515.
36. Hector, A.; Parkin, I. P., Convenient, Low-Energy, Solid-Liquid Metathesis Reactions - Synthesis of TiN, TiO_2, VN, VO_2 and Ti_xV_yN (X+Y = 1). *Journal of the Chemical Society-Chemical Communications* **1993**, 1095-1096.
37. Gillan, E. G.; Kaner, R. B., Rapid Solid-State Synthesis of Refractory Nitrides. *Inorganic Chemistry* **1994**, *33*, 5693-5700.
38. Hector, A. L.; Parkin, I. P., Magnesium and Calcium Nitrides as Nitrogen-Sources in Metathetical Reactions to Produce Metal Nitrides. *Chemistry of Materials* **1995**, *7*, 1728-1733.
39. Parkin, I. P., Solid State Metathesis Reaction for Metal Borides, Silicides, Pnictides and Chalcogenides: Ionic or Elemental Pathways. *Chemical Society Reviews* **1996**, *25*, 199-+.
40. Ernst, W.; Neidhardt, J.; Willmann, H.; Sartory, B.; Mayrhofer, P. H.; Mitterer, C., Thermal Decomposition Routes of Crn Hard Coatings Synthesized by Reactive Arc Evaporation and Magnetron Sputtering. *Thin Solid Films* **2008**, *517*, 568-574.
41. Choi, J.; Gillan, E. G., Solvothermal Metal Azide Decomposition Routes to Nanocrystalline Metastable Nickel, Iron, and Manganese Nitrides. *Inorganic Chemistry* **2009**, *48*, 4470-4477.
42. Lerch, M.; Fuglein, E.; Wrba, J., Synthesis, Crystal Structure, and High Temperature Behavior of Zr_3N_4. *Zeitschrift Fur Anorganische Und Allgemeine Chemie* **1996**, *622*, 367-372.
43. Clarke, S. J.; Michie, C. W.; Rosseinsky, M. J., Structure of Zr_2ON_2 by Neutron Powder Diffraction: The Absence of Nitride-Oxide Ordering. *Journal of Solid State Chemistry* **1999**, *146*, 399-405.
44. Gao, Q. S.; Giordano, C.; Antonietti, M., Controlled Synthesis of Tantalum Oxynitride and Nitride Nanoparticles. *Small* **2011**, *7*, 3334-3340.
45. Bassett, W. A., Diamond Anvil Cell, 50th Birthday. *High Pressure Research* **2009**, *29*, CP5-186.
46. Boehler, R., Laser Heating in the Diamond Cell: Techniques and Applications. *Hyperfine Interact*. **2000**, *128*, 307-321.
47. Salamat, A.; Fischer, R. A.; Briggs, R.; McMahon, M. I.; Petitgirard, S., In Situ Synchrotron X-Ray Diffraction in the Laser-Heated Diamond Anvil Cell: Melting Phenomena and Synthesis of New Materials. *Coordination Chemistry Reviews* **2014**, *277*, 15-30.
48. Bykov, M., et al., High-Pressure Synthesis of Ultraincompressible Hard Rhenium Nitride Pernitride $Re_2(N_2)(N)_{(2)}$ Stable at Ambient Conditions. *Nat. Commun*. **2019**, *10*, 8.
49. Liebermann, R. C., Multi-Anvil, High Pressure Apparatus: A Half-Century of Development and Progress. *High Pressure Research* **2011**, *31*, 493-532.
50. Jones, R. O., Density Functional Theory: Its Origins, Rise to Prominence, and Future. *Reviews of Modern Physics* **2015**, *87*, 897-923.
51. Capelle, K., A Bird's-Eye View of Density-Functional Theory. *Brazilian Journal of Physics* **2006**, *36*, 1318-1343.
52. Cramer, C. J., *Essentials of Computational Chemistry Theories and Models*, 2nd ed.; Wiley: Chichester, West Sussex, England, 2004.

53. Kohn, W., Nobel Lecture: Electronic Structure of Matter-Wave Functions and Density Functionals. *Reviews of Modern Physics* **1999**, *71*, 1253-1266.
54. Kresse, G., Ab-Initio Molecular-Dynamics for Liquid-Metals. *Journal of Non-Crystalline Solids* **1995**, *193*, 222-229.
55. Kresse, G.; Furthmuller, J., Efficiency of Ab-Initio Total Energy Calculations for Metals and Semiconductors Using a Plane-Wave Basis Set. *Computational Materials Science* **1996**, *6*, 15-50.
56. Hohenberg, P.; Kohn, W., Inhomogeneous Electron Gas. *Physical Review B* **1964**, *136*, B864-+.
57. Kresse, G.; Hafner, J., Ab-Initio Molecular-Dynamics Simulation of the Liquid-Metal Amorphous-Semiconductor Transition in Germanium. *Physical Review B* **1994**, *49*, 14251-14269.
58. Sun, J. W.; Ruzsinszky, A.; Perdew, J. P., Strongly Constrained and Appropriately Normed Semilocal Density Functional. *Physical Review Letters* **2015**, *115*.
59. Pickard, C. J.; Needs, R. J., Ab Initio Random Structure Searching. *Journal of Physics-Condensed Matter* **2011**, *23*, 23.
60. Oganov, A. R.; Ma, Y. M.; Lyakhov, A. O.; Valle, M.; Gatti, C., Evolutionary Crystal Structure Prediction as a Method for the Discovery of Minerals and Materials. In *Theoretical and Computational Methods in Mineral Physics: Geophysical Applications*, Wentzcovitch, R.; Stixrude, L., Eds. 2010; Vol. 71, pp 271-298.
61. Lonie, D. C.; Zurek, E., Xtalopt: An Open-Source Evolutionary Algorithm for Crystal Structure Prediction. *Comput. Phys. Commun.* **2011**, *182*, 372-387.
62. Wang, Y. C.; Lv, J. A.; Zhu, L.; Ma, Y. M., Crystal Structure Prediction Via Particle-Swarm Optimization. *Physical Review B* **2010**, *82*, 8.
63. Young, D. A., *Phase Diagrams of the Elements*: Reprint 2020. University of California Press, 1991.
64. Jiang, S. Q.; Holtgrewe, N.; Lobanov, S. S.; Su, F. H.; Mahmood, M. F.; McWilliams, R. S.; Goncharov, A. F., Metallization and Molecular Dissociation of Dense Fluid Nitrogen. *Nature Communications* **2018**, *9*.
65. Turnbull, R.; Hanfland, M.; Binns, J.; Martinez-Canales, M.; Frost, M.; Marques, M.; Howie, R. T.; Gregoryanz, E., Unusually Complex Phase of Dense Nitrogen at Extreme Conditions. *Nature Communications* **2018**, *9*.
66. Zerr, A.; Miehe, G.; Serghiou, G.; Schwarz, M.; Kroke, E.; Riedel, R.; Fuess, H.; Kroll, P.; Boehler, R., Synthesis of Cubic Silicon Nitride. *Nature* **1999**, *400*, 340-342.
67. Leinenweber, K.; O'Keeffe, M.; Somayazulu, M.; Hubert, H.; McMillan, P. F.; Wolf, G. H., Synthesis and Structure Refinement of the Spinel, γ-Ge_3N_4. *Chemistry-a European Journal* **1999**, *5*, 3076-3078.
68. Serghiou, G.; Miehe, G.; Tschauner, O.; Zerr, A.; Boehler, R., Synthesis of a Cubic Ge_3N_4 Phase at High Pressures and Temperatures. *Journal of Chemical Physics* **1999**, *111*, 4659-4662.
69. Shemkunas, M. P.; Petuskey, W. T.; Chizmeshya, A. V. G.; Leinenweber, K.; Wolf, G. H., Hardness, Elasticity, and Fracture Toughness of Polycrystalline Spinel Germanium Nitride and Tin Nitride. *Journal of Materials Research* **2004**, *19*, 1392-1399.
70. Weihrich, R.; Eyert, V.; Matar, S. F., Structure and Electronic Properties of New Model Dinitride Systems: A Density-Functional Study of CN_2, SiN_2, and GeN_2. *Chem Phys Lett* **2003**, *373*, 636-641.

71. Chen, C. B.; Xu, Y.; Sun, X. P.; Wang, S. H.; Tian, F. B., The Stability, Electronic Properties, and Hardness of SiN_2 under High Pressure. *Rsc Adv* **2014**, *4*, 55023-55027.
72. Niwa, K.; Ogasawara, H.; Hasegawa, M., Pyrite Form of Group-14 Element Pernitrides Synthesized at High Pressure and High Temperature. *Dalton Transactions* **2017**, *46*, 9750-9754.
73. Landskron, K.; Huppertz, H.; Senker, J.; Schnick, W., High-Pressure Synthesis of γ-P_3N_5 at 11 GPa and 1500 Degrees C in a Multianvil Assembly: A Binary Phosphorus(V) Nitride with a Three-Dimensional Network Structure from PN_4 Tetrahedra and Tetragonal PN_5 Pyramids. *Angewandte Chemie-International Edition* **2001**, *40*, 2643-2645.
74. Schneider, S. B.; Frankovsky, R.; Schnick, W., High-Pressure Synthesis and Characterization of the Alkali Diazenide Li_2N_2. *Angewandte Chemie-International Edition* **2012**, *51*, 1873-1875.
75. Laniel, D.; Weck, G.; Loubeyre, P., Direct Reaction of Nitrogen and Lithium up to 75 Gpa: Synthesis of the Li_3N, LiN, LiN_2, and LiN_5 Compounds. *Inorganic Chemistry* **2018**, *57*, 10685-10693.
76. Zhou, M.; Sui, M. H.; Shi, X. H.; Zhao, Z. T.; Guo, L. L.; Liu, B.; Liu, R.; Wang, P.; Liu, B. B., Lithium Pentazolate Synthesized by Laser Heating-Compressed Lithium Azide and Nitrogen. *Journal of Physical Chemistry C* **2020**, *124*, 11825-11830.
77. Bykov, M.; Tasca, K. R.; Batyrev, I. G.; Smith, D.; Glazyrin, K.; Chariton, S.; Mahmood, M.; Goncharov, A. F., Dinitrogen as a Universal Electron Acceptor in Solid-State Chemistry: An Example of Uncommon Metallic Compounds $Na_3(N_2)_{(4)}$ and NaN_2. *Inorganic Chemistry* **2020**, *59*, 14819-14826.
78. Steele, B. A.; Stavrou, E.; Crowhurst, J. C.; Zaug, J. M.; Prakapenka, V. B.; Oleynik, II, High-Pressure Synthesis of a Pentazolate Salt. *Chemistry of Materials* **2017**, *29*, 735-741.
79. Hao, J.; Li, Y. W.; Wang, J. S.; Ma, C. L.; Huang, L. Y.; Liu, R.; Cui, Q. L.; Zou, G. T.; Liu, J.; Li, X. D., Experimental Determinations of the High-Pressure Crystal Structures of Ca_3N_2. *Journal of Physical Chemistry C* **2010**, *114*, 16750-16755.
80. Hao, J., et al., Structural Phase Transformations of Mg_3N_2 at High Pressure: Experimental and Theoretical Studies. *Inorganic Chemistry* **2009**, *48*, 9737-9741.
81. Laniel, D.; Winkler, B.; Koemets, E.; Fedotenko, T.; Bykov, M.; Bykova, E.; Dubrovinsky, L.; Dubrovinskaia, N., Synthesis of Magnesium-Nitrogen Salts of Polynitrogen Anions. *Nature Communications* **2019**, *10*.
82. Bykov, M., et al., High-Pressure Synthesis of Dirac Materials: Layered Van Der Waals Bonded BeN_4 Polymorph. *Physical Review Letters* **2021**, *126*.
83. Zhang, C. Z.; Sun, Q., A Honeycomb BeN_2 Sheet with a Desirable Direct Band Gap and High Carrier Mobility. *Journal of Physical Chemistry Letters* **2016**, *7*, 2664-2670.
84. Chen, C. P.; Huang, B.; Wu, J. P., Be3n2 Monolayer: A Graphene-Like 2-Dimensional Material and Its Derivative Nanoribbons. *Aip Advances* **2018**, *8*.
85. Du, H. F.; Ge, Y. F.; Zhu, J. L.; Guo, W.; Yao, Y. G., Pressure-Induced Novel Nitrogen-Rich Aluminum Nitrides: AlN_6, Al_2N_7 and AlN_7 with Polymeric Nitrogen Chains and Rings. *Physical Chemistry Chemical Physics* **2021**, *23*, 12350-12359.

86. Liu, Z.; Li, D.; Wei, S. L.; Wang, W. J.; Tian, F. B.; Bao, K.; Duan, D. F.; Yu, H. Y.; Liu, B. B.; Cui, T. A., Bonding Properties of Aluminum Nitride at High Pressure. *Inorganic Chemistry* **2017**, *56*, 7494-7500.
87. Huang, B. W.; Frapper, G., Barium-Nitrogen Phases under Pressure: Emergence of Structural Diversity and Nitrogen-Rich Compounds. *Chemistry of Materials* **2018**, *30*, 7623-7636.
88. Xia, K.; Zheng, X. X.; Yuan, J. A.; Liu, C.; Gao, H.; Wu, Q.; Sun, J., Pressure-Stabilized High-Energy-Density Alkaline-Earth-Metal Pentazolate Salts. *Journal of Physical Chemistry C* **2019**, *123*, 10205-10211.
89. Zerr, A.; Miehe, G.; Riedel, R., Synthesis of Cubic Zirconium and Hafnium Nitride Having Th_3P_4 Structure. *Nature Materials* **2003**, *2*, 185-189.
90. Kroll, P., Hafnium Nitride with Thorium Phosphide Structure: Physical Properties and an Assessment of the Hf-N, Zr-N, and Ti-N Phase Diagrams at High Pressures and Temperatures. *Physical Review Letters* **2003**, *90*.
91. Kroll, P., Assessment of the Hf-N, Zr-N and Ti-N Phase Diagrams at High Pressures and Temperatures: Balancing between Mn and M3n4 (M = Hf, Zr, Ti). *Journal of Physics-Condensed Matter* **2004**, *16*, S1235-S1244.
92. Yu, S. Y.; Zeng, Q. F.; Oganov, A. R.; Frapper, G.; Zhang, L. T., Phase Stability, Chemical Bonding and Mechanical Properties of Titanium Nitrides: A First-Principles Study. *Phys Chem Chem Phys* **2015**, *17*, 11763-11769.
93. Bhadram, V. S.; Kim, D. Y.; Strobel, T. A., High-Pressure Synthesis and Characterization of Incompressible Titanium Pernitride. *Chemistry of Materials* **2016**, *28*, 1616-1620.
94. Bhadram, V. S.; Liu, H. Y.; Xu, E. S.; Li, T. S.; Prakapenka, V. B.; Hrubiak, R.; Lany, S.; Strobel, T. A., Semiconducting Cubic Titanium Nitride in the Th_3P_4 Structure. *Physical Review Materials* **2018**, *2*.
95. Kroll, P.; Schroter, T.; Peters, M., Prediction of Novel Phases of Tantalum(V) Nitride and Tungsten(Vi) Nitride That Can Be Synthesized under High Pressure and High Temperature. *Angewandte Chemie-International Edition* **2005**, *44*, 4249-4254.
96. Jiang, C.; Lin, Z. J.; Zhao, Y. S., Thermodynamic and Mechanical Stabilities of Tantalum Nitride. *Physical Review Letters* **2009**, *103*.
97. Zhang, J. D.; Wang, H. F., First-Principles Calculations of Structural and Electronic Properties of Ta_2N_3 under High Pressures. *Physica B* **2013**, *428*, 89-93.
98. Li, D.; Tian, F. B.; Duan, D. F.; Bao, K.; Chu, B. H.; Sha, X. J.; Liu, B. B.; Cui, T., Mechanical and Metallic Properties of Tantalum Nitrides from First-Principles Calculations. *Rsc Advances* **2014**, *4*, 10133-10139.
99. Weinberger, C. R.; Yu, X. X.; Yu, H.; Thompson, G. B., Ab Initio Investigations of the Phase Stability in Group Ivb and Vb Transition Metal Nitrides. *Computational Materials Science* **2017**, *138*, 333-345.
100. Xing, W. D.; Wei, Z. J.; Yu, R.; Meng, F. Y., Prediction of Stable High-Pressure Structures of Tantalum Nitride Tan2. *J. Mater. Sci. Technol.* **2019**, *35*, 2297-2304.
101. Salamat, A.; Hector, A. L.; Kroll, P.; McMillan, P. F., Nitrogen-Rich Transition Metal Nitrides. *Coordination Chemistry Reviews* **2013**, *257*, 2063-2072.
102. Zerr, A., et al., High-Pressure Synthesis of Tantalum Nitride Having Orthorhombic U_2S_3 Type Structure. *Advanced Functional Materials* **2009**, *19*, 2282-2288.

103. Friedrich, A.; Winkler, B.; Bayarjargal, L.; Arellano, E. A. J.; Morgenroth, W.; Biehler, J.; Schroder, F.; Yan, J. Y.; Clark, S. M., In Situ Observation of the Reaction of Tantalum with Nitrogen in a Laser Heated Diamond Anvil Cell. *Journal of Alloys and Compounds* **2010**, *502*, 5-12.
104. Salamat, A.; Woodhead, K.; Shah, S. I. U.; Hector, A. L.; McMillan, P. F., Synthesis of U3se5 and U3te5 Type Polymorphs of Ta_3N_5 by Combining High Pressure-Temperature Pathways with a Chemical Precursor Approach. *Chemical Communications* **2014**, *50*, 10041-10044.
105. Bykov, M.; Bykova, E.; Ponomareva, A. V.; Abrikosov, I. A.; Chariton, S.; Prakapenka, V. B.; Mahmood, M. F.; Dubrovinsky, L.; Goncharov, A. F., Stabilization of Polynitrogen Anions in Tantalum-Nitrogen Compounds at High Pressure. *Angewandte Chemie-International Edition* **2021**, *60*, 9003-9008.
106. Ivashchenko, V. I.; Turchi, P. E. A.; Olifan, E. I., Phase Stability and Mechanical Properties of Niobium Nitrides. *Physical Review B* **2010**, *82*.
107. Zhao, Z. L.; Bao, K.; Tian, F. B.; Duan, D. F.; Liu, B. B.; Cui, T., Phase Diagram, Mechanical Properties, and Electronic Structure of Nb-N Compounds under Pressure. *Physical Chemistry Chemical Physics* **2015**, *17*, 22837-22845.
108. Wang, S. M., et al., Synthesis, Crystal Structure, and Elastic Properties of Novel Tungsten Nitrides. *Chemistry of Materials* **2012**, *24*, 3023-3028.
109. Liu, K.; Wang, S. M.; Zhou, X. L.; Chang, J., Theoretical Calculations for Structural, Elastic, and Thermodynamic Properties of C-W_3N_4 under High Pressure. *Journal of Applied Physics* **2013**, *114*.
110. Xing, W. D.; Miao, X. J.; Meng, F. Y.; Yu, R., Crystal Structure of and Displacive Phase Transition in Tungsten Nitride Wn. *Journal of Alloys and Compounds* **2017**, *722*, 517-524.
111. Wang, C. C.; Tao, Q.; Dong, S. S.; Wang, X.; Zhu, P. W., Synthesis and Mechanical Character of Hexagonal Phase Delta-Wn. *Inorganic Chemistry* **2017**, *56*, 3970-3975.
112. Sasaki, T.; Ikoma, T.; Sago, K.; Liu, Z.; Niwa, K.; Ohsuna, T.; Hasegawa, M., High-Pressure Synthesis and Crystal Structure of Moc-Type Tungsten Nitride by Nitridation with Ammonium Chloride. *Inorganic Chemistry* **2019**, *58*, 16379-16386.
113. Kawamura, F.; Yusa, H.; Taniguchi, T., Synthesis of Hexagonal Phases of WN and $W_{2.25}N_3$ by High-Pressure Metathesis Reaction. *Journal of the American Ceramic Society* **2018**, *101*, 949-956.
114. Wang, Y. T.; Zhao, E. J.; Zhao, J. D.; Fu, L.; Ying, C.; Lin, L., Prediction of Novel Ground State and High Pressure Phases for W_2N_3: First-Principles. *Computational Materials Science* **2019**, *156*, 215-223.
115. Zhang, J. D.; Cheng, X. L., Theoretical Investigations of Structural, Elastic and Electronic Properties of M_2N_3 (M = Zr, Hf, W and Re) with U2s3 Structure. *Computational Materials Science* **2015**, *99*, 43-46.
116. Wang, H.; Li, Q.; Li, Y. E.; Xu, Y.; Cui, T.; Oganov, A. R.; Ma, Y. M., Ultra-Incompressible Phases of Tungsten Dinitride Predicted from First Principles. *Physical Review B* **2009**, *79*.
117. Soto, G., Computational Study of Hf, Ta, W, Re, Ir, Os and Pt Pernitrides. *Computational Materials Science* **2012**, *61*, 1-5.

118. Zhao, Z. L.; Bao, K.; Duan, D. F.; Tian, F. B.; Huang, Y. P.; Yu, H. Y.; Liu, Y. X.; Liu, B. B.; Cui, T., The Low Coordination Number of Nitrogen in Hard Tungsten Nitrides: A First-Principles Study. *Physical Chemistry Chemical Physics* **2015**, *17*, 13397-13402.
119. Song, L.; Wang, Y. X., First-Principles Study of W, WN, WN_2, and WN_3. *Physica Status Solidi B-Basic Solid State Physics* **2010**, *247*, 54-58.
120. Li, Q.; Sha, L.; Zhu, C.; Yao, Y., New Multifunctional Tungsten Nitride with Energetic N_6 and Extreme Hardness Predicted from First Principles. *Epl* **2017**, *118*.
121. Xia, K.; Gao, H.; Liu, C.; Yuan, J. N.; Sun, J.; Wang, H. T.; Xing, D. Y., A Novel Superhard Tungsten Nitride Predicted by Machine-Learning Accelerated Crystal Structure Search. *Science Bulletin* **2018**, *63*, 817-824.
122. Kang, Z. X.; He, H. Y.; Ding, R.; Chen, J. L.; Pan, B. C., Structures of W_xN_y Crystals and Their Intrinsic Properties: First Principles Calculations. *Crystal Growth & Design* **2018**, *18*, 2270-2278.
123. Mehl, M. J.; Finkenstadt, D.; Dane, C.; Hart, G. L. W.; Curtarolo, S., Finding the Stable Structures of N1-Xwx with an Ab Initio High-Throughput Approach. *Physical Review B* **2015**, *91*.
124. Bykov, M., et al., High-Pressure Synthesis of Metal-Inorganic Frameworks $Hf_4N_{20}.N_2$, $WN_8.N_2$, and $Os_5N_{28}.3N_2$ with Polymeric Nitrogen Linkers. *Angewandte Chemie-International Edition*, 7.
125. Salke, N. P.; Xia, K.; Fu, S. Y.; Zhang, Y. J.; Greenberg, E.; Prakapenka, V. B.; Liu, J.; Sun, J.; Lin, J. F., Tungsten Hexanitride with Single-Bonded Armchairlike Hexazine Structure at High Pressure. *Physical Review Letters* **2021**, *126*.
126. Wei, Q.; Zhao, C. Y.; Zhang, M. G.; Yan, H. Y.; Wei, B., High-Pressure Phases and Pressure-Induced Phase Transition of MoN_6 and ReN_6. *Physics Letters A* **2019**, *383*, 2429-2435.
127. Si, P. Z.; Jiang, W.; Wang, H. X.; Zhong, M.; Ge, H. L.; Chul-Jin, C.; Jung-Goo, L., The High Nitrogen Pressure Synthesis of Manganese Nitride. *Chinese Physics Letters* **2012**, *29*.
128. Friedrich, A.; Winkler, B.; Bayarjargal, L.; Morgenroth, W.; Juarez-Arellano, E. A.; Milman, V.; Refson, K.; Kunz, M.; Chen, K., Novel Rhenium Nitrides. *Physical Review Letters* **2010**, *105*.
129. Kawamura, F.; Yusa, H.; Taniguchi, T., Synthesis of Rhenium Nitride Crystals with MoS_2 Structure. *Applied Physics Letters* **2012**, *100*.
130. Bykov, M., et al., High-Pressure Synthesis of Ultraincompressible Hard Rhenium Nitride Pernitride $Re_2(N_2)(N)_{(2)}$ Stable at Ambient Conditions. *Nature Communications* **2019**, *10*.
131. Wang, Y. C.; Yao, T. K.; Yao, J. L.; Zhang, J. W.; Gou, H. Y., Does the Real ReN_2 Have the MoS_2 Structure. *Physical Chemistry Chemical Physics* **2013**, *15*, 183-187.
132. Young, A. F.; Sanloup, C.; Gregoryanz, E.; Scandolo, S.; Hemley, R. J.; Mao, H. K., Synthesis of Novel Transition Metal Nitrides IrN_2 and OsN_2. *Physical Review Letters* **2006**, *96*.
133. Gregoryanz, E.; Sanloup, C.; Somayazulu, M.; Badro, J.; Fiquet, G.; Mao, H. K.; Hemley, R. J., Synthesis and Characterization of a Binary Noble Metal Nitride. *Nature Materials* **2004**, *3*, 294-297.

134. Jacobs, H.; Rechenbach, D.; Zachwieja, U., Structure Determination of γ'-Fe_4N and ε-Fe_3N. *Journal of Alloys and Compounds* **1995**, *227*, 10-17.
135. Guo, K.; Rau, D.; von Appen, J.; Prots, Y.; Schnelle, W.; Dronskowski, R.; Niewa, R.; Schwarz, U., High Pressure High-Temperature Behavior and Magnetic Properties of Fe_4N: Experiment and Theory. *High Pressure Research* **2013**, *33*, 684-696.
136. Wriedt, H. A., Gokcen, N.A. & Nafziger, R.H. , The Fe-N (Iron-Nitrogen) System. *Bulletin of Alloy Phase Diagrams* **1987**, *8*, 355–377
137. Clark, W. P.; Steinberg, S.; Dronskowski, R.; McCammon, C.; Kupenko, I.; Bykov, M.; Dubrovinsky, L.; Akselrud, L. G.; Schwarz, U.; Niewa, R., High-Pressure Nias-Type Modification of FeN. *Angewandte Chemie-International Edition* **2017**, *56*, 7302-7306.
138. Niwa, K.; Terabe, T.; Kato, D.; Takayama, S.; Kato, M.; Soda, K.; Hasegawa, M., Highly Coordinated Iron and Cobalt Nitrides Synthesized at High Pressures and High Temperatures. *Inorganic Chemistry* **2017**, *56*, 6410-6418.
139. Laniel, D.; Dewaele, A.; Garbarino, G., High Pressure and High Temperature Synthesis of the Iron Pernitride FeN_2. *Inorganic Chemistry* **2018**, *57*, 6245-6251.
140. Bykov, M.; Khandarkhaeva, S.; Fedotenko, T.; Sedmak, P.; Dubrovinskaia, N.; Dubrovinsky, L., Synthesis of FeN_4 at 180 GPa and Its Crystal Structure from a Submicron-Sized Grain. *Acta Crystallographica Section E-Crystallographic Communications* **2018**, *74*, 1392-+.
141. Bykov, M., et al., Fe-N System at High Pressure Reveals a Compound Featuring Polymeric Nitrogen Chains. *Nature Communications* **2018**, *9*.
142. Hasegawa, M.; Yagi, T., Systematic Study of Formation and Crystal Structure of 3d-Transition Metal Nitrides Synthesized in a Supercritical Nitrogen Fluid under 10 Gpa and 1800 K Using Diamond Anvil Cell and Yag Laser Heating. *Journal of Alloys and Compounds* **2005**, *403*, 131-142.
143. Fang, C. M.; van Huis, M. A.; Zandbergen, H. W., Stability and Structures of the Epsilon-Phases of Iron Nitrides and Iron Carbides from First Principles. *Scripta Materialia* **2011**, *64*, 296-299.
144. Wang, Z. Y.; Li, Y. C.; Li, H. T.; Harran, I.; Jia, M. Z.; Wang, H.; Chen, Y. Z.; Wang, H. Y.; Wu, N. N., Prediction and Characterization of the Marcasite Phase of Iron Pernitride under High Pressure. *Journal of Alloys and Compounds* **2017**, *702*, 132-137.
145. Chen, Y. Z.; Cai, X. Y.; Wang, H. Y.; Wang, H. B.; Wang, H., Novel Triadius-Like N_4 Specie of Iron Nitride Compounds under High Pressure. *Scientific Reports* **2018**, *8*.
146. Wu, L. L.; Tian, R. F.; Wan, B.; Liu, H. Y.; Gong, N.; Chen, P.; Shen, T. D.; Yao, Y. S.; Gou, H. Y.; Gao, F. M., Prediction of Stable Iron Nitrides at Ambient and High Pressures with Progressive Formation of New Polynitrogen Species. *Chemistry of Materials* **2018**, *30*, 8476-8485.
147. Suzuki, K.; Kaneko, T.; Yoshida, H.; Morita, H.; Fujimori, H., Crystal-Structure and Magnetic-Properties of the Compound Con. *Journal of Alloys and Compounds* **1995**, *224*, 232-236.
148. Yu, R.; Zhan, Q.; De Jonghe, L. C., Crystal Structures of and Displacive Transitions in Osn2, Irn2, RuN_2, and Rh N_2. *Angewandte Chemie-International Edition* **2007**, *46*, 1136-1140.

149. Hernandez, E. R.; Canadell, E., Marcasite Vs. Arsenopyrite Structural Choice in MN_2 (M = Ir, Os and Rh) Transition Metal Nitrides. *Journal of Materials Chemistry* **2008**, *18*, 2090-2095.
150. Niwa, K.; Dzivenko, D.; Suzuki, K.; Riedel, R.; Troyan, I.; Eremets, M.; Hasegawa, M., High Pressure Synthesis of Marcasite-Type Rhodium Pernitride. *Inorganic Chemistry* **2014**, *53*, 697-699.
151. Bykov, M.; Yusenko, K. V.; Bykova, E.; Pakhomova, A.; Kraus, W.; Dubrovinskaia, N.; Dubrovinsky, L., Synthesis of Arsenopyrite-Type Rhodium Pernitride RhN_2 from a Single-Source Azide Precursor. *European Journal of Inorganic Chemistry* **2019**, *2019*, 3667-3671.
152. Crowhurst, J. C.; Goncharov, A. F.; Sadigh, B.; Evans, C. L.; Morrall, P. G.; Ferreira, J. L.; Nelson, A. J., Synthesis and Characterization of the Nitrides of Platinum and Iridium. *Science* **2006**, *311*, 1275-1278.
153. Du, X.; Yao, Y. S.; Wang, J.; Yang, Q. P.; Yang, G. C., IrN_4 and IrN_7 as Potential High-Energy-Density Materials. *Journal of Chemical Physics* **2021**, *154*.
154. Niwa, K.; Fukui, R.; Terabe, T.; Kawada, T.; Kato, D.; Sasaki, T.; Soda, K.; Hasegawa, M., High-Pressure Synthesis and Phase Stability of Nickel Pernitride. *European Journal of Inorganic Chemistry* **2019**, *2019*, 3753-3757.
155. Liu, X. H.; George, J.; Maintz, S.; Dronskowski, R., β-CuN_3: The Overlooked Ground-State Polymorph of Copper Azide with Heterographene-Like Layers. *Angewandte Chemie-International Edition* **2015**, *54*, 1954-1959.
156. Binns, J.; Donnelly, M. E.; Pena-Alvarez, M.; Wang, M. N.; Gregoryanz, E.; Hermann, A.; Dalladay-Simpson, P.; Howie, R. T., Direct Reaction between Copper and Nitrogen at High Pressures and Temperatures. *Journal of Physical Chemistry Letters* **2019**, *10*, 1109-1114.

COMPUTATIONAL METHOD:

First-Principles calculations

Calculations of total energy are done within Density Functional Theory (DFT) as implemented in Vienna Ab Initio Simulation Package (VASP).[1-4] We use the Strongly Conserved and Appropriately Normed (SCAN) functional [5] together with the projector-augmented-wave (PAW) method.[6-7] Consistency checks have been done with the Generalized Gradient Approximation (GGA-PBE) as well. [8-9] All results are obtained using a plane wave cut-off energy of 500 eV with forces converged to better than 1 meV/Å. The Brillouin zone of each structure is sampled by k-point meshes with grid sizes smaller than 0.03 $Å^{-1}$. With the parameters above, enthalpy differences between structures are converged to better than 1 meV.

For every structure we compute energy E as a function of volume V, reducing V stepwise to simulate higher densities and pressures. The resulting E–V data yields pressure p by numerical differentiation, $p = -\partial E/\partial V$, and enthalpy $H = E + pV$ figure 1.

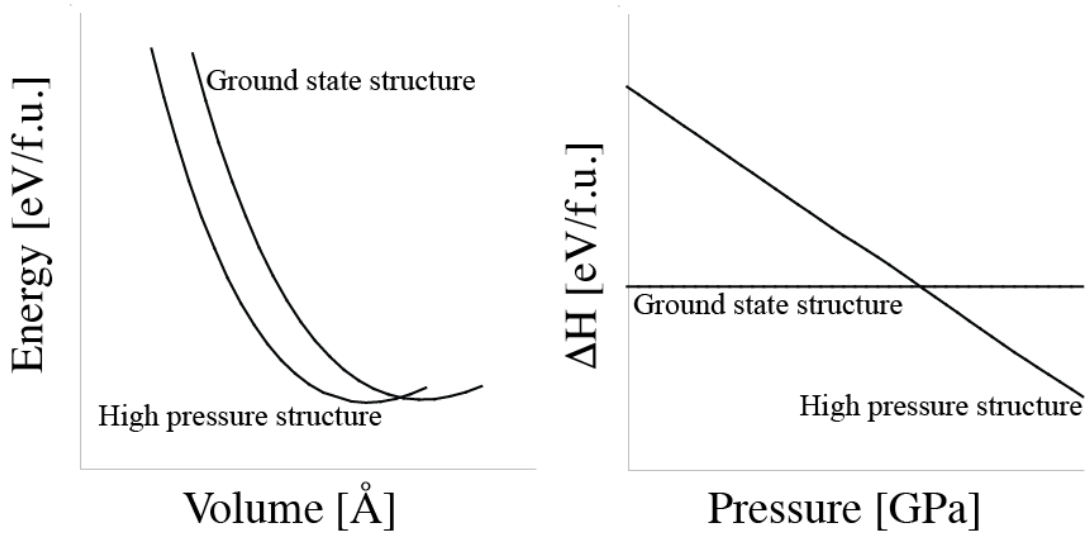

Figure 1. Energy-volume (E-V) diagram (left) and Enthalpy-pressure (ΔH-p) diagram (right)

Reaction enthalpies ΔH as a function of pressure at zero temperature are computed based on enthalpies of products and reactants. This data is commonly used to identify the convex hull of a phase system. Neglecting further impact of temperature and of entropy differences, reaction Gibbs energies $\Delta G = \Delta H - T \cdot \Delta S$ are approximated by ΔH. Locating ΔH=0 then yields estimates of transition pressures. These estimates are excellent guidelines predicting solid state reactions at constant composition, not at least because entropy differences that contribute to reaction Gibbs energies ΔG for solid-state reactions are usually small in comparison to changes of ΔH within a few GPa of pressure. Computing enthalpy differences in GGA-PBE and SCAN functional are consistent and typically deviate less than 5 meV per atom. In very few cases we find slightly larger differences between GGA-PBE and SCAN functional. For instance, while the energy difference between ε-TaN and ϑ-TaN is 0.025 eV/TaN using GGA-PBE, using the SCAN functional ϑ-TaN is more favorable than ε-TaN by 0.013 eV/TaN at 0 GPa. Consequently, while the pressure for the transition ε-TaN to ϑ-TaN is 2.5 GPa using GGA-PBE, using SCAN there appears no transition between ε-TaN and ϑ-TaN at elevated pressuresusing SCAN, and the transition pressure between ε-TaN and ϑ-TaN is 2.5 GPa using GGA-PBE. Instead, a negative pressure of –1.7 GPa is computed. For instance, the enthalpy differences between ε-TaN and ϑ-TaN are 0.0005 eV/TaN using SCAN and 0.0219 eV/TaN using GGA-PBE. The differences in the transition pressures among TaN phases are within 2 GPa. For instance, the transition pressures between ε-TaN and ϑ-TaN at 0.5 GPa using SCAN and 2.5 GPa using GGA-PBE Figure 2. Thus, within the SCAN functional mononitride ε-TaN has a slightly higher energy at zero pressure than ϑ-TaN.This results changes the pressure-temperature phase diagram, since within SCAN ϑ-TaN will be the only stable TaN structure.

For the structure searches we use structures reported previously together with various algorithms and programs [Ab initio random structure searching (AIRSS)[10], Universal

Structure Predictor: Evolutionary Xtallography (USPEX)[11], XTALOPT [12], Crystal Structure Prediction via Particle Swarm Optimization (CALYPSO)[13]]. For the structure searches by USPEX we start with variable composition searches to identify potential compositions with high nitrogen content. Ensembles of 50 structures are followed for 20 generations. For each new generation, 40% of structures are taken by heredity, 20% randomly, 20% through lattice mutations, and 20% by atom mutation. This process is repeated with new seed structures 20 times. Thereafter promising compositions – identified by negative enthalpy of formation (from elements and/or from neighboring compositions) at least at some pressure – are followed in more detail with searches at constant composition. This includes compositions with high nitrogen content.

References

1. Hohenberg, P.; Kohn, W., Inhomogeneous Electron Gas. *Physical Review* **1964**, *136*, B864-B871.
2. Kresse, G.; Hafner, J., Ab Initio Molecular Dynamics for Liquid Metals. *Physical Review B* **1993**, *47*, 558-561.
3. Kresse, G.; Hafner, J., \Textit{Ab Initio} Molecular-Dynamics Simulation of the Liquid-Metal Char21 Amorphous-Semiconductor Transition in Germanium. *Physical Review B* **1994**, *49*, 14251-14269.
4. Kresse, G.; Furthmüller, J., Efficiency of Ab-Initio Total Energy Calculations for Metals and Semiconductors Using a Plane-Wave Basis Set. *Computational Materials Science* **1996**, *6*, 15-50.
5. Sun, J. W.; Ruzsinszky, A.; Perdew, J. P., Strongly Constrained and Appropriately Normed Semilocal Density Functional. *Phys Rev Lett* **2015**, *115*.
6. Blöchl, P. E., Projector Augmented-Wave Method. *Physical Review B* **1994**, *50*, 17953-17979.
7. Kresse, G.; Joubert, D., From Ultrasoft Pseudopotentials to the Projector Augmented-Wave Method. *Physical Review B* **1999**, *59*, 1758-1775.
8. Perdew, J. P.; Burke, K.; Ernzerhof, M., Generalized Gradient Approximation Made Simple. *Phys Rev Lett* **1996**, *77*, 3865-3868.
9. Perdew, J. P.; Burke, K.; Ernzerhof, M., Generalized Gradient Approximation Made Simple [Phys. Rev. Lett. 77, 3865 (1996)]. *Phys Rev Lett* **1997**, *78*, 1396-1396.
10. Pickard, C. J.; Needs, R. J., Ab Initio Random Structure Searching. *Journal of Physics-Condensed Matter* **2011**, *23*, 23.
11. Oganov, A. R.; Ma, Y. M.; Lyakhov, A. O.; Valle, M.; Gatti, C., Evolutionary Crystal Structure Prediction as a Method for the Discovery of Minerals and Materials. In *Theoretical and Computational Methods in Mineral Physics: Geophysical Applications*, Wentzcovitch, R.; Stixrude, L., Eds. 2010; Vol. 71, pp 271-298.
12. Lonie, D. C.; Zurek, E., Xtalopt: An Open-Source Evolutionary Algorithm for Crystal Structure Prediction. *Comput. Phys. Commun.* **2011**, *182*, 372-387.
13. Wang, Y. C.; Lv, J. A.; Zhu, L.; Ma, Y. M., Crystal Structure Prediction Via Particle-Swarm Optimization. *Physical Review B* **2010**, *82*, 8.

PART I: CHEMICAL POTENTIAL OF NITROGEN AT HIGH PRESSURE AND HIGH TEMPERATURE

CHAPTER 1: CHEMICAL POTENTIAL OF NITROGEN AT HIGH PRESSUER AND HIGH TEMPERATURE: APPLICATION TO NITROGEN AND NITROGEN-rich PHASE DIAGRAM CALCULATIONS

Hanof Alkhaldi and Peter Kroll. Chemical Potential of Nitrogen at High Pressure and High Temperature: Application to Nitrogen and Nitrogen-Rich Phase Diagram Calculations. *The Journal of Physical Chemistry C* **2019** 123 (12), 7054-7060.

CHEMICAL POTENTIAL OF NITROGEN AT HIGH PRESSUER AND HIGH TEMPERATURE: APPLICATION TO NITROGEN AND NITROGEN-rich PHASE DIAGRAM CALCULATIONS

INTRODUCTORY REMARKS

The following article provides a detailed accounting of contributions to the chemical potential of nitrogen at high pressures and high temperatures. The method establishes a computational pathway to attain pressure–temperature phase diagrams of nitrogen-rich compounds at high pressures and high temperatures – conditions that are relevant for chemical synthesis in a diamond-anvil-cell. The validity of the approach is demonstrated for three characteristic systems: pure nitrogen, and nitrogen-rich Si-N as well as Ti-N phases. Besides corroborating experimental data, another outcome is that the "moderate extrapolation" explored in our study yields the best match between computation and experiment for experiments carried out between 2000 and 3000 K.

Chemical Potential of Nitrogen at High Pressure and High Temperature: Application to Nitrogen and Nitrogen-rich Phase Diagram Calculations

Hanof Alkhaldi and Peter Kroll[a]

Department of Chemistry and Biochemistry, The University of Texas at Arlington, 700 Planetarium Place, Arlington, Texas 76019, United States.

* Corresponding authors: pkroll@uta.edu

Abstract

The chemical potential change of nitrogen at high-pressure/high-temperature is a crucial ingredient for predicting the formation of nitrogen-rich compounds. Here we provide intelligible data for the chemical potential change of molecular nitrogen at temperature and pressure conditions relevant for experiments in the diamond-anvil-cell. In combination with first-principles calculations we derive pressure-temperature phase diagrams readily accessible to guide experimental efforts. We show the validity of our approach for three characteristic systems: pure nitrogen, and nitrogen-rich Si-N and Ti-N phases appearing at high-pressure/high-temperature.

Introduction

High-pressure nitrogen chemistry has seen tremendous advances over the last three decades thanks to diligent experimental work. The pursuit of super-hard and high energy-density materials has driven many endeavors, and several new nitrogen-rich compounds have been synthesized.[1-13] With the advent of accurate density functional calculations it became possible to predict new phases and the range of pressure they will emerge.[1, 14-15] The availability of massive high-performance computers today makes high-troughput searches employing a variety of structure search algorithms feasible and even more compound systems involving nitrogen are explored.[16-21]

In a recent comprehensive work, Sun et al. identified stable and metastable nitrogen-rich compounds and analyzed their enthalpy of formation from the elements.[20] Their work highlights the importance of the chemical potential of nitrogen for a successful synthesis of nitrogen containing compounds. Evidently, molar enthalpy equals chemical potential in the pure state only at absolute zero. Elevated temperature and pressure as well as the chemical environment, however, yield substantial differences between the two.[22]

Our focus is the chemical potential of nitrogen at high-pressure/high-temperature conditions (h-p/h-T), above 5 GPa and from 1500 K to 4000 K. These conditions are characteristic for laser-heated experiments carried out in the diamond-anvil-cell (DAC), where a synthesis of nitrogen-rich compounds may occur via direct synthesis from the elements.[1, 3] Even if fluid molecular nitrogen is not used as a pressure medium, it may evolve from reactants during heating and has to be accounted for in a reaction mixture. Standard textbook approaches relate the chemical potential change of nitrogen at h-p/h-T to its fugacity, which can adopt astronomical values even at experimentally accessible pressure. [23] We have previously described estimates for the fugacity of molecular nitrogen for h-p/h-T.[24] Here we provide intelligible data for the chemical potential change

of molecular nitrogen at temperature and pressure conditions relevant for experiments in the DAC. We then combine the thermochemical data with first-principles calculations into thermodynamic calculations of pressure-temperature phase diagrams. We consider three characteristic compound systems, N, Si-N, and Ti-N, to highlight the difference between estimates of phase stability based on enthalpy alone and predictions involving the impact of chemical potential changes at h-p/h-T conditions. and to show the validity of our approach.

Computational method:

First-Principles calculations

Calculations of total energy and volume are done within density functional theory (DFT) as implemented in Vienna abs initio simulation package (VASP).[25-28] We use the Strongly Conserved and Appropriately Normed (SCAN) functional [29] together with the projector-augmented-wave (PAW) method.[30-31] Consistency checks have been done with the Generalized Gradient Approximation (GGA-PBE) as well. [32-33] All results are obtained using a plane wave cut-off energy of 500 eV with forces converged to better than 1 meV/Å. The Brillouin zone of each structure is sampled by k-point meshes with grid sizes smaller than 0.03 $Å^{-1}$. With the parameters above, enthalpy differences between structures are converged to better than 1 meV.

For every structure we compute energy E as a function of volume V, reducing V stepwise to simulate higher densities and pressures. The resulting E–V data yields pressure p by numerical differentiation, $p = -\partial E/\partial V$, and enthalpy $H = E + pV$. Reaction enthalpies ΔH as a function of pressure at zero temperature are computed based on enthalpies of products and reactants. This data is commonly used to identify the convex hull of a phase system. Neglecting further impact of temperature and of entropy differences, reaction Gibbs energies $\Delta G = \Delta H - T \cdot \Delta S$ are approximated by ΔH. Locating

ΔH=0 then yields an estimate of transition pressures. These estimates are excellent guidelines predicting solid state reactions at constant composition, not at least because entropy differences that contribute to reaction Gibbs energies ΔG for solid-state reactions are usually small in comparison to changes of ΔH within a few GPa of pressure.

Once a gaseous or fluid reactant or product is involved, however, effects of entropy must be included. This is imperative for reactions involving pure nitrogen, which is why a consideration of the chemical potential μ of nitrogen, it Gibbs molar energy, and its increment relative to molar enthalpy, is important. [15, 20, 24]

Thermodynamic calculations

The chemical potential of nitrogen gas $\mu(T, p_{N_2})$ depends on temperature T and nitrogen partial pressure p_{N_2} via:

$$\mu(T, p_{N_2}) = \mu(T, p_0) + kT \ln\left(\frac{f}{p_0}\right) = \mu(T, p_0) + kT \ln\left(\frac{\gamma p_{N_2}}{p_0}\right) = \mu(T, p_0) + kT \ln\left(\frac{p_{N_2}}{p_0}\right) + kT \ln\gamma$$

Herein, f is the fugacity of nitrogen, p_0 is a reference nitrogen partial pressure for which we choose 1 bar (0.1 MPa), and k is the Boltzmann constant. The second equality relates fugacity f to nitrogen partial pressure p_{N_2} and introduces the fugacity coefficient γ. For a perfect gas $f = p_{N_2}$ and $\gamma = 1$ holds. The last term in the equation, kT ln γ, then shows the impact of a deviation from perfect gas behavior on the chemical potential. To provide examples: $\ln\gamma = 20$, thus $f \approx 10^9 \cdot p_{N_2}$ describes experimental data of nitrogen at 300 K and 2 GPa, while at 2000 K and 2 GPa $\ln\gamma = 2.3$. [23, 34]

There is currently no rigorous theoretical framework available to assess fugacity of nitrogen at elevated temperatures and pressures for different chemical environments. However, changes of the nitrogen chemical potential above the boiling point at ambient pressure, $\Delta\mu(T, p_{N_2})$, have been well documented in thermochemical tables.[22] Since

changes of μ in the gaseous state dominate those in the solid and liquid state by far, it is justified to neglect the increment of μ from absolute zero up to the boiling point and approximate the chemical potential at these conditions simply by enthalpy H of a solid molecular phase of nitrogen. We thus receive

$$\mu(T, p_{N_2}) \approx H(p_{N_2}) + \Delta\mu(T, p_{N_2})$$

and the chemical potential increment $\Delta\mu(T, p_{N_2})$ is given by

$$\Delta\mu(T, p_{N_2}) = \Delta\mu(T, p_0) + kT \ln\left(\frac{p_{N_2}}{p_0}\right) + kT \ln\gamma$$

The first term in this equation reflects the tabulated thermochemical data, while the second term describes the dependence of the chemical potential of a perfect gas on pressure. The third term accounts for all deviations from perfect behavior, collected in the fugacity. For a perfect gas, $\gamma = 1$, thus $\ln\gamma = 0$, and the third term vanishes. In general, fugacity γ will depend on all parameters of a system, but especially on partial pressure of the gas and on temperature.

In previous work we provided three different approaches to account for $\Delta\mu(T, p_{N_2})$ at high temperatures and high pressures. A first approach assumes perfect gas behavior, thus $\ln\gamma = 0$.[15, 35] A second proposal follows a moderate extrapolation of experimental data:[24]

$$\ln\gamma = \alpha(T) \cdot \left[1 - \exp\left(-\beta(T) p_{N_2}\right)\right] \qquad \text{(Eqn. f1)}$$

with $\alpha(T) = \alpha_1/T + \alpha_2/T^2 + \alpha_3/T^3$, and $\beta(T) = \beta_0 + \beta_1/T + \beta_2/T^2$.

Coefficients are: α_1=14.0707, α_2=2.40815, α_3=0.86685, β_0=0.29775, β_1=0.09503, β_2=0.00996. A third estimate of γ extrapolates experimental data in a more progressive way:[24]

$$\ln\gamma = \alpha/T \cdot \ln\left(1 + \beta p_{N_2}\right) \qquad \text{(Eqn. f2)}$$

with α=10.4583 and β=0.3879. In both extrapolation formulas the temperature T is given in units of 1000 K and the pressure p_{N_2} in GPa. For convenience, we provide data of $\Delta\mu(T, p_{N_2})$ based on these approaches for conditions relevant to high-pressure/high-temperature syntheses of nitride compounds in Tables 1, 2, and 3.

$\Delta\mu(T, p_{N_2})$	20 GPa	40 GPa	60 GPa	80 GPa	100 GPa	120 GPa	140 GPa
1500 K	-0.89	-0.85	-0.82	-0.80	-0.79	-0.78	-0.77
2000 K	-1.27	-1.21	-1.18	-1.15	-1.13	-1.12	-1.10
2500 K	-1.67	-1.60	-1.55	-1.52	-1.50	-1.48	-1.46
3000 K	-2.09	-2.00	-1.95	-1.91	-1.88	-1.86	-1.84

Table 1: Changes of chemical potential, $\Delta\mu(T, p_{N_2})$ (in eV/atom), of nitrogen, treating nitrogen as perfect gas, γ = 1 (ln γ = 0).

$\Delta\mu(T, p_{N_2})$	20 GPa	40 GPa	60 GPa	80 GPa	100 GPa	120 GPa	140 GPa
1500 K	-0.21	-0.16	-0.13	-0.11	-0.10	-0.08	-0.07
2000 K	-0.61	-0.54	-0.51	-0.48	-0.46	-0.45	-0.44
2500 K	-1.02	-0.94	-0.90	-0.87	-0.84	-0.82	-0.81
3000 K	-1.45	-1.36	-1.31	-1.27	-1.24	-1.22	-1.20

Table 2: Changes of chemical potential, $\Delta\mu(T, p_{N_2})$ (in eV/atom), of nitrogen, with fugacity approximated using the moderate extrapolation, Eqn. f1.

$\Delta\mu(T, p_{N_2})$	20 GPa	40 GPa	60 GPa	80 GPa	100 GPa	120 GPa	140 GPa
1500 K	0.09	0.42	0.62	0.76	0.87	0.96	1.04
2000 K	-0.29	0.05	0.26	0.41	0.53	0.63	0.71
2500 K	-0.69	-0.33	-0.12	0.04	0.16	0.26	0.35
3000 K	-1.11	-0.74	-0.51	-0.35	-0.22	-0.12	-0.03

Table 3: Changes of chemical potential, $\Delta\mu(T, p_{N_2})$ (in eV/atom), of nitrogen, with fugacity approximated using the progressive extrapolation, Eqn. f2.

Using the thermodynamic data together with the various extrapolation formulas it is now straightforward to compute the chemical potential $\mu(T, p_{N_2})$ of nitrogen at high temperatures and high pressures. Assuming, furthermore, that the increment $\Delta\mu(T, p_{N_2})$ dominate all further temperature effects, especially the entropy differences between solid-state products and reactants, we can combine the thermodynamic calculations with first-

principles calculations of enthalpy and compute reaction Gibbs energies ΔG. Locating equilibrium lines and identifying the most stable system at a given temperature and pressure, finally, results in temperature-pressure phase diagrams.

Results:

On the Nitrogen Phase Diagram

We first apply the approach combining first-principles computations with thermodynamic calculations to identify the phase boundary between molecular nitrogen and polymeric nitrogen. Triple-bonded molecular nitrogen is represented using the crystal structure of ε-N_2 (SpGr. R-3c (167), Z=16). Choosing α-N_2 (SpGr. Pa-3 (205), Z=8) instead provides equivalent enthalpy-pressure data, if a pressure-induced distortion of the cubic into an orthorhombic (Cmca) structure is allowed. Both ε- and α-phase remain "molecular" comprising isolated N_2 molecules up to about 200 GPa, when they "polymerize" spontaneously. Single-bonded polymeric nitrogen, also termed cubic-gauche phase, cg-N, adopts a cubic structure (SpGr. $I2_13$ (199), Z=8).

At experimental conditions, cg-N emerges at pressures above 110 GPa and temperatures above 2000K. [4]. Additional experiments report formation of transparent cg-N at 120–130 GPa above 2000 K, [36], at 165 GPa in excess of 2000 K, [37], and at 140 GPa when heating above 1450 K. All reports agree that formation of cg-N at high-pressure high-temperature conditions is a complex kinetic process passing through multiple intermediates. Longer heating enhances the phase content of polymeric nitrogen, while heating at higher temperatures accelerates its formation.

Calculating the energy-volume (E-V) data for molecular and polymeric nitrogen and deriving the corresponding ΔH-p diagram (Figure 1) yields a transition pressure p_t for the transformation between the two phases of 59.3 GPa (53.3 GPa using PBE). This is in-line with previous reports of computed values of p_t, [14, 38] but obviously not corresponding to

the experimental conditions listed above. At 110 GPa, the lowest reported transition pressure, the enthalpy difference between and ε-N_2 and cg-N is 0.48 eV/atom (0.55 eV/atom using PBE), clearly favoring the polymeric form of nitrogen. Assuming that the experimental conditions (110 GPa, 2000 K) reflect equilibrium between molecular N_2 and cg-N, the chemical potential of both phases is equal at these conditions. Consequently, the computed enthalpy for molecular nitrogen is augmented by an increment of -0.48 eV/atom (negative relative to cg-N) to yield its chemical potential. Therefore, $\Delta\mu$(2000 K, 110 GPa) = -0.48 eV/atom. This value of $\Delta\mu$ is in agreement with the data derived using the moderate extrapolation of fugacity, Table 2. The more progressive estimate may not be ruled out, since many times temperatures have been described as "in excess of 2000 K". Consequently, experimental data for synthesis of cg-N supports our proposal that the two extrapolations can be regarded as lower and upper boundary for the fugacity of nitrogen at high pressures.

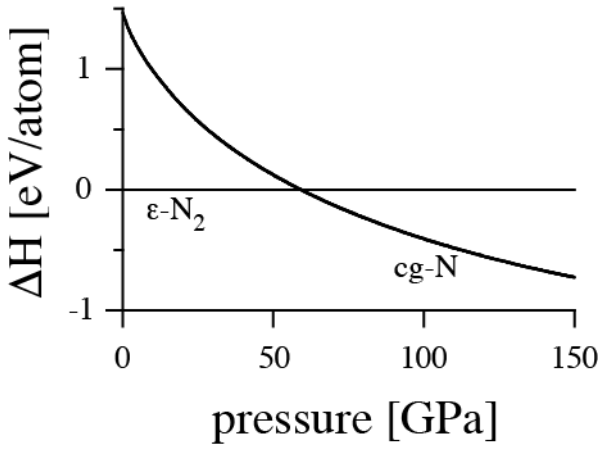

Figure 1: Enthalpy-pressure (ΔH-p) of polymeric-N relative to molecular ε-N_2 computed using the SCAN functional. The enthalpy difference ΔH is given in eV per atom.

We now combine for molecular nitrogen the first-principles calculations of enthalpy as a function of pressure with the thermodynamic calculations of chemical potential changes as a function of temperature and pressure. On the other side, Gibbs energy of the solid

cubic-gauche phase of nitrogen is approximated by its enthalpy. This approach neglects contribution by vibrational entropy and further effects. However, this error occurs on both sides of the equilibrium equation and will, to a large extend, cancel out. Besides, those contributions are dwarfed by the chemical potential change for molecular nitrogen (and by its uncertainty). We acknowledge that the dominant error in these calculations is within the estimate of $\Delta\mu(T, p_{N_2})$, and more experiments will be helpful to yield more accurate estimates of $\Delta\mu(T, p_{N_2})$. The phase boundary between molecular nitrogen and the phase of cg-N is then located by equating the Gibbs energies of the two phases and results are shown in Figure 2. Obviously, the experimental results – the phase boundary between molecular and polymeric nitrogen – are well characterized through either the moderate or progressive extrapolation of fugacity for molecular nitrogen. Treating nitrogen as a perfect gas does not yield a thermodynamically stable cg-N at 110 GPa and 2000 K, while the two extrapolating approximations do.

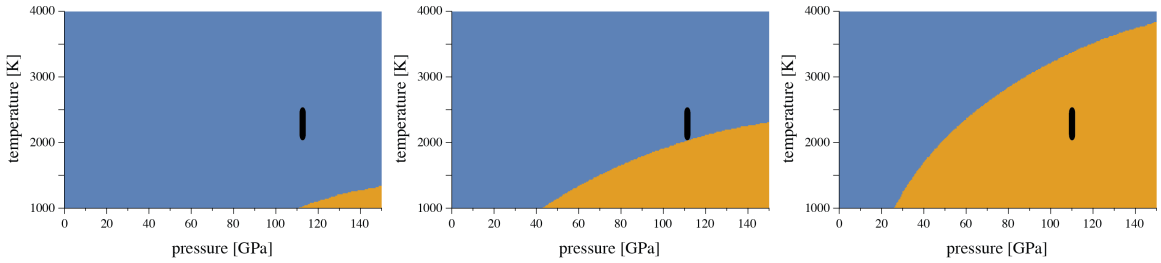

Figure 2: Pressure-temperature phase diagram of nitrogen showing the phase boundary between molecular (ε-N_2) and polymeric (cg-N) nitrogen based on a combination of first principles (SCAN functional) and thermodynamic calculations. For the fugacity of nitrogen we use (left) the perfect gas approximation, (middle) the moderate and (right) the progressive extrapolation formula. The thick line in each diagram indicates reported experimental conditions from Ref. [4] for the formation of polymeric nitrogen.

On the Silicon-Nitrogen Phase Diagram

We apply the computational approach next to the Si-N phase system, focusing on the surprising synthesis of SiN_2. Until 1999, α- and β-Si_3N_4 were the only known crystalline ambient pressure modifications of silicon nitride. Zerr et al. then synthesized a spinel-

type γ-Si_3N_4 (SpGr. Fd-3m (227), Z=8) by reacting silicon and molecular nitrogen at 15 GPa and 2000 K.[1] A post-spinel modification δ-Si_3N_4 was later been predicted to adopt a $CaTi_2O_4$-type structure and succeed γ-Si_3N_4 above 160 GPa.[39] SiN_2 with a pyrite-type structure (SpGr. Pa-3 (205), Z=4) comprising the pernitride N_2^{4-}-anion was first considered by Weihrich et al.. [40] In 2014 Chen et al. computed the pyrite-type SiN_2 to be enthalpically favored over a combination of γ-Si_3N_4 and N_2 at pressures above 17 GPa.[41] Subsequently, this phase was obtained through direct synthesis from the elements using laser heating at approximately 60 GPa.[42] Unfortunately, no estimate of the temperature during synthesis of SiN_2 has been given. Notably, applying only 50 GPa of pressure but the same temperature conditions yields only γ-Si_3N_4 and not SiN_2, indicating a boundary between the two phases. At this point it is possible to think of Si-N phases with even higher nitrogen content. As one example, we consider SiN_4 with a structure related to the calcite-type of $CaCO_3$ (SpGr. R-3c (167), Z=6). At 71 GPa (62 GPa in PBE) this candidate type of SiN_4 will become more favorable by enthalpy relative to SiN_2 and molecular nitrogen, see Figure 3. In other words, it will appear on the convex hull of the Si-N phase system between SiN_2 and N.

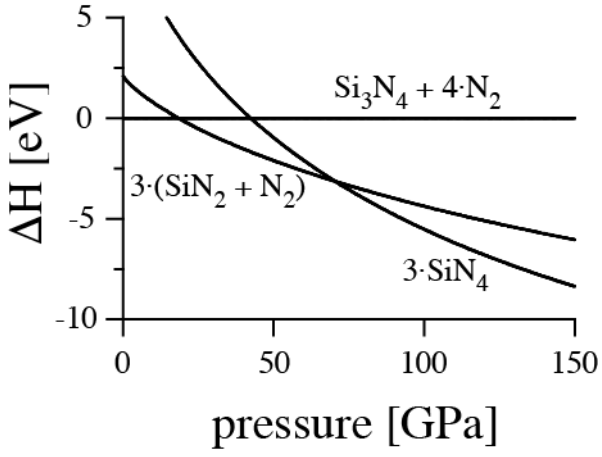

Figure 3: Relative enthalpy-pressure (ΔH-p) diagram comparing $Si_3N_4 + 4{\cdot}N_2$, $3{\cdot}(SiN_2 + N_2)$, and $3{\cdot}SiN_4$ computed using the SCAN functional. Enthalpy is given relative to γ-Si_3N_4 and molecular ε-N_2.

As in the nitrogen phase system, we note a discrepancy between computed and observed phase boundary between γ-Si_3N_4 and SiN_2. Once again, we can relate the significant shift in transition pressure to the chemical potential increment of molecular nitrogen involved in the phase change. According to Figure 3, the enthalpy difference between 3 SiN_2 and γ-Si_3N_4 + N_2 at 60 GPa is 2.6 eV (2.9 eV in PBE). Assuming that both phases are in equilibrium, this implies that at experimental conditions, where the pressure refers to the partial pressure of nitrogen, p_{N_2}, the chemical potential of nitrogen is 1.3 eV per N atom lower than its computed enthalpy. Therefore, $\Delta\mu(T_{syn}, 60\text{GPa}) = -1.3$ eV/atom. It is justified to expect that the temperature of synthesis T_{syn} exceeds 2000 K in these experiments.[1] Inspecting the values of $\Delta\mu$ at 60 GPa in Tables 1-3, we find corresponding data, for example using perfect gas data (~2300 K) or the moderate extrapolation of fugacity of nitrogen (~3000 K). As to the likelihood of SiN_4 emerging at high nitrogen pressure, Figure 3 yields that the enthalpy difference between SiN_2 + N_2 and SiN_4 at 100 GPa is 1/3 · 1.15 eV = 0.38 eV. Thus, we expect formation of SiN_4 only if the chemical potential increment $\Delta\mu$ is larger than -0.19 eV. Assuming the moderate extrapolation formula to be valid this can only happen below 1600 K at 100 GPa. Note that above 110 GPa formation of cg-N is observed.

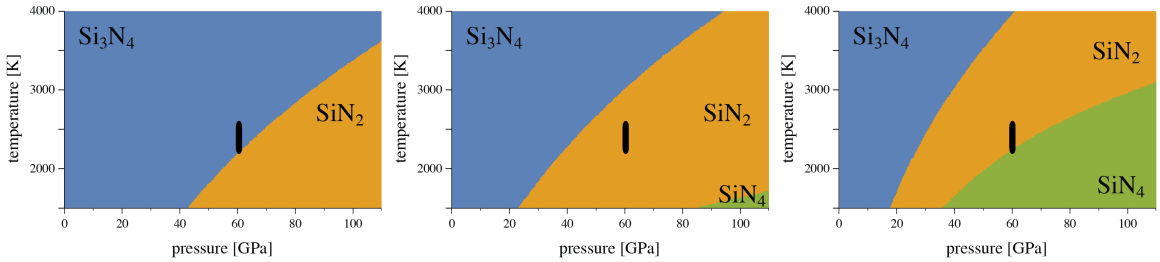

Figure 4: Temperature-pressure phase diagrams for the silicon-nitrogen system involving Si_3N_4, SiN_2, and SiN_4. Pressure refers to nitrogen partial pressure, p_{N_2}. For the fugacity of nitrogen we use the (left) perfect gas approximation, (middle) the moderate and (right) the progressive extrapolation formula. The thick line in each diagram indicates the pressure (60 GPa) for the formation of SiN_2 reported in Ref. [42] together with a good-

faith estimate of the temperature of synthesis. The transition from α/β-Si_3N_4 to γ-Si_3N_4 occurring at about 15 GPa had been omitted from the diagrams.

Combining first-principles and thermodynamic calculations we derive the phase diagrams collectively shown in Figure 4. Focusing on a pressure of 60 GPa, we find that the moderate extrapolation formula for the fugacity of nitrogen yields fitting result, if we assume typical temperatures between 2000 K and 3000 K in such a Laser-heating experiment.[1] Even if we treat nitrogen as a perfect gas, a pernitride SiN_2 has a small range of stability above 2000 K at 60 GPa, before it will decompose into Si_3N_4 and nitrogen at higher temperatures. A reduced fugacity of nitrogen would also describe the formation of γ-Si_3N_4 at 50 GPa from the elements. Based on the more moderate approximation of fugacity, synthesis of SiN_4 will require pressures at about 100 GPa, and may eventually impossible due to the appearance of cg-N. Indeed, we find that SiN_4 is less favorable by enthalpy than SiN_2 and cg-N at any pressure.

On the Titanium-Nitrogen Phase Diagram

Our third application of combining first-principles and thermodynamic calculations addresses the nitrogen-rich part of the titanium-nitrogen phase diagram. A first account of the Ti-N phase diagram involving rocksalt TiN (SpGr. Fm-3m (225), Z=4) and Th_3P_4-type Ti_3N_4 (SpGr. I-43d (220), Z=4), while treating nitrogen as a perfect gas, located the phase boundary between TiN and Ti_3N_4 between 75 GPa and 100 GPa, at 2000 K and 2800 K, respectively.[15, 35]. Subsequent structure searches discovered a pernitride TiN_2 (SpGr. I4/mcm (140), Z=4) to appear on the convex hull for pressures above 26.6 GPa, surpassing Ti_3N_4 at any higher pressure.[17] Experimental studies first reported synthesis of TiN_2 at 73 GPa and 2300 K.[43] Subsequently, a similar experiment (75 GPa, 2400 K) produced the long-sought Th_3P_4-type Ti_3N_4.[44] Careful analysis of both experiments indicate that pernitride TiN_2 and Th_3P_4-type Ti_3N_4 were produced each time at different locations of the reaction chambers.[44]

Computing energies and enthalpies for the three systems 3 TiN + 3/2 N_2, Ti_3N_4 + N_2, and 3 TiN_2 yields the enthalpy pressure diagram of Figure 5, left. We find that below 24.6 GPa the TiN + ½ N_2 system is favored by enthalpy, while above this pressure TiN_2 is the most favorable compound. As to the question whether Ti_3N_4 may appear [44] or may not appear [17] on the convex hull, we find the reaction 2 TiN + TiN_2 -> Ti_3N_4 to be exothermic above 65.4 GPa (Figure 5, right). Thus, Ti_3N_4 appears on the convex hull between TiN and TiN_2 — but how will this relate to thermodynamical stability at elevated temperatures?

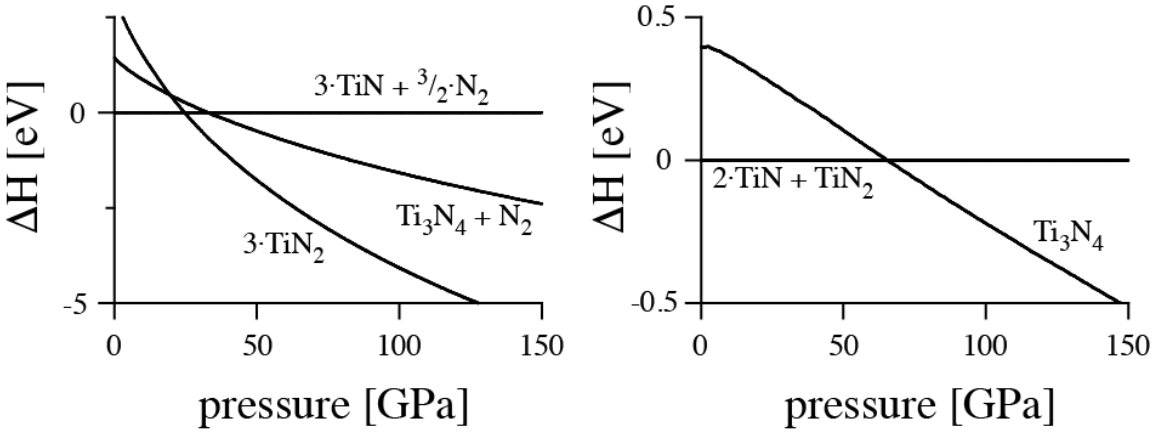

Figure 5: (Left) Relative enthalpy-pressure (ΔH-p) diagram comparing 3·TiN + 3/2·N_2, Ti_3N_4 + N_2, and 3·TiN_2 computed using the SCAN functional. Enthalpy is given relative to TiN and molecular ε-N_2. (Right) Enthalpy of reaction for 2 TiN + TiN_2 -> Ti_3N_4. Enthalpy is given per formula unit Ti_3N_4.

The results of phase diagrams calculations are shown in Figure 6. A common feature is the small wedge of the stability field of Ti_3N_4 between the much larger regions corresponding to TiN and TiN_2. The wedge starts at about 62 GPa and emerges at quite different temperatures depending on the approximation for fugacity of nitrogen. However, in each approximation it widens its range with increasing pressure. At 75 GPa, its width is 200 K, and enlarges to 500 K at 110 GPa. With respect to experimental condition, 75 GPa and 2400 K, it appears that the moderate approximation to fugacity of

nitrogen predicts best the outcome of the experiment. Temperature conditions in the diamond anvil cell are not equal throughout the chamber, and large variations can appear. Thus, an apparent "coexistence" of Ti_3N_4 and TiN_2 is likely related to different temperature conditions, with each phase being synthesized at its thermodynamical stable conditions before being quenched rapidly.

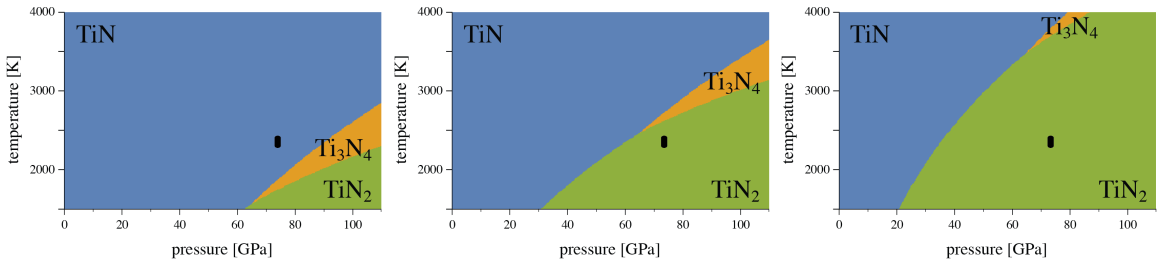

Figure 6: Temperature-pressure phase diagrams for the titanium-nitrogen system involving TiN, Ti_3N_4, and TiN_2. Pressure refers to nitrogen partial pressure, p_{N_2}. For the fugacity of nitrogen we use the (left) perfect gas approximation, (middle) the moderate and (right) the progressive extrapolation formula. The thick line in each diagram indicates the experimental conditions for the formation of Ti_3N_4 and TiN_2 reported in Refs. [43] and [44].

Discussion

Predicting the chemical synthesis of new high-pressure nitride phases from their elements in standard laser-heated diamond-anvil experiments requires consideration of reaction equilibria of nitride compounds with molecular nitrogen – as a function of pressure and temperature. Considering a "convex hull" of relative enthalpy involving nitrogen may serve as an initial guideline, but the substantial decrease of the chemical potential of nitrogen above the boiling point (in the range of –1.5 to –3.5 eV per N atom for 1500 to 3000 K, respectively [22]) limits its predictive value. At higher pressure this effect is countered, and experimental data suggests that nitrogen becomes extremely active as expressed through its fugacity.

Comparing experimental data for the synthesis of cg-N with the computed phase diagrams of Figure 2 undoubtedly supports a significant change of chemical potential as well as a substantial magnitude of fugacity of nitrogen at elevated pressure and temperature. For the pure system, the extrapolation formulas (Eqns. f1 and f2) provide lower and upper boundary for the fugacity of nitrogen at high pressures and temperatures. Analysis of computed Si-N and Ti-N phase diagrams and the available experimental data corroborate the notion that the moderate approach to fugacity (Eqn. f1) carries a higher weight. The case of simultaneous synthesis of Ti_3N_4 and TiN_2 shows the delicacy of the approach. Indeed, at 75 GPa Ti_3N_4 has only a small temperature stability window ($\Delta T \approx 200K$) avaulable for its synthesis, and this condition was hit at some spots in the experiment.

Additional support stems from the synthesis of RuN_2. Early predictions located the phase boundary between 25 and 40 GPa at temperatures between 2000 and 3000 K.[45] RuN_2 was then synthesize at pressures above 32 GPa, and while no temperature measurements were made there was indication that the temperature exceeded 2000 K.[46] Up to 20 GPa even the treatment of nitrogen as perfect gas can yield reasonable estimates of phase boundaries at high temperature.[15, 35]

The major source of error in our phase diagram calculations originates from limited knowledge about the fugacity of nitrogen. Note that for high pressure nitrides typical contributions of vibrational entropy differences to ΔG remain very small. At 2000 K these contributions are well below 0.1 eV/atom [19, 47]. Configurational entropy caused by defects or via mixing may in principle contribute up to 0.1 eV at 2000 K per active site, if we assume ideal mixing. In most compound systems such contributions are compensated by a few GPa of pressure change. In comparison, the uncertainty in chemical potential change is larger, and taking the moderate extrapolation formula as a base we estimate a margin of +/- 0.2 eV per nitrogen atom. To evaluate, how such an error propagates into

pressure or temperature imprecisions, one can plot the "convex hull" for a particular temperature or make plots of relative Gibbs energy (ΔG) at a certain temperature as a function of pressure. Likewise, it is possible to plot ΔG for a given pressure as a function of temperature. These "slices" through the computed phase diagram will also help to indentify phases, which are closely above the minimum Gibbs energy system.

Of course, the combination of first-principles and thermodynamic calculations requires the input of good structure candidates, making the various methods of structure searches indispensible for the exploration of new materials.[17, 20] Together with the method we deliver, they provide a comprehensive tool to guide synthesis of nitrogen-rich compounds at high pressure and high temperature.

Last we note that we have chosen simple extrapolation formulas and only consider the impact of nitrogen partial pressure and temperature on fugacity. Further experimental pressure and temperature data is needed to provide better estimates for fugacity and chemical potential change of nitrogen at high-pressure high-temperature conditions in different chemical environments.

Conclusion

We provide a pathway to compute pressure-temperature phase diagrams of nitrogen-rich compounds combining experimental thermochemical data with first-principles calculations. The approach is validated by comparison to experimental data for the synthesis of polymeric nitrogen, the phase boundary between silicon nitride and silicon pernitride, and the appearance of three nitrogen-rich Ti-N phases within a small pressure-temperature range. Overall, we deliver a rational strategy to predict temperature-pressure conditions for the synthesis of nitrogen-rich compounds. High-pressure researchers can apply the approach to identify new nitrogen-rich materials attainable via direct synthesis from the elements.

Acknowledgement

This work was supported by the National Science Foundation (NSF) through award OISE-1743701. The computational work was made possible through generous grants by the Texas Advance Computing Center in Austin, TACC, Texas, and by the High Performance Computing facilities at UTA. H.A. achnowledges support by the government of Saudi Arabia.

References

1. Zerr, A.; Miehe, G.; Serghiou, G.; Schwarz, M.; Kroke, E.; Riedel, R.; Fuess, H.; Kroll, P.; Boehler, R., Synthesis of Cubic Silicon Nitride. *Nature* **1999**, *400*, 340-342.
2. Landskron, K.; Huppertz, H.; Senker, J.; Schnick, W., High-Pressure Synthesis of γ-P_3N_5 at 11 GPa and 1500 Degrees C in a Multianvil Assembly: A Binary Phosphorus(V) Nitride with a Three-Dimensional Network Structure from Pn4 Tetrahedra and Tetragonal Pn5 Pyramids. *Angew Chem Int Edit* **2001**, *40*, 2643-2645.
3. Zerr, A.; Miehe, G.; Riedel, R., Synthesis of Cubic Zirconium and Hafnium Nitride Having Th_3P_4 Structure. *Nat Mater* **2003**, *2*, 185-189.
4. Eremets, M. I.; Gavriliuk, A. G.; Trojan, I. A.; Dzivenko, D. A.; Boehler, R., Single-Bonded Cubic Form of Nitrogen. *Nat Mater* **2004**, *3*, 558-563.
5. Gregoryanz, E.; Sanloup, C.; Somayazulu, M.; Badro, J.; Fiquet, G.; Mao, H. K.; Hemley, R. J., Synthesis and Characterization of a Binary Noble Metal Nitride. *Nat Mater* **2004**, *3*, 294-297.
6. Zerr, A., et al., High-Pressure Synthesis of Tantalum Nitride Having Orthorhombic U_2S_3 Type Structure. *Adv Funct Mater* **2009**, *19*, 2282-2288.
7. Bykov, M., et al., Fe-N System at High Pressure Reveals a Compound Featuring Polymeric Nitrogen Chains. *Nat Commun* **2018**, *9*.
8. Bykov, M., et al., High-Pressure Synthesis of a Nitrogen-Rich Inclusion Compound $ReN_{(8)}.N_{(2)}$ with Conjugated Polymeric Nitrogen Chains. *Angew Chem Int Edit* **2018**, *57*, 9048-9053.
9. Laniel, D.; Dewaele, A.; Garbarino, G., High Pressure and High Temperature Synthesis of the Iron Pernitride FeN_2. *Inorg Chem* **2018**, *57*, 6245-6251.
10. Laniel, D.; Weck, G.; Loubeyre, P., Direct Reaction of Nitrogen and Lithium up to 75 Gpa: Synthesis of the Li_3N, LiN, LiN_2, and LiN_5 Compounds. *Inorg Chem* **2018**, *57*, 10685-10693.
11. Zerr, A.; Riedel, R.; Sekine, T.; Lowther, J. E.; Ching, W. Y.; Tanaka, I., Recent Advances in New Hard High-Pressure Nitrides. *Adv. Mater.* **2006**, *18*, 2933-2948.
12. Horvath-Bordon, E.; Riedel, R.; Zerr, A.; McMillan, P. F.; Auffermann, G.; Prots, Y.; Bronger, W.; Kniep, R.; Kroll, P., High-Pressure Chemistry of Nitride-Based Materials. *Chem. Soc. Rev.* **2006**, *35*, 987-1014.
13. Salamat, A.; Hector, A. L.; Kroll, P.; McMillan, P. F., Nitrogen-Rich Transition Metal Nitrides. *Coord. Chem. Rev.* **2013**, *257*, 2063-2072.
14. Mailhiot, C.; Yang, L. H.; Mcmahan, A. K., Polymeric Nitrogen. *Physical Review B* **1992**, *46*, 14419-14435.
15. Kroll, P., Hafnium Nitride with Thorium Phosphide Structure: Physical Properties and an Assessment of the Hf-N, Zr-N, and Ti-N Phase Diagrams at High Pressures and Temperatures. *Phys Rev Lett* **2003**, *90*.
16. Zhao, Z. L.; Bao, K.; Tian, F. B.; Duan, D. F.; Liu, B. B.; Cui, T., Phase Diagram, Mechanical Properties, and Electronic Structure of Nb-N Compounds under Pressure. *Phys Chem Chem Phys* **2015**, *17*, 22837-22845.
17. Yu, S. Y.; Zeng, Q. F.; Oganov, A. R.; Frapper, G.; Zhang, L. T., Phase Stability, Chemical Bonding and Mechanical Properties of Titanium Nitrides: A First-Principles Study. *Phys Chem Chem Phys* **2015**, *17*, 11763-11769.

18. Liu, Z.; Li, D.; Wei, S. L.; Wang, W. J.; Tian, F. B.; Bao, K.; Duan, D. F.; Yu, H. Y.; Liu, B. B.; Cui, T. A., Bonding Properties of Aluminum Nitride at High Pressure. *Inorg Chem* **2017**, *56*, 7494-7500.
19. Zhang, J.; Oganov, A. R.; Li, X. F.; Niu, H. Y., Pressure-Stabilized Hafnium Nitrides and Their Properties. *Physical Review B* **2017**, *95*, 5.
20. Sun, W. H.; Holder, A.; Orvananos, B.; Arca, E.; Zakutayev, A.; Lany, S.; Ceder, G., Thermodynamic Routes to Novel Metastable Nitrogen-Rich Nitrides. *Chem Mater* **2017**, *29*, 6936-6946.
21. Huang, B. W.; Frapper, G., Barium-Nitrogen Phases under Pressure: Emergence of Structural Diversity and Nitrogen-Rich Compounds. *Chem Mater* **2018**, *30*, 7623-7636.
22. Chase, M. W., Nist-Janaf Thermochemical Tables; . *NIST Standard Reference Database* **1998**, *13;* https://kinetics.nist.gov/janaf.
23. Jacobsen, R. T.; Stewart, R. B.; Jahangiri, M., Thermodynamic Properties of Nitrogen from the Freezing Line to 2000-K at Pressures to 1000-MPa. *J Phys Chem Ref Data* **1986**, *15*, 735-909.
24. Kroll, P.; Schroter, T.; Peters, M., Prediction of Novel Phases of Tantalum(V) Nitride and Tungsten(Vi) Nitride That Can Be Synthesized under High Pressure and High Temperature. *Angew Chem Int Edit* **2005**, *44*, 4249-4254.
25. Hohenberg, P.; Kohn, W., Inhomogeneous Electron Gas. *Physical Review* **1964**, *136*, B864-B871.
26. Kresse, G.; Hafner, J., \Textit{Ab Initio} Molecular Dynamics for Liquid Metals. *Physical Review B* **1993**, *47*, 558-561.
27. Kresse, G.; Hafner, J., \Textit{Ab Initio} Molecular-Dynamics Simulation of the Liquid-Metal\Char21{}Amorphous-Semiconductor Transition in Germanium. *Physical Review B* **1994**, *49*, 14251-14269.
28. Kresse, G.; Furthmüller, J., Efficiency of Ab-Initio Total Energy Calculations for Metals and Semiconductors Using a Plane-Wave Basis Set. *Computational Materials Science* **1996**, *6*, 15-50.
29. Sun, J. W.; Ruzsinszky, A.; Perdew, J. P., Strongly Constrained and Appropriately Normed Semilocal Density Functional. *Phys Rev Lett* **2015**, *115*.
30. Blöchl, P. E., Projector Augmented-Wave Method. *Physical Review B* **1994**, *50*, 17953-17979.
31. Kresse, G.; Joubert, D., From Ultrasoft Pseudopotentials to the Projector Augmented-Wave Method. *Physical Review B* **1999**, *59*, 1758-1775.
32. Perdew, J. P.; Burke, K.; Ernzerhof, M., Generalized Gradient Approximation Made Simple. *Phys Rev Lett* **1996**, *77*, 3865-3868.
33. Perdew, J. P.; Burke, K.; Ernzerhof, M., Generalized Gradient Approximation Made Simple [Phys. Rev. Lett. 77, 3865 (1996)]. *Phys Rev Lett* **1997**, *78*, 1396-1396.
34. Unland, J.; Onderka, B.; Davydov, A.; Schmid-Fetzer, R., Thermodynamics and Phase Stability in the Ga-N System. *J Cryst Growth* **2003**, *256*, 33-51.
35. Kroll, P., Assessment of the Hf-N, Zr-N and Ti-N Phase Diagrams at High Pressures and Temperatures: Balancing between Mn and M_3N_4 (M = Hf, Zr, Ti). *J Phys-Condens Mat* **2004**, *16*, S1235-S1244.

36. Lipp, M. J.; Klepeis, J. P.; Baer, B. J.; Cynn, H.; Evans, W. J.; Iota, V.; Yoo, C. S., Transformation of Molecular Nitrogen to Nonmolecular Phases at Megabar Pressures by Direct Laser Heating. *Physical Review B* **2007**, *76*.
37. Gregoryanz, E.; Goncharov, A. F.; Sanloup, C.; Somayazulu, M.; Mao, H. K.; Hemley, R. J., High P-T Transformations of Nitrogen to 170 GPa. *J Chem Phys* **2007**, *126*.
38. Mattson, W. D.; Sanchez-Portal, D.; Chiesa, S.; Martin, R. M., Prediction of New Phases of Nitrogen at High Pressure from First-Principles Simulations. *Phys Rev Lett* **2004**, *93*.
39. Kroll, P.; von Appen, J., Post-Spinel Phases of Silicon Nitride. *Phys Status Solidi B* **2001**, *226*, R6-R7.
40. Weihrich, R.; Eyert, V.; Matar, S. F., Structure and Electronic Properties of New Model Dinitride Systems: A Density-Functional Study of CN_2, SiN_2, and GeN_2. *Chem Phys Lett* **2003**, *373*, 636-641.
41. Chen, C. B.; Xu, Y.; Sun, X. P.; Wang, S. H.; Tian, F. B., The Stability, Electronic Properties, and Hardness of SiN_2 under High Pressure. *Rsc Adv* **2014**, *4*, 55023-55027.
42. Niwa, K.; Ogasawara, H.; Hasegawa, M., Pyrite Form of Group-14 Element Pernitrides Synthesized at High Pressure and High Temperature. *Dalton T* **2017**, *46*, 9750-9754.
43. Bhadram, V. S.; Kim, D. Y.; Strobel, T. A., High-Pressure Synthesis and Characterization of Incompressible Titanium Pernitride. *Chem Mater* **2016**, *28*, 1616-1620.
44. Bhadram, V. S.; Liu, H. Y.; Xu, E. S.; Li, T. S.; Prakapenka, V. B.; Hrubiak, R.; Lany, S.; Strobel, T. A., Semiconducting Cubic Titanium Nitride in the Th_3P_4 Structure. *Phy Rev Mater* **2018**, *2*.
45. Kroll, P., Advances in Computation of Temperature-Pressure Phase Diagrams of High-Pressure Nitrides. *Key Eng Mat* **2009**, *403*, 77-80.
46. Niwa, K.; Suzuki, K.; Muto, S.; Tatsumi, K.; Soda, K.; Kikegawa, T.; Hasegawa, M., Discovery of the Last Remaining Binary Platinum-Group Pernitride RuN_2. *Chem-Eur J* **2014**, *20*, 13885-13888.
47. Togo, A.; Kroll, P., First-Principles Lattice Dynamics Calculations of the Phase Boundary between β-Si_3N_4 and γ-Si_3N_4 at Elevated Temperatures and Pressures. *J. Comput. Chem.* **2008**, *29*, 2255-2259.

PART II: COMPUTING METAL–NITROGEN PHASE DIAGRAM AT HIGH PRESSURE AND HIGH TEMPERATURE

CHAPTER 1: COMPUTING THE TANTALUM–NITROGEN PHASE DIAGRAM AT HIGH PRESSUER AND HIGH TEMPERATURE

Hanof Alkhaldi and Peter Kroll. Computing the Tantalum–Nitrogen Phase Diagram at High Pressure and High Temperature. *The Journal of Physical Chemistry C* **2020** 124 (40), 22221-22227.

COMPUTING THE TANTALUM–NITROGEN PHASE DIAGRAM AT HIGH PRESSUER AND HIGH TEMPERATURE

INTRODUCTORY REMARKS

The following article applies the approach established in the previous work to the tantalum–nitrogen system. In comparison to the earlier work, a system with great structural diversity is encountered – no less than eleven different structures are reported to occur. The work locates all experimentally reported phases and predicts new tantalum–nitrogen compounds $Ta_2N_2(N_2)$ and Ta_2N_8. It also engages into a discussion which polymorphs of Ta_3N_5 likely had been synthesized in recent experiments. The work not only provides the minimum Gibbs energy structures, but also indicates Gibbs energy difference between Ta–N phases in pressure–temperature space. Such an examination locates optimum conditions that display maximum driving force for the synthesis of Ta–N compounds.

Computing the Tantalum–Nitrogen Phase Diagram at High Pressure and High Temperature

Hanof Alkhaldi and Peter Kroll*

Department of Chemistry and Biochemistry, The University of Texas at Arlington, 700 Planetarium Place, Arlington, Texas 76019, United States.

* Corresponding authors: pkroll@uta.edu

Abstract:

We investigate the pressure-temperature phase diagram of the tantalum–nitrogen system through a combination of density functional theory computations and thermodynamic calculations. Accounting for the chemical potential of nitrogen at high pressure and high temperature we obtain a Gibbs energy surface for every Ta-N phase in pressure-temperature space. Combining the data yields a coherent stability map that identifies the one most favorable Ta-N structure at given *p,T* conditions in the presence of excess nitrogen. Slices through the phase diagram at constant pressure or constant temperature examine the manifold of competing structures and locate optimum conditions with maximum driving force for successful syntheses. We rationalize high pressure experiments that synthesized new Ta–N polymorphs and predict temperature and pressure conditions necessary to synthesize $Ta_2N_2(N_2)$ and Ta_2N_8.

Introduction:

Progress in experimental high pressure/high temperature (HPHT) techniques over the last two decades yielded many new transition metal nitrogen (TM-N) compounds.[1] These include nitrides,[2] pernitrides,[3-4] mixed nitride-pernitrides,[5], compounds comprising complex polyatomic nitrogen anions,[6] and compounds with extended anionic nitrogen chains [7] — just to provide few examples from a continuously growing list. There are two major experimental pathways towards novel TM-N compounds at HPHT. One combines reactants, elements or pre-existing TM-N compounds, with an excess of nitrogen loaded in a diamond anvil cells (DAC) and applies Laser heating.[8-10] The other approach starts with solid-state compounds, for instance a low-pressure polymorph or a nitrogen-rich single-source precursor, potentially in combination with a nitrogen-rich reactant. This approach can be applied either in a DAC or in a large-volume press, e.g. a multi-anvil apparatus.[5] After the initial compression temperature is raised to usually 1500 K and higher to initiate reactions between reactants and nitrogen, or to induce phase transformations and decompositions. Though it is thinkable that stronger "kinetic control" may be possible at lower temperatures, such methods are still in their nascent stage.

Experimental studies have been motivated or examined by computational efforts, and synergy between different approaches drives new explorations. Advances in computer resources and suitable algorithms and programs [Ab initio random structure searching (AIRSS) [11], Universal Structure Predictor: Evolutionary Xtallography (USPEX) [12], XTALOPT [13], Crystal Structure Prediction via Particle Swarm Optimization (CALYPSO) [14]] make high-throughput calculations feasible to search for structures, and it appears that far more new TM-N structures have been envisioned than have been realized in experiments. With nitrogen as one reactant during synthesis fidelity of computational predictions depend on how well the chemical potential of nitrogen is assessed at high temperature and high pressure.[15-17] We recently provided intelligible data for the chemical

potential change of molecular nitrogen relative to its enthalpy at temperature and pressure conditions.[18] Here we apply the combination of thermochemical data with first-principles calculations to explore the pressure–temperature phase diagram of tantalum-nitrogen.

Tantalum–nitrogen compounds attained in experiments include crystalline structures of Ta_2N, TaN, Ta_5N_6, Ta_4N_5, Ta_2N_3, and Ta_3N_5.[1] Much computational work has been devoted to identify additional Ta-N structures that can be attained in high-pressure experiments.[19-23] Our early assessment of the pressure-temperature phase diagram of nitrogen-rich tantalum nitride addressed a phase boundary between TaN and Ta_3N_5 at high temperature and high pressure.[16] Motivated by this work three experimental endeavors were reported. Zerr et al. used crystalline Ta_3N_5 as starting material in a multi-anvil apparatus (large-volume press).[24] At both 11 GPa and 1773 K and at 20 GPa and 1973 K they obtained η-Ta_2N_3 with marginal contamination with oxygen. Friedrich et al. performed experiments in a Laser-heated DAC starting with tantalum embedded in excess nitrogen.[25] They synthesized η-Ta_2N_3 in several experiments between 9 and 27 GPa and temperatures estimated to be between 1600 and 2000 K. Salamat et al. loaded a diamond-anvil cell (DAC) with an amorphous polymeric N-rich Ta-N precursor, which at ambient pressure could also be crystallized to yield the ambient pressure modification Ta_3N_5-I.[26] After increasing pressure to 20 GPa and Laser-heating at 1500-2000 K they obtained a phase assemblage which was analyzed to consist of Ta_3N_5–II and the U_3Se_5–type of Ta_3N_5 together with small amounts of η-Ta_2N_3 and ε-N_2.

In this contribution, we will first outline the computational approach and then present computed pressure–temperature phase diagrams for the tantalum nitrogen system that identify thermodynamically stable phases and their respective stability field. We then provide slices through the phase diagram at constant pressure and at constant temperature, respectively, that help experimentalists to locate conditions of maximum

driving force for successful syntheses. We then contrast convex-hull data based on formation enthalpy and on formation Gibbs energy, and close with a discussion.

Computational method:

Calculations of total energy and volume were done within density functional theory (DFT) as implemented in Vienna ab initio simulation package (VASP)[27-30]. We used pseudopotentials based on the projector-augmented-wave (PAW)[31-32] method together with the strongly constrained and appropriately normed (SCAN) semilocal density functional[33]. Brillouin zone integration happened for each structure through appropriate k-point meshes with grid sizes smaller than 0.03 $Å^{-1}$. All reported results rely on a plane wave cut-off energy of 500 eV, and forces were converged to better than 1 meV/Å, yielding energy and enthalpy differences between structures converged to better than 1 meV per atom.

For structural explorations we first computed the wealth of previously reported structures in the Ta–N system.[19-23] We then augmented the data base by structures attained via an evolutionary algorithm (USPEX[12]) as well as through random structure search (AIRSS[11]). Searches were performed at 40, 80, 120, and 160 GPa (and T=0K) with up to 20 and more atoms in a simulation cell. We also added models originally received for different transition metal nitride compounds to our search.[34-35] Overall, two previously unreported polymorphs (Ta_3N_5-III and TaN_2-II, described below) emerged from this approach.

To acquire enthalpy–pressure (H-p) data we proceed as described previously:[36] for a given structure we optimize its structural parameters at a given volume. We then vary volume systematically and for each new volume we optimize the structure and compute its energy. The resulting E–V data yields pressure p by numerical differentiation, $p = -\partial E/\partial V$, and we compute enthalpy by $H = E + pV$. For solid-state reactions, reaction

Gibbs energies $\Delta G = \Delta H - T \cdot \Delta S$ are well approximated by reaction enthalpies ΔH, because entropy contributions to ΔG are usually small in comparison to changes of ΔH within a few GPa. A similar argument is made in light of a possible temperature dependency of enthalpies: heat capacities of solid reactants and products at high temperature do not differ to an extent that exceeds changes of ΔH within a few GPa.

Once a gaseous or fluid component participates in the reaction, however, the impact of temperature is important and will often determine the outcome of an experiment. Therefore, in reactions involving nitrogen, its chemical potential μ (Gibbs molar energy) and its increment $\Delta\mu$ relative to molar enthalpy must be taken in consideration at any temperature and pressure. In previous works, we specified approaches to quantify $\Delta\mu$ at high temperatures and high-pressures[16]. Besides perfect gas behavior, we provided a moderate and a more progressive extrapolation for the fugacity of nitrogen under these conditions. In Table 1, 2, and 3 we summarize results for the chemical potential increment $\Delta\mu(T, p_{N_2})$ of nitrogen.[18] Note that the data at 0 GPa corresponds to NIST tabulated data,[37] with only small variations for the two extrapolations due to their particular functional form. Detailed discussions of the approach and applications to various systems can be found in references [16] and [18].

Table 1: $\Delta\mu(T, p_{N_2})$ (in eV/atom) of nitrogen, treating nitrogen as perfect gas, $\gamma = 1$ ($\ln \gamma = 0$).

$\Delta\mu(T, p_{N_2})$	0 GPa	20 GPa	40 GPa	60 GPa	80 GPa	100 GPa	120 GPa	140 GPa
1500 K	-1.23	-0.89	-0.85	-0.82	-0.80	-0.79	-0.78	-0.77
2000 K	-1.72	-1.27	-1.21	-1.18	-1.15	-1.13	-1.12	-1.10
2500 K	-2.24	-1.67	-1.60	-1.55	-1.52	-1.50	-1.48	-1.46
3000 K	-2.77	-2.09	-2.00	-1.95	-1.91	-1.88	-1.86	-1.84

Table 2: $\Delta\mu(T, p_{N_2})$ (in eV/atom) of nitrogen within the moderate extrapolation.

$\Delta\mu(T, p_{N_2})$	0 GPa	20 GPa	40 GPa	60 GPa	80 GPa	100 GPa	120 GPa	140 GPa
1500 K	-1.21	-0.21	-0.16	-0.13	-0.11	-0.10	-0.08	-0.07
2000 K	-1.71	-0.61	-0.54	-0.51	-0.48	-0.46	-0.45	-0.44
2500 K	-2.22	-1.02	-0.94	-0.90	-0.87	-0.84	-0.82	-0.81
3000 K	-2.76	-1.45	-1.36	-1.31	-1.27	-1.24	-1.22	-1.20

Table 3: $\Delta\mu(T, p_{N_2})$ (in eV/atom) of nitrogen within the progressive extrapolation.

$\Delta\mu(T, p_{N_2})$	0 GPa	20 GPa	40 GPa	60 GPa	80 GPa	100 GPa	120 GPa	140 GPa
1500 K	-1.21	0.09	0.42	0.62	0.76	0.87	0.96	1.04
2000 K	-1.71	-0.29	0.05	0.26	0.41	0.53	0.63	0.71
2500 K	-2.22	-0.69	-0.33	-0.12	0.04	0.16	0.26	0.35
3000 K	-2.76	-1.11	-0.74	-0.51	-0.35	-0.22	-0.12	-0.03

Using computed enthalpies of all tantalum-nitrogen compounds, including tantalum and molecular nitrogen (ε-N_2), together with the chemical potential increment $\Delta\mu(T, p_{N_2})$ of nitrogen we can now assess Gibbs energy for each system, locate phase boundaries ($\Delta G=0$), and identify the thermodynamically most stable phase with its structure in the temperature-pressure phase diagram. Within this approach, "thermodynamic stability" refers to a system with excess nitrogen and with pressure equal to the partial pressure of nitrogen. Temperature-pressure conditions we explore are typically realized in DAC-experiments using nitrogen as pressure medium together with Laser heating. To display phase diagrams, we chose the temperature 1000 to 4000 K and the pressure range 0 to 140 GPa. Throughout, the source for excess nitrogen (our reference) is molecular nitrogen (ε-N_2). It is known that polymeric nitrogen forms at 110 GPa and 2000K.[10] Thus, going beyond these pressure and temperature conditions neglects a potential transformation into the extended form of nitrogen. A computational assessment of the phase boundaries between molecular and polymeric nitrogen has recently been given elsewhere.[18]

Results:

Combining first-principles computations with thermodynamic calculations we compute the pressure–temperature (p,T) phase diagram for the tantalum–nitrogen system. Three diagrams resulting from using the three different approximations for the chemical potential of nitrogen are shown in Figure 1. Each diagram displays the thermodynamically most stable Ta-N phase at given p,T-conditions in the presence of excess nitrogen.

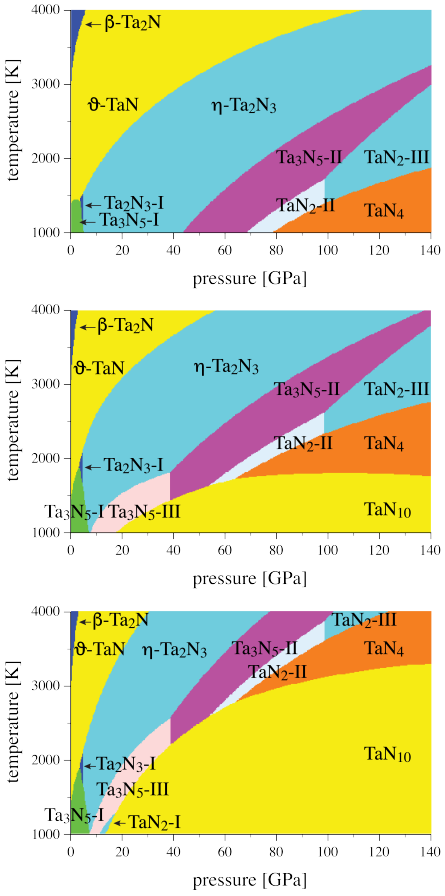

Figure 1: Tantalum-nitrogen pressure-temperature phase diagrams computed by combining of first principles (SCAN functional) and thermodynamic calculations. The pressure axes refer to partial pressure of nitrogen ($p(N_2)$). For the fugacity of nitrogen we use (top) the perfect gas approximation, (middle) the moderate, and (bottom) the progressive extrapolation formula. Structures of the individual phases are explained in the text.

At low pressure and low temperature the computed Ta-N phase diagrams display the structure of Ta_3N_5-I, the lowest energy orthorhombic polymorph of Ta_3N_5 with space group symmetry *Cmcm* (no. 62).[38] At higher temperature hexagonal ϑ-TaN (*P*-6*m*2 (187)) emerges, and above 3000K we find β-Ta_2N (*P*31*m* (157)). Within the SCAN functional we compute the rival mononitride ε-TaN with a slightly higher energy at zero pressure than ϑ-TaN. Since the latter has the more a favorable pressure behavior, it is the only TaN structure stable in the phase diagram.

A significant part of the phase diagram is then occupied by η-Ta_2N_3, the orthorhombic U_2S_3-type structure (*Pnma* (62)).[24] Interestingly, our calculations yield a small stability range of tetragonal Ta_2N_3 (*P*-4*m*2 (115) below 5.8 GPa as well, consistent in all approximations for the chemical potential of nitrogen. This phase was proposed to precede η-Ta_2N_3 at lower pressures.[19]

Increasing the pressure further yields two more structures of Ta_3N_5. Above 38 GPa the previously predicted U_3Te_5-type of Ta_3N_5–II (*Pnma* (62)) will appear.[16] Yet another orthorhombic structure, Ta_3N_5–III (*Pmmn* (59)), is intermediate between the ambient pressure modification Ta_3N_5–I and the high-pressure modification Ta_3N_5–II. Ta_3N_5–III appears above 1000 K only when using the moderate or progressive extrapolation. Since Ta_3N_5–III borders to η-Ta_2N_3 at higher temperatures, temperature has significant impact on a potential synthesis of Ta_3N_5–III, as will be addressed in the discussion below.

At even higher pressures we observe two polymorphs with composition TaN_2. Monoclinic (*P*2_1/*c* (14)) TaN_2–II followed at 98 GPa by orthorhombic (*Cmca* (64)) TaN_2–III. Our labels (II and III) have been chosen to allow for a low-pressure monoclinic polymorph TaN_2–I (*C*2/*m* (12)), which occurs only in the phase diagram computed using the progressive extrapolation formula for the chemical potential change of nitrogen. Polymorphs I and III have been proposed previously for TaN_2 and NbN_2.[23, 35] All three

TaN_2 structures are mixed nitride-per-nitrides, TaN_2 == $Ta_2N_2(N_2)$. Two more phases with high nitrogen content emerge at high pressures. Monoclinic TaN_4 ($P2_1/c$ (14)) displays a finite chain of nitrogen atoms forming a complex N_8^{10-}-anion, hence TaN_4 == $Ta_2(N_8)$. This structure has been proposed previously as well.[23, 35] Finally, we include orthorhombic TaN_{10} (*Immm* (71)) that displays infinite chains of nitrogen together with enclosed N_2 molecules. This structure has been predicted for HfN_{10} already.[39]

Among the structures that do not have a stability field in the computed phase diagram are the nitrides ε-TaN, Ta_5N_6, Ta_4N_5, Ta_3N_4, and TaN_3. This is in part due to the SCAN functional chosen in our work, but also to the conditions stated: in the presence of excess nitrogen below 140 GPa and temperatures above 1000 K these phases are not thermodynamically stable.

Phase diagrams as displayed in Figure 1 are essential for materials synthesis and for understanding phase relations. We need to keep in mind, however, that they display only the minimum Gibbs energy structure at a given *p,T*-condition. The diagrams do not show – for instance – competitive structures, some of which may have a kinetic advantage during synthesis. It is also quite difficult to provide error bars showing uncertainties in phase boundaries. These can be large in cases where the relative slopes of the intersecting Gibbs energy landscapes are shallow rather than steep. To provide more insight into the phase diagram, and ultimately to provide support for experimentalists, we display relative Gibb's energy versus temperature data (ΔG-T) and relative Gibb's energy versus pressure data (ΔG-p) for tantalum-nitrogen phases. We will restrict this discussion to the moderate extrapolation for the chemical potential of nitrogen. Our recent comparison of experimental and computed data in the titanium-nitrogen system and indicates that its outcomes are closest to experimental observations.[18]

In Laser-heated DAC experiments targeting synthesis of new nitrides the reactant is typically embedded in nitrogen as pressure medium. Thereafter the pressure is increased to a desired level, and then Laser-heating is applied to increase temperature. We have this experimental procedure in mind for Δ*G*-*T* diagrams at 40 and 80 GPa shown in Figure 2. These are "slices" through the phase diagram of Ta-N phases in the presence of excess nitrogen at constant pressure. Each line represents the Gibbs energy of a system comprised of a structure with given composition plus appropriate amounts of nitrogen relative to the Gibbs energy of Ta_3N_5-II. Assuming equilibrium to be established, the system with lowest Gibbs energy (here Δ*G*) will form at the respective temperature. Phase boundaries in the phase diagram shown in Figure 1 (middle), therefore, will align with line crossings in the Δ*G*-*T* graphs shown in Figure 2. At 40 GPa we have the sequence: $TaN_{10} \xrightarrow{1450\,K} Ta_3N_5\text{–II} \xrightarrow{1850\,K} \eta\text{-}Ta_2N_3 \xrightarrow{3650\,K} \vartheta\text{-TaN}$; at 80 GPa we compute $TaN_{10} \xrightarrow{1800\,K} TaN_4 \xrightarrow{2000\,K} TaN_2\text{–II} \xrightarrow{2250\,K} Ta_3N_5\text{–III} \xrightarrow{2950\,K} \eta\text{-}Ta_2N_3$. The data is easily used to quantify the driving force (ΔG) for a conversion and to locate "optimum" conditions for a synthesis, where ΔG is maximized. For instance, at 80 GPa the Ta_3N_5-II structure will be favorable between 2250 and 2950 K. Its thermodynamic stability is optimal at a temperature of 2500 K, favored by about 0.18 eV per Ta_3N_5 over its closest competitors TaN_2-I and η-Ta_2N_3. In addition, the graphs allow fair estimates about impacts of structural defects or systematic errors in the computational approach on reaction outcomes.

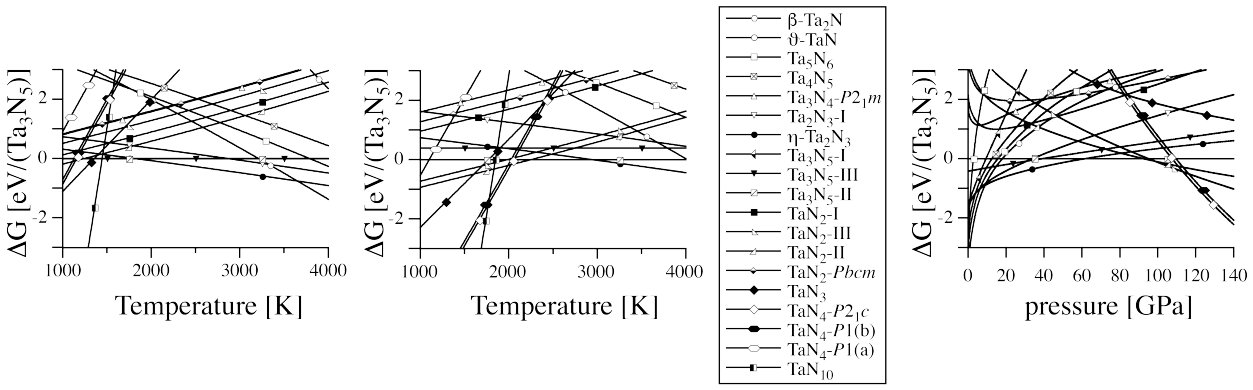

Figure 2: (left side of legend) Relative Gibbs energy versus temperature, Δ*G*-*T*, of Ta-N phases in excess nitrogen at 40 GPa and 80 GPa, respectively. (right side of legend) Relative Gibbs energy versus pressure, Δ*G*-*p*, of Ta-N phases in excess nitrogen at 2500 K. Symbols in the respective diagrams refer to structures listed in the boxed legend. Note that in each diagram energy refers to an overall composition Ta_3N_5. For all phases, thus, a proper amount of molecular nitrogen is added (or subtracted). E.g. $1½ \cdot Ta_2N_3 + ¼ \cdot N_2 \rightarrow Ta_3N_5$.

In a similar way, we show relative Gibbs energies at constant temperature as a function of pressure, Δ*G*-*p*, for tantalum-nitrogen phases. For a temperature of 2500 K this is shown in in Figure 2 on the right side. We find the sequence $\vartheta\text{-TaN} \xrightarrow{9\ \text{GPa}} \eta\text{-}Ta_2N_3 \xrightarrow{61\ \text{GPa}} Ta_3N_5\text{–II} \xrightarrow{93\ \text{GPa}} TaN_2\text{-II} \xrightarrow{98\ \text{GPa}} TaN_2\text{-III} \xrightarrow{116\ \text{GPa}} TaN_4$. Once again, the data can be used to identify best conditions for synthesizing a particular structure. While the thermodynamic stability of Ta_3N_5-II at 2500 K extends from 61 to 93 GPa, the largest ΔG of about 0.18 eV per Ta_3N_5 relative to competitors (TaN_2-I and η-Ta_2N_3) is found at 81 GPa.

A different concept invoked for discussing thermodynamic stability of compounds is that of a "convex hull". A convex hull is a set of phases, all which have positive reaction energies for a decomposition into any combination of neighboring phases. It is founded on formation energies of compounds and can be worked out from experimental as well as computational data. Convex hulls are frequently used in chemistry to display thermodynamic stability even in broader context, e.g. Frost-Ebsworth diagrams in

electrochemistry. In high-pressure science, however, these are typically composition-formation enthalpy convex-hulls constructed from results obtained at zero K. Therefore, they address relative stabilities of compounds under constant composition, but have only limited applicability in predicting thermodynamic stable phases in the presence of excess nitrogen at elevated temperature. In other words, they predict the outcome of a solid-state reaction (e.g. $TaN + Ta_3N_5 \rightarrow 2\ Ta_2N_3$), but cannot address simultaneous competing reactions with nitrogen (e.g. $2\ Ta_2N_3 \rightarrow 4\ TaN + N_2$ or $Ta_3N_5 \rightarrow 3\ TaN + N_2$).

We show convex hulls based on enthalpy and based on Gibbs energy at 2500 K for different pressures in Figure 3. For the latter approach, we augment the enthalpy of nitrogen by the chemical potential change according to the moderate extrapolation for the fugacity of nitrogen as given in Table 2. Note that we use the same data as in Figure 1 and Figure 2, but only present it in different ways. All convex hulls refer to the formation from the elements, $n{\cdot}Ta + m{\cdot}\frac{1}{2}N_2 \rightarrow Ta_nN_m$. The most noticeable difference between the diagrams based on enthalpy and on Gibbs energy is that nitrogen-rich phases appear on the latter only at very high pressure and are noticeable absent at low pressures. This is simply a consequence of molecular nitrogen having significantly lower chemical potential at elevated temperatures. Thus, Ta_3N_4 and Ta_2N_3 appear on the enthalpy-based convex hull at 0 GPa, while they both do not appear in the corresponding diagram based on Gibbs energy at 2500 K. Another example is TaN_{10}, which appears on the enthalpy-based convex hull at 40 GPa. However, this phase does not appear at 2500 K even at 120 GPa on the convex hull based on Gibbs energy. A convex hull based on Gibbs energy has yet another helpful characteristic: the most nitrogen-rich phase appearing on it is also the thermodynamically most stable one at the given conditions in the presence of excess nitrogen. Hence, it correctly predicts the outcome of DAC experiments at the applied temperature and pressure conditions, if nitrogen is used as reactant and pressure medium.

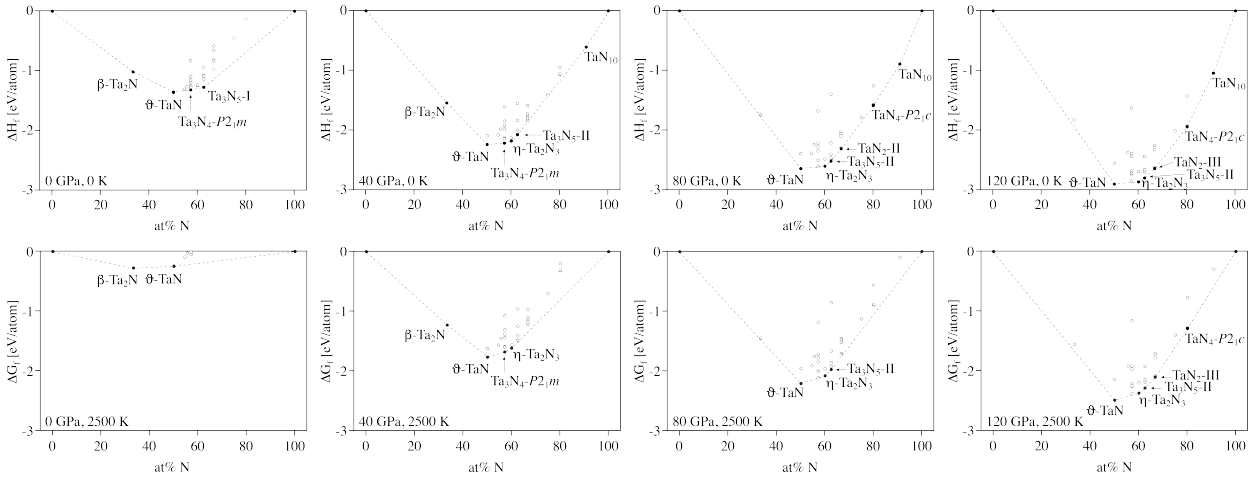

Figure 3: Convex hulls for the Ta-N system at 0, 40, 80, and 120 GPa. The top row refers to formation enthalpy (ΔH, in eV/atom). The bottom row refers to formation Gibbs energy (ΔG, in eV/atom) at 2500 K applying the moderate extrapolation given in Table 2. Phases stable against decomposition into any of its neighboring phases are indicated by filled black dots as well as by their structure name (see also legend in Figure 2). For the various compositions nitrogen contents are given (in at-%): Ta (0), Ta_2N (33), TaN (50), Ta_5N_6 (55), Ta_4N_5 (56), Ta_3N_4 (57), Ta_2N_3 (60), Ta_3N_5 (63), TaN_2 (67), TaN_3 (75), TaN_4 (80), TaN_{10} (91), N_2 (100).

Discussion:

Our assessment of the tantalum-nitrogen phase diagram at high-temperature and high-pressure targets chemical synthesis of new compounds in state-of-the-art laser-heated diamond anvil experiments that use nitrogen as reactant and as pressure medium. The approach is a practical guide that augments quantum-chemical calculations with thermochemical data. For every Ta-N phase system it yields a Gibbs energy surface in pressure-temperature space. The tantalum-nitrogen *p,T*-phase diagram then identifies for every *p,T*-condition the one thermodynamically most stable phase and its structure in the presence of excess nitrogen (see Figure 1). This information in itself is most helpful, but applies to ideal conditions (homogeneous isotropic system and infinite time to establish equilibrium). In a real experiment, conditions vary at different location of the reaction zone and kinetics do play a significant role. Hence, the manifold of alternative structures,

some of which– under peculiar circumstances – may form as well, is of interest as well. This manifold is explored by appropriate "slices" into the phase diagram made at constant pressure or at constant temperature (see Figure 2). Gibbs energy differences may be interpreted similar to a statistical weight, indicating the likelihood of a structure to emerge. Using the "slices" then also offers the opportunity to locate optimum experimental conditions to realize a particular structure in its stability field.

Calculations of a "convex hull" relying on relative enthalpies can serve as a guideline for experimentalists. However, such measures refer to 0 K only and have limited fidelity predicting synthesis of compounds with high nitrogen content given the substantial decrease of the chemical potential of nitrogen by –1.2 to –2.8 eV (per N atom) for 1000 to 3000 K at 0 GPa. Even at pressures of 40 or 80 GPa the chemical potential of nitrogen is lowered by –0.4 to –1.2 eV (per N atom) at 2000 to 3000 K, respectively, relative to its enthalpy. Computing "convex hulls" at different temperatures and pressures by augmenting enthalpy of nitrogen with chemical potential change resolves this issue and enhances fidelity in predictions. "Convex hulls" based on Gibbs energy have also the characteristic to readily identify the thermodynamically most stable structure at the given pressure and temperature in the presence of excess nitrogen.

In this study, we presented data only for results using the SCAN functional. Calculations using the generalized-gradient-approximation (GGA) in form of the PBE functional[40] yield similar but not identical results. Enthalpy differences vary by up to 5 meV per atom, and have the impact that ε-TaN and Ta_5N_6 do not appear in the convex hull, in contrast to previous calculations.[22, 23] For comparison with experimental data, we stress that in all calculations we consider perfect ideal crystals only, while the nature of defects in a solid and its surface chemistry have additional impact on Gibbs energy. Additionally, pathways and kinetics of decomposition or formation reactions or uneven

reaction conditions may yield transient meta-stable intermediates or by-products in an experiment.[26, 41]

A critical ingredient for our calculations is the assessment of the chemical potential of nitrogen at high temperature and high pressure.[18] Detailed experimental studies are needed and will further help to refine the analytical model. Previous high-pressure experiments in the Ta-N system by Zerr et al. and Friedrich et al. operated with pressures between 15 and 27 GPa and temperatures around 2000 K.[24-25] This is well in the stability range of η-Ta_2N_3 when using either the perfect gas and moderate extrapolation approach for the chemical potential change of nitrogen. The experiments, thus, render the progressive extrapolation less likely in this pressure range. A special consideration is needed for the experiments by Salamat et al..[26] Loading a diamond-anvil cell (DAC) with an amorphous polymeric N-rich Ta-N precursor, which at ambient pressure could also be crystallized to yield the ambient pressure modification Ta_3N_5-I, they increased pressure to 20 GPa and performed Laser-heating for several minutes at 1500-2000K. Subsequence XRD characterization at ambient temperature indicated a pressure of 22 GPa in the cell. The powder pattern of the product was analyzed to contain a phase assemblage of Ta_3N_5–II and the U_3Se_5–type of Ta_3N_5 together with small amounts of η-Ta_2N_3 and ε-N_2. We reason, based on the computed thermochemical data, that the second major component in the product besides Ta_3N_5–II is Ta_3N_5–III rather than the U_3Se_5–type. Indeed, at 22 GPa the orthorhombic (Pmmn) structure of Ta_3N_5–III is -0.15 eV/Ta_3N_5 more favorable than Ta_3N_5-II, while the U_3Se_5-type is 0.42 eV/Ta_3N_5 less favorable than Ta_3N_5–II. The two structures Ta_3N_5–III and U_3Se_5-type also have similar lattice parameters at 22 GPa (one parameter of Ta_3N_5–III is just half of one of the U_3Se_5-type). Note that Salamat et al. were not aware of a Ta_3N_5–III structure at the time of their analysis. The broad lines of their experimental powder pattern, however, makes a clear phase determination difficult, as had been pointed out be the authors as well. The simultaneous appearance of η-Ta_2N_3 and

ε-N_2 is further rationalized by thermochemical data. Based on enthalpy, they system 3/2 · η-Ta_2N_3 + ¼ · ε-N_2 is favored by -0.04 eV/Ta_3N_5 relative to Ta_3N_5-II, but still less favorable than Ta_3N_5–III by +0.11 eV/Ta_3N_5. A possible formation of tetragonal Ta_2N_3 and ε-N_2 is penalized by +0.16 eV/Ta_3N_5 relative to Ta_3N_5-II. At 1500 to 2000 K an assemblage of η-Ta_2N_3 and ε-N_2 drops by -0.1 to -0.3 eV due to the chemical potential change of nitrogen within the moderate extrapolation data. Hence, the experimental conditions chosen by Salamat et al. are close to the phase boundary between Ta_3N_5–III and η-Ta_2N_3, which is also reflected in Figure 1 (middle). Clever choice of a N-rich precursor and slow kinetics at lower temperatures in comparison to experiments carried out by Friedrich et al. may further helped to attain Ta_3N_5 polymorphs. Thus, the experiments of Salamat et al. give credibility to the moderate extrapolation data for the chemical potential change of nitrogen, but do not fully exclude a more perfect gas behavior.

To synthesize pure Ta_3N_5-II within its large stability field in the *p,T*-phase diagram experimentalists can choose optimum conditions of 2500 K and 80 GPa, assuming the moderate extrapolation for nitrogen fugacity to hold. Such pressures and temperatures are not uncommon and have been applied in recent experiments.[5-7] Besides, more fascinating Ta-N polymorphs are attainable at even higher pressures, the mixed nitride-per-nitrides of TaN_2 (= $Ta_2N_2(N_2)$) between 93 and 116 GPa, and TaN_4 with its polyatomic N_8^{10-}-anion at pressures beyond.

Conclusion:

We provide a practical and comprehensive approach to work out pressure-temperature phase diagrams. It combines density functional theory computations with thermodynamic calculations and includes proposed data for the chemical potential of nitrogen at high pressure and high temperature. Applying the method to the tantalum–nitrogen system we

receive a phase diagram for pressures up to 140 GPa and temperatures between 1000 and 4000 K. The phase diagram identifies stability fields of Ta-N structures in the presence of excess nitrogen, therefore, under conditions typical to state-of-the-art DAC experiments. Optimum conditions with maximum driving force for successful syntheses are found by slicing the phase diagram at constant pressure or at constant temperature. Our results allow us not only to account for the outcome of recent high pressure experiments that synthesized new Ta–N polymorphs, but also to predict *p*,*T*–conditions necessary to synthesize proposed $Ta_2N_2(N_2)$ and Ta_2N_8. Overall, much computed data obtained in recent years can be brought to more use for experimentalists with this method.

Acknowledgement

This work was supported by the National Science Foundation (NSF) through award OISE-1743701. The computational work was made possible through generous grants by the Texas Advance Computing Center in Austin, TACC, Texas, and by the High Performance Computing facilities at UTA. H.A. acknowledges support by the government of Saudi Arabia.

References:

1. Salamat, A.; Hector, A. L.; Kroll, P.; McMillan, P. F., Nitrogen-Rich Transition Metal Nitrides. *Coordination Chemistry Reviews* **2013**, *257*, 2063-2072.
2. Zerr, A.; Miehe, G.; Riedel, R., Synthesis of Cubic Zirconium and Hafnium Nitride Having Th_3P_4 Structure. *Nature Materials* **2003**, *2*, 185-189.
3. Crowhurst, J. C.; Goncharov, A. F.; Sadigh, B.; Evans, C. L.; Morrall, P. G.; Ferreira, J. L.; Nelson, A. J., Synthesis and Characterization of the Nitrides of Platinum and Iridium. *Science* **2006**, *311*, 1275-1278.
4. Niwa, K.; Fukui, R.; Terabe, T.; Kawada, T.; Kato, D.; Sasaki, T.; Soda, K.; Hasegawa, M., High-Pressure Synthesis and Phase Stability of Nickel Pernitride. *European Journal of Inorganic Chemistry* **2019**, *33*, 3753-3757.
5. Bykov, M., et al., High-Pressure Synthesis of Ultraincompressible Hard Rhenium Nitride Pernitride $Re_2(N_2)(N)_2$ Stable at Ambient Conditions. *Nat. Commun.* **2019**, *10*, 8.
6. Bykov, M.; Khandarkhaeva, S.; Fedotenko, T.; Sedmak, P.; Dubrovinskaia, N.; Dubrovinsky, L., Synthesis of FeN_4 at 180 GPa and Its Crystal Structure from a Submicron-Sized Grain. *Acta Crystallogr. Sect. E.-Crystallogr. Commun.* **2018**, *74*, 1392.
7. Bykov, M., et al., Fe-N System at High Pressure Reveals a Compound Featuring Polymeric Nitrogen Chains. *Nat. Commun.* **2018**, *9*.
8. Bassett, W. A., Diamond Anvil Cell, 50th Birthday. *High Pressure Research* **2009**, *29*, CP5-186.
9. Boehler, R., Laser Heating in the Diamond Cell: Techniques and Applications. *Hyperfine Interact.* **2000**, *128*, 307-321.
10. Eremets, M. I.; Gavriliuk, A. G.; Trojan, I. A.; Dzivenko, D. A.; Boehler, R., Single-Bonded Cubic Form of Nitrogen. *Nature Materials* **2004**, *3*, 558-563.
11. Pickard, C. J.; Needs, R. J., Ab Initio Random Structure Searching. *Journal of Physics-Condensed Matter* **2011**, *23*, 23.
12. Oganov, A. R.; Ma, Y. M.; Lyakhov, A. O.; Valle, M.; Gatti, C., Evolutionary Crystal Structure Prediction as a Method for the Discovery of Minerals and Materials. In *Theoretical and Computational Methods in Mineral Physics: Geophysical Applications*, Wentzcovitch, R.; Stixrude, L., Eds. **2010**; Vol. 71, pp 271-298.
13. Lonie, D. C.; Zurek, E., Xtalopt: An Open-Source Evolutionary Algorithm for Crystal Structure Prediction. *Comput. Phys. Commun.* **2011**, *182*, 372-387.
14. Wang, Y. C.; Lv, J. A.; Zhu, L.; Ma, Y. M., Crystal Structure Prediction Via Particle-Swarm Optimization. *Physical Review B* **2010**, *82*, 8.
15. Kroll, P., Hafnium Nitride with Thorium Phosphide Structure: Physical Properties and an Assessment of the Hf-N, Zr-N, and Ti-N Phase Diagrams at High Pressures and Temperatures. *Physical Review Letters* **2003**, *90*.
16. Kroll, P.; Schröter, T.; Peters, M., Prediction of Novel Phases of Tantalum(V) Nitride and Tungsten(VI) Nitride That Can Be Synthesized under High Pressure and High Temperature. *Angew Chem Int Edit* **2005**, *44*, 4249-4254.
17. Sun, W. H.; Holder, A.; Orvananos, B.; Arca, E.; Zakutayev, A.; Lany, S.; Ceder, G., Thermodynamic Routes to Novel Metastable Nitrogen-Rich Nitrides. *Chem Mater* **2017**, *29*, 6936-6946.

18. Alkhaldi, H.; Kroll, P., Chemical Potential of Nitrogen at High Pressure and High Temperature: Application to Nitrogen and Nitrogen-Rich Phase Diagram Calculations. *Journal of Physical Chemistry C* **2019**, *123*, 7054-7060.
19. Jiang, C.; Lin, Z. J.; Zhao, Y. S., Thermodynamic and Mechanical Stabilities of Tantalum Nitride. *Physical Review Letters* **2009**, *103*.
20. Zhang, J. D.; Wang, H. F., First-Principles Calculations of Structural and Electronic Properties of Ta_2N_3 under High Pressures. *Physica B* **2013**, *428*, 89-93.
21. Li, D.; Tian, F. B.; Duan, D. F.; Bao, K.; Chu, B. H.; Sha, X. J.; Liu, B. B.; Cui, T., Mechanical and Metallic Properties of Tantalum Nitrides from First-Principles Calculations. *Rsc Advances* **2014**, *4*, 10133-10139.
22. Weinberger, C. R.; Yu, X. X.; Yu, H.; Thompson, G. B., Ab Initio Investigations of the Phase Stability in Group IVb and Vb Transition Metal Nitrides. *Computational Materials Science* **2017**, *138*, 333-345.
23. Xing, W. D.; Wei, Z. J.; Yu, R.; Meng, F. Y., Prediction of Stable High-Pressure Structures of Tantalum Nitride TaN_2. *J. Mater. Sci. Technol.* **2019**, *35*, 2297-2304.
24. Zerr, A., et al., High-Pressure Synthesis of Tantalum Nitride Having Orthorhombic U_2S_3 Type Structure. *Advanced Functional Materials* **2009**, *19*, 2282-2288.
25. Friedrich, A.; Winkler, B.; Bayarjargal, L.; Arellano, E. A. J.; Morgenroth, W.; Biehler, J.; Schroder, F.; Yan, J. Y.; Clark, S. M., In Situ Observation of the Reaction of Tantalum with Nitrogen in a Laser Heated Diamond Anvil Cell. *Journal of Alloys and Compounds* **2010**, *502*, 5-12.
26. Salamat, A.; Woodhead, K.; Shah, S. I. U.; Hector, A. L.; McMillan, P. F., Synthesis of U_3Se_5 and U_3Te_5 Type Polymorphs of Ta_3N_5 by Combining High Pressure-Temperature Pathways with a Chemical Precursor Approach. *Chemical Communications* **2014**, *50*, 10041-10044.
27. Hohenberg, P.; Kohn, W., Inhomogeneous Electron Gas. *Physical Review B* **1964**, *136*, B864-+.
28. Kresse, G., Ab-Initio Molecular-Dynamics for Liquid-Metals. *J Non-Cryst Solids* **1995**, *193*, 222-229.
29. Kresse, G.; Hafner, J., Ab-Initio Molecular-Dynamics Simulation of the Liquid-Metal Amorphous-Semiconductor Transition in Germanium. *Physical Review B* **1994**, *49*, 14251-14269.
30. Kresse, G.; Furthmüller, J., Efficiency of Ab-Initio Total Energy Calculations for Metals and Semiconductors Using a Plane-Wave Basis Set. *Computational Materials Science* **1996**, *6*, 15-50.
31. Blochl, P. E., Projector Augmented-Wave Method. *Physical Review B* **1994**, *50*, 17953-17979.
32. Kresse, G.; Joubert, D., From Ultrasoft Pseudopotentials to the Projector Augmented-Wave Method. *Physical Review B* **1999**, *59*, 1758-1775.
33. Sun, J. W.; Ruzsinszky, A.; Perdew, J. P., Strongly Constrained and Appropriately Normed Semilocal Density Functional. *Physical Review Letters* **2015**, *115*, 036402.
34. Kroll, P., Advances in Computation of Temperature-Pressure Phase Diagrams of High-Pressure Nitrides. *Key Eng Mat* **2009**, *403*, 77-80.

35. Zhao, Z. L.; Bao, K.; Tian, F. B.; Duan, D. F.; Liu, B. B.; Cui, T., Phase Diagram, Mechanical Properties, and Electronic Structure of Nb-N Compounds under Pressure. *Phys. Chem. Chem. Phys.* **2015**, *17*, 22837-22845.
36. Kroll, P., Pathways to Metastable Nitride Structures. *J. Solid State Chem.* **2003**, *176*, 530-537.
37. Jacobsen, R. T.; Stewart, R. B.; Jahangiri, M., Thermodynamic Properties of Nitrogen from the Freezing Line to 2000-K at Pressures to 1000-MPa. *J Phys Chem Ref Data* **1986**, *15*, 735-909.
38. Strähle, J., Die Kristallstruktur des Tantal(V)-Nitrids Ta3N5. *Zeitschrift für anorganische und allgemeine Chemie* **1973**, *402*, 47-57.
39. Zhang, J.; Oganov, A. R.; Li, X. F.; Niu, H. Y., Pressure-Stabilized Hafnium Nitrides and Their Properties. *Physical Review B* **2017**, *95*.
40. Perdew, J. P.; Burke, K.; Ernzerhof, M., Generalized Gradient Approximation Made Simple. *Physical Review Letters* **1996**, *77*, 3865-3868.
41. Bhadram, V. S.; Liu, H. Y.; Xu, E. S.; Li, T. S.; Prakapenka, V. B.; Hrubiak, R.; Lany, S.; Strobel, T. A., Semiconducting Cubic Titanium Nitride in the Th_3P_4 Structure. *Phy Rev Mater* **2018**, *2*.

CHAPTER 2: COMPUTING THE IRON–NITROGEN PHASE DIAGRAM AT HIGH PRESSURE AND HIGH TEMPERATURE

COMPUTING THE IRON–NITROGEN PHASE DIAGRAM AT HIGH PRESSURE AND HIGH TEMPERATURE

INTRODUCTORY REMARKS

While the previous work showcases pressure and temperature conditions relevant to synthesis of new high–pressure nitrogen–rich compounds in diamond-anvil-cell (DAC) experiments, the following article finds its strongest relevance in planetary science and it related to the earth's interior. Systematically the pressure–temperature phase diagram of the iron–nitrogen system is explored and phase boundaries outlined. Slice through the phase diagram – either at constant pressure or at constant temperature – are provided in order to compare Gibbs energy differences of various Fe–N compounds and to rationalize experimental findings – with implications to the inner core of our planet.

Computing the Iron–Nitrogen Phase Diagram

at High Pressure and High Temperature

Hanof Alkhaldi and Peter Kroll[a]

Department of Chemistry and Biochemistry, The University of Texas at Arlington, 700 Planetarium Place, Arlington, Texas 76019, United States.

* Corresponding authors: pkroll@uta.edu

Abstract:

Locating pressure and temperature conditions relevant to concurrent diamond-anvil-cell (DAC) experiments is imperative for the discovery of new high–pressure nitrogen-rich compounds. In this work we provide a pressure-temperature phase diagram of the iron–nitrogen system for pressures up to 200 GPa and temperatures up to 4000 K through a combination of Density Functional Theory computations and thermodynamic calculations. The work includes an assessment of the chemical potential of nitrogen and its change at high pressure and high temperature. We deliver stability fields of various Fe–N compounds in the presence of excess nitrogen. Our results are in agreement with recent synthesis of FeN_2 and FeN_4, and predict a hitherto unknown FeN_8 attainable at 100 GPa and 1500K.

Keywords:

High-pressure Iron-nitrogen compounds; phase diagram; chemical potential nitrogen

Introduction:

A variety of new nitrogen-rich compounds of main group elements and transition metals have been synthesized over the last two decades.[1-12] Advances in experimental techniques to attain high pressure/high temperature (HPHT) conditions facilitate this progress, in good parts driven and supported by computational studies.[1, 13-15] New transition metal nitrogen (TM-N) compounds include nitrides,[3] pernitrides,[16] mixed nitride-pernitrides, compounds comprising complex polyatomic nitrogen anions, and compounds with extended anionic nitrogen chains.[7]

The iron-nitrogen system is particularly relevant to industrial applications[17] as well as to planetary cores.[18-22] Binary Fe–N compounds synthesized at ambient pressure include crystalline structures of Fe_4N, Fe_3N, and Fe_2N.[23-25] Recently, more nitrogen–rich compounds Fe_3N_2, FeN, FeN_2, and FeN_4 have been synthesized at high pressure and high temperature.[7, 26-30] Much computational work has been devoted to investigate these and to identify further Fe-N polymorphs. This includes structures of Fe_4N, Fe_3N, Fe_4N_3, Fe_7N_3, Fe_2N, FeN, FeN_2, FeN_4, FeN_6 FeN_8, and FeN_{10}.[31-36] Computed data has been used to construct composition–formation enthalpy convex hulls of the Fe–N system for pressures up to 300 GPa, and based on those several phase transitions of nitrogen–rich Fe-N compounds have been proposed.[32, 33, 37] For instance, the most favorable structure of FeN at ambient pressure is a ZnS-type structure (sp.gr. *F4-3m* (216)), which transfers to a NiAs-type structure (sp.gr. *P63/mmc* (194)) at about 24 GPa. The NiAs-type of FeN exhibits remarkable magnetic properties even at high pressure.[38] At 79 GPa a MnP-type structure of FeN (sp.gr. *Pnma* (62)) then becomes preferred. A marcasite-type structure of FeN_2 (sp.gr. *Pnmm* (194)) was proposed to become accessible above 22 GPa, and a FeN_4 (sp.gr. *P-1* (2)) with unprecedented structure above 30 GPa.[32, 33, 37] Notably, both compounds FeN_2 and FeN_4 were subsequently

synthesized in high pressure experiments.[7, 28, 29] Other Fe-N polymorphs proposed to be attainable up to 300 GPa include Fe_3N_8, FeN_3, FeN_6, and FeN_8.[32, 33, 37]
The target of our contribution is to explore thermodynamic stability of Fe–N compounds at experimental conditions and, thus, to provide a useful guide for experimentalists. In a typical high pressure synthesis experiment iron is placed into a diamond anvil cell, which is then loaded with nitrogen.[7, 39] Excess nitrogen in the cell acts both as pressure transmitting medium as well as reactant. After compression to a desired pressure, the iron is heated by irradiation through a laser-heating system to overcome activation barriers and enable reactions with nitrogen at high pressures. To achieve our goal, we combine quantum-chemical and thermodynamic calculations to provide a pressure–temperature phase diagram of Fe–N under excess nitrogen. The phase diagram predicts synthesis conditions of thermodynamically stable Fe–N phases accessible through DAC experiments using nitrogen as pressure medium.

Computational method:

All calculations of total energy are performed within Density Functional Theory (DFT) as implemented in Vienna Ab-initio Simulation Package (VASP).[40-43] We use pseudopotentials based on the projector-augmented-wave (PAW) method.[44, 45] We apply strongly constrained and appropriately normed semilocal density functional (SCAN)[46]. With the goal to predict phase boundaries at temperatures well above 1000 K, we do not explicitly search for magnetic order. Hence, calculations are performed without spin-polarization. The Brillouin zone of each structure is sampled by k-point meshes with grid sizes smaller than 0.03 $Å^{-1}$. All calculations depend on well forces converged to better than 1 meV/Å with a plane wave cut-off energy of (500 eV) which yields energy and enthalpy differences between structures converged to better than 1 meV per atom.

We started our endeavor by computing Fe–N structures reported previously.[7, 26, 28, 29, 37, 47] We then used the Universal Structure Predictor Evolutionary Xtallography (USPEX)[48] code to identify known and to locate potential new polymorphs. For the structure searches by USPEX we start with variable composition searches at 80 GPa to identify potential compositions with high nitrogen content. Ensembles of 50 structures are followed for 20 generations. For each new generation, 40% of structures are taken by heredity, 20% randomly, 20% through lattice mutations, and 20% by atom mutation. This process is repeated with new seed structures 20 times. Promising compositions – identified by negative enthalpy of formation (from elements and/or from neighboring compositions) at least at some pressure – are followed in more detail with searches at constant composition. This includes compositions with high nitrogen content such as FeN_4, FeN_6 and FeN_8. We search crystal structures with at least 20 atoms in their primitive unit cell and perform (at least each 20 independent) searches at 40, 80, 120, and 160 GPa. Ensembles of 15-25 structures are evolved for up to 45 generations (50% heredity, 10% random, 20% lattice mutations, 20 atomic mutations). We augmented the structure data base by models obtained earlier for different transition metal nitride compounds.[49] The most nitrogen–rich composition we studied was FeN_{10}. It turns out that all structures encountered in this study have been reported before, with exception of a new polymorph of FeN_8.

Enthalpy-pressure data of every structure is acquired using standard techniques described earlier.[50] In brief: energy–volume data of each structure is converted to enthalpy-pressure data by numerical differentiation. For all reaction involving solid state structures the enthalpy of reaction ΔH is equated to reaction Gibbs energies ΔG, because entropy changes that contribute to ΔG are much smaller than changes of ΔH within a few GPa of pressure. For reaction involving nitrogen, we augment reaction Gibbs energies ΔG with chemical potential changes of nitrogen, $\Delta\mu(p,T)$, as outlined in previous

studies.[51, 52] Experimental data of $\Delta\mu$(p,T) for nitrogen is available for low pressures from the freezing point to 4000K.[53] The data is extrapolated to high pressure and high temperature using the "moderate extrapolation" for fugacity of nitrogen.[51] As result we obtain quantitative data of chemical potential for every phase system and can compare reaction Gibbs energies at high pressure and high temperature conditions. Note that the approach assumes the presence of an excess of nitrogen as reactant, hence it applies to a standard experiment in a diamond-anvil-cell (DAC) loaded with nitrogen. The approach has shown good agreement between experiment and calculations for several systems to at least 80 GPa[52, 54]. For instance, it provides a rational for the simultaneous appearance of Ti_3N_4 and TiN_2 within a temperature range between 1800 and 2400 K at 74 GPa.[52, 55, 56]

Results and Discussion:

The computed pressure–temperature (*p,T*) phase diagram for the Iron–Nitrogen system is shown in Figure 1. It is a result of combining first-principles computations of crystal structures with thermodynamic calculations addressing the chemical potential of nitrogen. We emphasize that the phase diagram as shown applies to an experiment carried out under the condition of excess nitrogen.

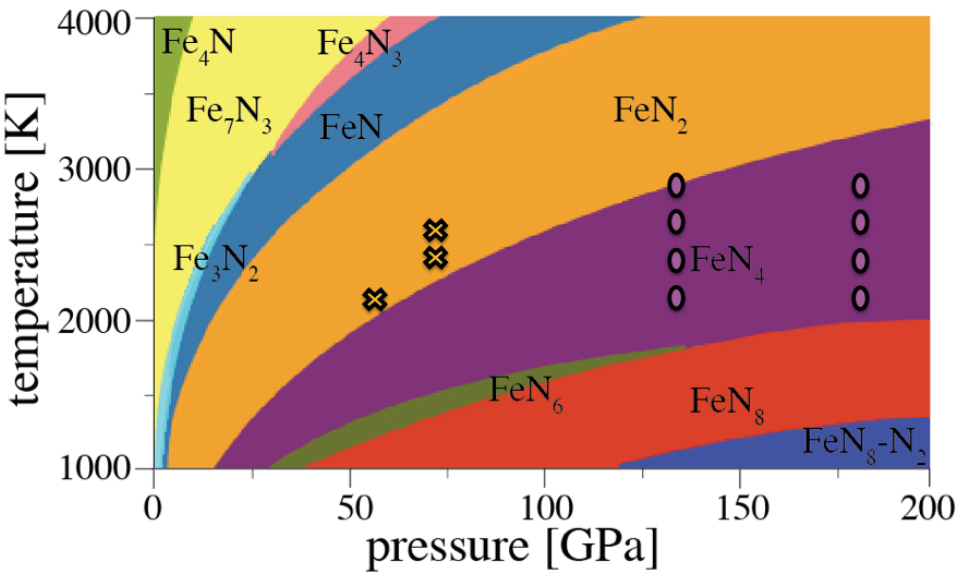

Figure 1: The iron-nitrogen pressure-temperature phase diagram computed by combining of first principles (SCAN functional) and thermodynamic calculations. Experimental conditions reported for the formation of FeN_2[7, 28] and of FeN_4[7, 29] are indicated by crosses and circles, respectively.

At low pressure the computed Fe-N phase diagrams displays perovskite-type γ'-Fe_4N, which is commonly observed at ambient conditions.[23] Increasing pressure yields Fe_7N_3, with a stability field ranging up to 25 and 50 GPa at 3000 and 4000 K, respectively. At such high temperatures magnetism is not expected to play a role, and, consequently, we obtain the orthorhombic structure (sp.gr. *Amm2* (38)) being preferred over ε-Fe_7N_3 in non-magnetic calculations. The thermodynamical stability of Fe_7N_3 then prevents appearance of orthorhombic ζ-Fe_2N. This Fe_2N phase was synthesized at 10 GPa at 1800 K using diamond anvil cell and laser heating.[30] The next phase we find to become thermodynamically stable in the presence of excess nitrogen, albeit with a very small stability range, is Fe_3N_2-II (sp.gr. *Fdd2* (43)[57]). This polymorph of Fe_3N_2 has not been observed in experiments. However, Fe_3N_2-I (sp.gr. *Pnma* (62)) was synthesized at 50 GPa and 1990 K.[7] We find that Fe_3N_2-I is a high-pressure phase of Fe_3N_2 and will follow Fe_3N_2-II as the most favorable Fe_3N_2 structure at 80 GPa. In our computed phase diagram Fe_3N_2-I does not appear, since at high pressures it is surpassed by phases with higher

nitrogen content, FeN, FeN_2, and FeN_4. We note that at temperatures above 3000 K and pressures between 30 and 70 GPa Fe_4N_3 (sp.gr. *Imm2* (44)) emerges.[35] The well-known FeN (sp.gr. *P63/mmc* (194); NiAs-type) follows next. This structure has emerged in various experiments at conditions ranging from 10 to 130 GPa and temperatures from 1300 to 2000 K.[7, 26, 27, 39] We compute its stability range to be smaller, for instance between 10 and 20 GPa at 2000 K. A large part of the phase diagram then is occupied by FeN_2 (sp.gr. *Pnmm* (194)) with marcasite-type structure. At 2000 K we compute it to be the thermodynamically most favorable Fe–N compound between 20 and 60 GPa. In experiments this phase was attained at 58.5 GPa and 2100 K,[7] but also at 72.5 GPa. Both these experimental conditions are located within the computed stability field for FeN_2. At 2000 K and above 60 GPa the only other structure appearing is FeN_4 (sp.gr. *P-1* (2)). This phase has been synthesized at more extreme conditions in experiments, 135 GPa and 2000 K,[7, 29] and 180 GPa and 2700 K.[7] We have indicated data of reported experimental conditions for the syntheses of FeN_2 and FeN_4 in Figure 1. At temperatures below 2000 K and high pressures we find several Fe–N compounds with high nitrogen content displaying infinite nitrogen chains. A small stability range is indicated for monoclinic FeN_6 (sp.gr. *C 2/m* (12)), a structure predicted earlier[37, 58]. At higher pressures FeN_8 (sp.gr. (*P-1* (2)[59])) emerges. This new structure bears similar features – an infinite N-chain and FeN_6–octahedrons – as the previously suggested modification of FeN_8.[37] However, the coordination environment of Fe is more regular, causing this structure to be lower in enthalpy for all pressures we computed. Finally, we include FeN_{10} (sp.gr. *Immm* (71)[60]), a structure that was first predicted for HfN_8-N_2 and then synthesized for ReN_8-N_{10} and WN_8-N_2.[49, 61].

Previous computational studies in the Fe-N system delivered thermochemical data that was conveniently displayed using the concept of a convex hull.[32, 33, 37] Note that a typical convex hull in high-pressure science data is based on composition-formation

enthalpy data obtained at zero K. Consequently, whenever such diagrams are used to infer "thermodynamic stability" of compounds, the impact of temperature or excess nitrogen is not included in considerations. Using the approach outlined above it is straight forward to attain convex hulls based on Gibbs energy, explicitly including temperature and presence of nitrogen. In Figure 2 we compare both types of convex hulls, one based on enthalpy and the other based on Gibbs energy at 2500 K. Evidently, the most significant difference between the two diagrams is that several nitrogen-rich Fe-N phases – in particular FeN_6, FeN_8, and FeN_{10} – are not thermodynamically stable at high pressure at 2500 K. In general, temperature shifts the appearance of a phase on the convex hull (indicating thermodynamic stability) towards higher pressure. This can be seen for FeN_4, which appears at 40 GPa on the enthalpy-based convex hull, while it requires more than 80 GPa to appear in the corresponding diagram based on Gibbs energy at 2500 K. A convex hull based on Gibbs energy, therefore, has more predictive power in identifying thermodynamically stable nitrogen-rich phases at the given conditions in the presence of excess nitrogen.

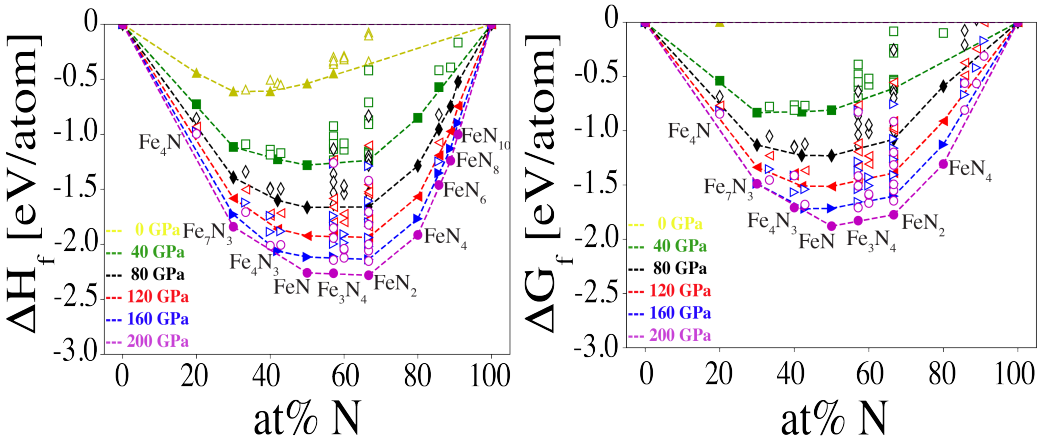

Figure 2: Convex hulls for the Fe-N system at 0, 40, 80, 120,160 and 200 GPa. The diagram on the left refers to formation enthalpy (ΔH, in eV/atom). On the right the diagram refers to formation Gibbs energy (ΔG, in eV/atom) at 2500 K. Phases stable against decomposition into any of its neighboring phases are indicated by filled symbol.

Phase diagrams as that shown in Figure 1 display phases with minimum Gibbs energy at a given *p,T*-condition. Unfortunately, they do not reveal competitive phases, nor do they provide error bars or uncertainties in phase boundaries. Such information, however, can be very helpful to rationalize experimental results. For instance, simultaneous appearance of Ti_3N_4 and TiN_2 in the same DAC experiment can be related to small differences in Gibbs energy between the two phases at 74 GPa and 2000 K.[52, 55, 56]. Therefore, we provide relative Gibbs energy versus temperature data (ΔG-T) and relative Gibbs energy versus pressure data (ΔG-p) for Iron-Nitrogen phases. Effectively, these are "slices" cut through the manifold of G(p,T) data of all structures at constant p or at constant T, respectively. ΔG-T data at constant p may be particularly helpful for experimentalists, since in many experiments pressure is first set to a desired level, and only thereafter is Laser-heating applied to increase temperature.

In Figure 3 (right) we present ΔG-T of Fe–N compounds at 58.5 GPa. Each line represents the Gibbs energy relative to FeN_2 for a system comprised of a structure with given composition plus appropriate amounts of nitrogen. The sequence of structures computed at 58.5 GPa then is $FeN_8 \xrightarrow{1200\,K} FeN_6 \xrightarrow{1340\,K} FeN_4 \xrightarrow{2000\,K} FeN_2 \xrightarrow{3120\,K} FeN \xrightarrow{3710\,K} Fe_4N_3 \xrightarrow{3935\,K} Fe_7N_3$, with the temperature of transition indicated above the arrow. Hence, computed data suggested that FeN_2 structure will be favorable between 2000 and 3120 K. The maximum driving force ΔG to attain the structure is at 2380 K, when it is favored by about 0.6 eV/FeN_2 over its closest competitor FeN. Likewise, Figure 3 (left) shows ΔG-p of Fe–N compounds at 2380 K. We find the sequence of $\gamma' - Fe_4N \xrightarrow{1.5\,GPa} Fe_7N_3 \xrightarrow{10.5\,GPa} Fe_3N_2\text{– II} \xrightarrow{15.5\,GPa} FeN \xrightarrow{27\,GPa} FeN_2 \xrightarrow{85\,GPa} FeN_4$. The thermodynamic stability of FeN_2 at 2380 K ranges from 26 to 85 GPa, with maximum ΔG of about 0.6 eV/FeN_2 relative to its competitor FeN_4 found at 58 GPa. We note that such data can be used to identify optimum *p,T*–conditions to synthesize a compound. And indeed, FeN_2 was synthesized using laser heated diamond anvil cell at pressure of 58.5 GPa and temperature between 2100 ± 200 K[7] – auspiciously close to the computed

optimum conditions. A similar analysis (not shown here) yields a maximum driving force at 2340 K and 135 GPa to synthesize FeN_4 — for which experimental conditions of 135 GPa and temperatures above 2000K have been reported.[7]

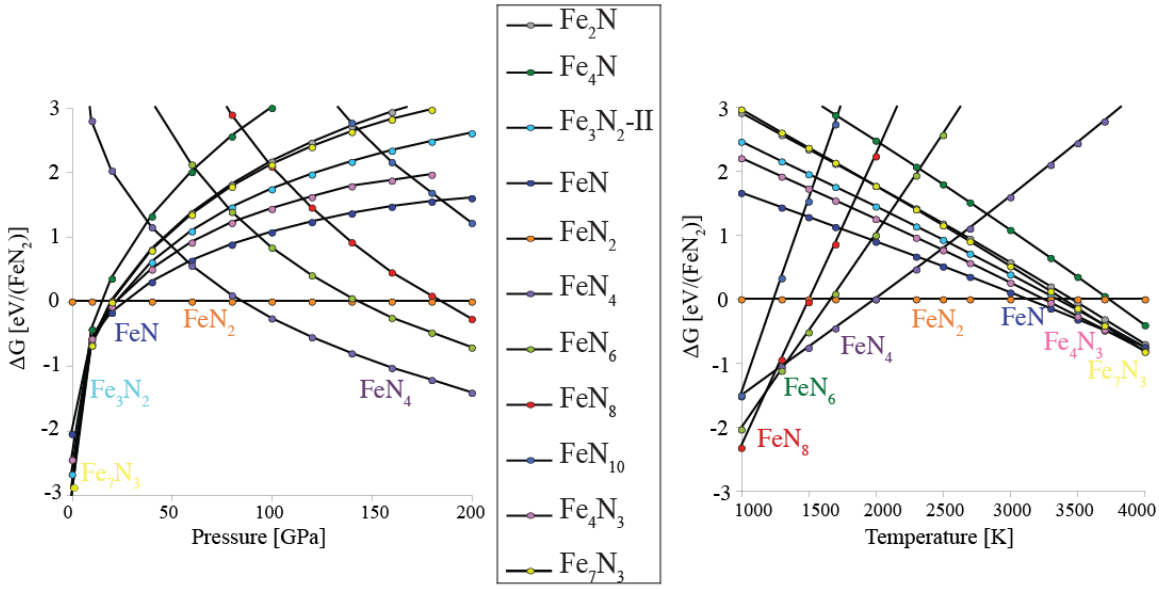

Figure 3: (Left side of legend) Relative Gibbs energy versus pressure, Δ*G*-*p*, of Fe-N phases in excess nitrogen at 2380 K. (Right side of legend) Relative Gibbs energy versus temperature, Δ*G*-*T*, of Fe-N phases in excess nitrogen at 58.5 GPa. Symbols in the respective diagrams refer to structures listed in the boxed legend. Note that in each diagram energy refers to an overall composition FeN_2.

Favorable reaction kinetics will be required to synthesize FeN_8 with its structure displaying infinite chains of nitrogen. Figure 1 indicates that the structure will become favorable only below 2000 K and that pressures exceeding 100 GPa are needed. It will be a challenge to attain this structure.

Summary and Conclusion:

We provide a comprehensive computation of the pressure-temperature phase diagram of the iron–nitrogen system for pressures up to 200 GPa and temperatures up to 4000 K. The work relies on a combination of Density Functional Theory computations with

thermodynamic calculations that includes an assessment of the chemical potential of nitrogen at high pressure and high temperature. We identify stability fields of Fe-N structures in the presence of excess nitrogen under conditions of typical DAC experiments. We made "slices" of the phase diagram at constant pressure or at constant temperature to determine maximum driving force in order to validate our approach with experimental data. Based on a comparison of experimental and computational data, we estimate an uncertainty of our method of +/- 300 K and +/- 5 GPa. This assessment assumes, however, that experimental conditions are indeed corresponding to uniform presence of excess nitrogen and that observed structures are free of defects. When such conditions are not established, this may result in phases not identified here as "thermodynamically stable" – further enriching the landscape of feasible compounds.

Acknowledgement

This work was supported by the National Science Foundation (NSF) through award OISE-1743701. The computational work was made possible through generous grants by the Texas Advance Computing Center in Austin, TACC, Texas, and by the High Performance Computing facilities at UTA. H.A. acknowledges support by the Saudi Arabian Cultural Mission.

References:

[1] A. Zerr, G. Miehe, G. Serghiou, M. Schwarz, E. Kroke, R. Riedel, H. Fuess, P. Kroll, R. Boehler, Synthesis of cubic silicon nitride, Nature, 400 (1999) 340-342.
[2] K. Landskron, H. Huppertz, J. Senker, W. Schnick, High-pressure synthesis of γ-P_3N_5 at 11 GPa and 1500 ºC in a multianvil assembly: A binary phosphorus(v) nitride with a three-dimensional network structure from PN_4 tetrahedra and tetragonal PN_5 pyramids, Angew. Chem.-Int. Edit., 40 (2001) 2643-2645.
[3] A. Zerr, G. Miehe, R. Riedel, Synthesis of cubic zirconium and hafnium nitride having Th_3P_4 structure, Nat. Mater., 2 (2003) 185-189.
[4] M.I. Eremets, A.G. Gavriliuk, I.A. Trojan, D.A. Dzivenko, R. Boehler, Single-bonded cubic form of nitrogen, Nat. Mater., 3 (2004) 558-563.
[5] E. Gregoryanz, C. Sanloup, M. Somayazulu, J. Badro, G. Fiquet, H.K. Mao, R.J. Hemley, Synthesis and characterization of a binary noble metal nitride, Nat. Mater., 3 (2004) 294-297.
[6] A. Zerr, G. Miehe, J.W. Li, D.A. Dzivenko, V.K. Bulatov, H. Hofer, N. Bolfan-Casanova, M. Fialin, G. Brey, T. Watanabe, M. Yoshimura, High-Pressure Synthesis of Tantalum Nitride Having Orthorhombic U_2S_3 Type Structure, Adv Funct Mater, 19 (2009) 2282-2288.
[7] M. Bykov, E. Bykova, G. Aprilis, K. Glazyrin, E. Koemets, I. Chuvashova, I. Kupenko, C. McCammon, M. Mezouar, V. Prakapenka, H.P. Liermann, F. Tasnadi, A.V. Ponomareva, I.A. Abrikosov, N. Dubrovinskaia, L. Dubrovinsky, Fe-N system at high pressure reveals a compound featuring polymeric nitrogen chains, Nature Communications, 9 (2018).
[8] M. Bykov, E. Bykova, E. Koemets, T. Fedotenko, G. Aprilis, K. Glazyrin, H.P. Liermann, A.V. Ponomareva, J. Tidholm, F. Tasnadi, I.A. Abrikosov, N. Dubrovinskaia, L. Dubrovinsky, High-Pressure Synthesis of a Nitrogen-Rich Inclusion Compound ReN_8.x N_2 with Conjugated Polymeric Nitrogen Chains, Angew. Chem.-Int. Edit., 57 (2018) 9048-9053.
[9] D. Laniel, G. Weck, P. Loubeyre, Direct Reaction of Nitrogen and Lithium up to 75 GPa: Synthesis of the Li_3N, LiN, LiN_2, and LiN_5 Compounds, Inorganic Chemistry, 57 (2018) 10685-10693.
[10] A. Zerr, R. Riedel, T. Sekine, J.E. Lowther, W.Y. Ching, I. Tanaka, Recent advances in new hard high-pressure nitrides, Adv. Mater., 18 (2006) 2933-2948.
[11] E. Horvath-Bordon, R. Riedel, A. Zerr, P.F. McMillan, G. Auffermann, Y. Prots, W. Bronger, R. Kniep, P. Kroll, High-pressure chemistry of nitride-based materials, Chem. Soc. Rev., 35 (2006) 987-1014.
[12] A. Salamat, A.L. Hector, P. Kroll, P.F. McMillan, Nitrogen-rich transition metal nitrides, Coord. Chem. Rev., 257 (2013) 2063-2072.
[13] C. Mailhiot, L.H. Yang, A.K. Mcmahan, Polymeric Nitrogen, Phys Rev B, 46 (1992) 14419-14435.
[14] P. Kroll, Hafnium nitride with thorium phosphide structure: Physical properties and an assessment of the Hf-N, Zr-N, and Ti-N phase diagrams at high pressures and temperatures, Physical Review Letters, 90 (2003).

[15] A.Y. Liu, M.L. Cohen, Structural properties and electronic structure of low-compressibility materials: β-Si_3N_4 and hypothetical β-C_3N_4, Phys Rev B, 41 (1990) 10727-10734.
[16] J.C. Crowhurst, A.F. Goncharov, B. Sadigh, C.L. Evans, P.G. Morrall, J.L. Ferreira, A.J. Nelson, Synthesis and characterization of the nitrides of platinum and iridium, Science, 311 (2006) 1275-1278.
[17] S.T. Oyama, The Chemistry of Transition Metal Carbides and Nitrides, Blackie Academic & Professional; Chapman & Hall: , Glasgow, Scotland, 1996.
[18] J.F. Adler, Q. Williams, A high-pressure X-ray diffraction study of iron nitrides: Implications for Earth's core, Journal of Geophysical Research-Solid Earth, 110 (2005).
[19] M. Roskosz, M.A. Bouhifd, A.P. Jephcoat, B. Marty, B.O. Mysen, Nitrogen solubility in molten metal and silicate at high pressure and temperature, Geochim. Cosmochim. Acta, 121 (2013) 15-28.
[20] K.D. Litasov, A.F. Shatskiy, Composition of the Earth's core: A review, Russ. Geol. Geophys., 57 (2016) 22-46.
[21] K.D. Litasov, A. Shatskiy, D.S. Ponomarev, P.N. Gavryushkin, Equations of state of iron nitrides ε-Fe_3N_x and γ-Fe_4N_y to 30GPa and 1200K and implication for nitrogen in the Earth's core, Journal of Geophysical Research-Solid Earth, 122 (2017) 3574-3584.
[22] Y.K. Zhuang, X.W. Su, N.P. Salke, Z.X. Cui, Q.Y. Hu, D.Z. Zhang, J. Liu, The effect of nitrogen on the compressibility and conductivity of iron at high pressure, Geosci Front, 12 (2021) 983-989.
[23] H. Jacobs, D. Rechenbach, U. Zachwieja, Structure determination of γ'-Fe_4N and ε-Fe_3N, J. Alloy. Compd., 227 (1995) 10-17.
[24] K. Guo, D. Rau, J. von Appen, Y. Prots, W. Schnelle, R. Dronskowski, R. Niewa, U. Schwarz, High pressure high-temperature behavior and magnetic properties of Fe_4N: experiment and theory, High Pressure Research, 33 (2013) 684-696.
[25] H.A. Wriedt, Gokcen, N.A. & Nafziger, R.H. , The Fe-N (Iron-Nitrogen) system, Bulletin of Alloy Phase Diagrams 8(1987) 355–377
[26] W.P. Clark, S. Steinberg, R. Dronskowski, C. McCammon, I. Kupenko, M. Bykov, L. Dubrovinsky, L.G. Akselrud, U. Schwarz, R. Niewa, High-Pressure NiAs-Type Modification of FeN, Angew. Chem.-Int. Edit., 56 (2017) 7302-7306.
[27] K. Niwa, T. Terabe, D. Kato, S. Takayama, M. Kato, K. Soda, M. Hasegawa, Highly Coordinated Iron and Cobalt Nitrides Synthesized at High Pressures and High Temperatures, Inorganic Chemistry, 56 (2017) 6410-6418.
[28] D. Laniel, A. Dewaele, G. Garbarino, High Pressure and High Temperature Synthesis of the Iron Pernitride FeN_2, Inorganic Chemistry, 57 (2018) 6245-6251.
[29] M. Bykov, S. Khandarkhaeva, T. Fedotenko, P. Sedmak, N. Dubrovinskaia, L. Dubrovinsky, Synthesis of FeN_4 at 180 GPa and its crystal structure from a submicron-sized grain, Acta Crystallographica Section E-Crystallographic Communications, 74 (2018) 1392-+.
[30] M. Hasegawa, T. Yagi, Systematic study of formation and crystal structure of 3d-transition metal nitrides synthesized in a supercritical nitrogen fluid under 10 GPa and 1800 K using diamond anvil cell and YAG laser heating, J. Alloy. Compd., 403 (2005) 131-142.

[31] C.M. Fang, M.A. van Huis, H.W. Zandbergen, Stability and structures of the ε-phases of iron nitrides and iron carbides from first principles, Scripta Materialia, 64 (2011) 296-299.
[32] Z.Y. Wang, Y.C. Li, H.T. Li, I. Harran, M.Z. Jia, H. Wang, Y.Z. Chen, H.Y. Wang, N.N. Wu, Prediction and characterization of the marcasite phase of iron pernitride under high pressure, J. Alloy. Compd., 702 (2017) 132-137.
[33] Y.Z. Chen, X.Y. Cai, H.Y. Wang, H.B. Wang, H. Wang, Novel triadius-like N_4 specie of iron nitride compounds under high pressure, Scientific Reports, 8 (2018).
[34] F.B. Jiao, C.Y. Zhang, W.Y. Xie, High-Pressure FeN_x: Stability, Phase Transition, and Energetic Characteristic, Journal of Physical Chemistry C, 124 (2020) 19953-19961.
[35] N.E. Sagatov, D.N. Sagatova, P.N. Gavryushkin, K.D. Litasov, Fe–N System at High Pressures and Its Relevance to the Earth's Core Composition, Crystal Growth & Design, 21 (2021) 6101-6109.
[36] N. Sagatov, P.N. Gavryushkin, T.M. Inerbaev, K.D. Litasov, New high-pressure phases of Fe_7N_3 and Fe_7C_3 stable at Earth's core conditions: evidences for carbon-nitrogen isomorphism in Fe-compounds, Rsc Adv, 9 (2019) 3577-3581.
[37] L.L. Wu, R.F. Tian, B. Wan, H.Y. Liu, N. Gong, P. Chen, T.D. Shen, Y.S. Yao, H.Y. Gou, F.M. Gao, Prediction of Stable Iron Nitrides at Ambient and High Pressures with Progressive Formation of New Polynitrogen Species, Chemistry of Materials, 30 (2018) 8476-8485.
[38] A. Kartsev, O.D. Feya, N. Bondarenko, A.G. Kvashnin, Stability and magnetism of FeN high-pressure phases, Phys Chem Chem Phys, 21 (2019) 5262-5273.
[39] D. Laniel, A. Dewaele, S. Anzellini, N. Guignot, Study of the iron nitride FeN into the megabar regime, J. Alloy. Compd., 733 (2018) 53-58.
[40] P. Hohenberg, W. Kohn, Inhomogeneous Electron Gas, Phys Rev B, 136 (1964) B864-+.
[41] G. Kresse, Ab-Initio Molecular-Dynamics for Liquid-Metals, J Non-Cryst Solids, 193 (1995) 222-229.
[42] G. Kresse, J. Hafner, Ab-Initio Molecular-Dynamics Simulation of the Liquid-Metal Amorphous-Semiconductor Transition in Germanium, Phys Rev B, 49 (1994) 14251-14269.
[43] G. Kresse, J. Furthmuller, Efficiency of ab-initio total energy calculations for metals and semiconductors using a plane-wave basis set, Comp Mater Sci, 6 (1996) 15-50.
[44] P.E. Blochl, Projector Augmented-Wave Method, Phys Rev B, 50 (1994) 17953-17979.
[45] G. Kresse, D. Joubert, From ultrasoft pseudopotentials to the projector augmented-wave method, Phys Rev B, 59 (1999) 1758-1775.
[46] J.W. Sun, A. Ruzsinszky, J.P. Perdew, Strongly Constrained and Appropriately Normed Semilocal Density Functional, Physical Review Letters, 115 (2015).
[47] M.H. Wetzel, M.R. Schwarz, A. Leineweber, High-pressure high-temperature study of the pressure induced decomposition of the iron nitride γ'-Fe4N, J. Alloy. Compd., 801 (2019) 438-448.
[48] A.R. Oganov, Y.M. Ma, A.O. Lyakhov, M. Valle, C. Gatti, Evolutionary Crystal Structure Prediction as a Method for the Discovery of Minerals and Materials, in: R. Wentzcovitch, L. Stixrude (Eds.) Theoretical and Computational Methods in Mineral Physics: Geophysical Applications, 2010, pp. 271-298.

[49] J. Zhang, A.R. Oganov, X.F. Li, H.Y. Niu, Pressure-stabilized hafnium nitrides and their properties, Phys Rev B, 95 (2017).
[50] P. Kroll, Pathways to metastable nitride structures, J. Solid State Chem., 176 (2003) 530-537.
[51] P. Kroll, T. Schroter, M. Peters, Prediction of novel phases of tantalum(V) nitride and tungsten(VI) nitride that can be synthesized under high pressure and high temperature, Angew. Chem.-Int. Edit., 44 (2005) 4249-4254.
[52] H. Alkhaldi, P. Kroll, Chemical Potential of Nitrogen at High Pressure and High Temperature: Application to Nitrogen and Nitrogen-Rich Phase Diagram Calculations, Journal of Physical Chemistry C, 123 (2019) 7054-7060.
[53] R.T. Jacobsen, R.B. Stewart, M. Jahangiri, Thermodynamic Properties of Nitrogen from the Freezing Line to 2000 K at Pressures to 1000 MPa, Journal of Physical and Chemical Reference Data, 15 (1986) 735-909.
[54] H. Alkhaldi, P. Kroll, Computing the Tantalum-Nitrogen Phase Diagram at High Pressure and High Temperature, Journal of Physical Chemistry C, 124 (2020) 22221-22227.
[55] V.S. Bhadram, D.Y. Kim, T.A. Strobel, High-Pressure Synthesis and Characterization of Incompressible Titanium Pernitride, Chemistry of Materials, 28 (2016) 1616-1620.
[56] V.S. Bhadram, H.Y. Liu, E.S. Xu, T.S. Li, V.B. Prakapenka, R. Hrubiak, S. Lany, T.A. Strobel, Semiconducting cubic titanium nitride in the Th_3P_4 structure, Physical Review Materials, 2 (2018).
[57] Fe_3N_2 adopts space group symmetry *Fdd2* (43) with lattice parameters a=6.94, b=6.08, and c=6.76. Atoms are Fe at (0, 0, -0.2239), N1 at (-0.1674, 0.0624, 0.2292), and N2 (0.3048, 0.0299, 0.4493)
[58] Y.L. Li, S.N. Wang, A.R. Oganov, H.Y. Gou, J.S. Smith, T.A. Strobel, Investigation of exotic stable calcium carbides using theory and experiment, Nature Communications, 6 (2015).
[59] FeN_8 adopts space group symmetry *P-1* (1) with lattice parameters a=4.14, b=4.31, c=3.44; and a=110.7°, b=83.43°, g=72.25°. Atoms are Fe at (0, 0,0), N1 at (-0.13171, -0.23095, -0.22887), N2 at (-0.03462, 0.36362, -0.00334), N3 at (-0.44232, 0.12528, 0.48929), and N4 at (0.40971, 0.29414, 0.27986)
[60] FeN_8-N_2 adopts space group symmetry *Immm* (71) with lattice parameters a=3.64, b=6.38, and c=5.87. Atoms are Fe at (0, 0, 0), N1 at (0.18074, -0.32342, 0.3121), and N2 at (-0.33998, 0.5, 0) (data at 102 GPa)
[61] M. Bykov, S. Chariton, E. Bykova, S. Khandarkhaeva, T. Fedotenko, A.V. Ponomareva, J. Tidholm, F. Tasnadi, I.A. Abrikosov, P. Sedmak, V. Prakapenka, M. Hanfland, H.P. Liermann, M. Mahmood, A.F. Goncharov, N. Dubrovinskaia, L. Dubrovinsky, High-Pressure Synthesis of Metal-Inorganic Frameworks $Hf_4N_{20}.N_2$, $WN_8.N_2$, and $Os_5N_{28}.3N_2$ with Polymeric Nitrogen Linkers, Angew. Chem.-Int. Edit., (2020) 7.

CHAPTER 3: COMPUTING THE TUNGSTEN–NITROGEN PHASE DIAGRAM AT HIGH PRESSURE AND HIGH TEMPERATURE AND FURTHER TERNARY W–N COMPOUNDS

COMPUTING THE TUNGSTEN–NITROGEN PHASE DIAGRAM AT HIGH PRESSURE AND HIGH TEMPERATURE AND FURTHER TERNARY W–N COMPOUNDS

INTRODUCTORY REMARKS

Ternary tungsten bronzes are a fascinating class of oxide materials that are formed when WO_3 is reduced. To explore a similar compound system among tungsten–nitrogen compounds, the first question to address is whether it is feasible to synthesize WN_2, with W in oxidation state +6. The resulting computed phase diagram of W–N is fascinating, albeit formations of compounds with W^{+6} are notably absent up to 200 GPa. Thus, we entered a more generalized question, as to whether an alloying metal can change preferences for W to adopt its highest oxidation state in high pressure experiments. Starting with Li_6WN_4, a compound accessible in experiments at ambient pressure, the two binary systems Li–N and W–N, as well as the ternary Li–W–N system are explored. Ternary Li–W–N compounds are being compared to mixtures of W–N and Li–N compounds to address their thermodynamic stability. In course of this endeavor, the ternary $LiWN_3$ == $LiW(N)(N_2)$, a mixed nitride-pernitride compound, is identified as a new high–pressure ternary Li–W–N structure. It will be attainable at 80 GPa and 2600 K.

Computing the Tungsten–Nitrogen Phase Diagram at High Pressure and High Temperature and Further Ternary W–N Compounds

Hanof Alkhaldi and Peter Kroll[a]

Department of Chemistry and Biochemistry, The University of Texas at Arlington, 700 Planetarium Place, Arlington, Texas 76019, United States.

* Corresponding authors: pkroll@uta.edu

Abstract:

We compute the tungsten–nitrogen (W–N) pressure–temperature phase diagram through a combination of density functional theory and thermodynamic calculations. Augmenting standard enthalpy-pressure calculations by the chemical potential change of nitrogen at high pressure and high temperature conditions, we estimate Gibbs energies under nitrogen-rich conditions. The approach allows to predict temperature and pressure conditions necessary to synthesize W–N polymorphs and to locate optimum pressure/temperature conditions. Our investigations include W_2N_3, W_3N_5, $W_2N_2(N_2)$, and recently synthesized WN_6 and WN_8-N_2. We further address ternary Li–W–N compounds with W in high oxidation state, namely $Li_6WN_{(2\cdot n)}$, with n=4 to 11. We predict in which ternary Li–W–N will decompose, and predict unknown $LiWN_3$ attainable at 80 GPa and 2500 K.

Introduction

Diatomic nitrogen ($N \equiv N$) is the most abundant molecule of Earth's atmosphere. It is highly stable and unreactive at ambient conditions due to the strong triple bond combined with its high ionization potential. The triple bond contains an average energy of ~954 kJ/mol, far more than three times that of a single bond (N–N; ~160 kJ/mol) and more than that of a double bond (N=N; 418 kJ/mol), respectively.[1] Further nitrogen phases comprising single and double bonds are formed under high pressure.[2-3] A particular example is "polymeric" cubic-gauche nitrogen – a structure in which each nitrogen forms single bonds with three adjacent nitrogen atoms.[4] Transformation or decomposition of polymeric nitrogen to diatomic nitrogen molecules is expected to release a large amount of energy. Consequently, nitrogen and its various compounds gained research interest not only due to their unique physical properties but also for the fact that they are promising high-energy-density materials (HEDMs).[5] These HEDMs have potential applications in impulse power engineering, high-voltage and high-power electrophysics, welding materials, and impact protection of space vehicles.[6] Besides elemental nitrogen compounds, several binary nitrogen compounds of main group elements and transition metals have been successfully attained at high pressure and high temperature (high-p,T). The research brought along discovery of various forms of complex nitrogen ions in nitrogen-rich compounds, including diazenides, pernitrides, mixed nitride-pernitrides, polyatomic nitrogen anions, and compounds with extended anionic nitrogen chains.

Nitrogen compounds of tungsten have been investigated thoroughly through first principle calculations. These include crystalline structures of W_3N, W_2N, W_3N_2, W_2N_3, WN, WN_2, WN_4, WN_6, and WN_8-N_2 – all of which were subsequently obtained in experiments. More details about prediction and synthesis of W–N compounds are provided below.[7-25] Noteworthy is WN_6 with a structure comprising armchair-like hexazine cyclo-N_6^{6-}. This anion is isoelectronic to cyclo-hexane, thus comprises $N - N$

single bonds, and balances the charge of W^{6+}, showing tungsten in oxidation state of 6+. $WN_8{-}N_2$ exhibits (neutral) dinitrogen molecules ($N \equiv N$) besides polydiazenediyl anions $2[N_4]^{2-}_{\infty}$). In this compound, W exhibits the oxidation state of 4+. Both compounds were synthesized at extremely high pressures, 126 GPa and 105 GPa, respectively. It is commonly observed that applying high pressure results in increased coordination and higher oxidation states. Conversely, the impact of increasing temperature is commonly a reduced oxidation state accompanied with lower coordination number. This follows Le Chatelier's principle, with pressure countering the impact of temperature. Alloying W–N compounds with an alkali or alkaline earth metal is an alternative approach that will yield W in high oxidation state at lower pressure compared to pure W–N compounds. To date the only synthesized ternary W-N compound is Li_6WN_4 adopts space group (*P42/nmc* (128)). It comprises nitride anions, which renders the oxidation state of W to be 6+. Li_6WN_4 is synthesized in a solid-state reaction at room temperature.[26] A single study addresses ternary W–N compounds at 0 K.[27] We show further below that the realm of possible ternary W–N compounds are much larger than it appears. It is our aim in this contribution to display a wide range of W–N and Li–W–N structures in which W will attain high oxidation states. To address the ternary system, we will first present computed pressure–temperature (p,T) phase diagrams for the respective binary systems, W–N and Li–N. Identifying thermodynamically stable binary phases and their respective stability field provides the foundation for our exploration of ternary compounds. Driven by the availability of Li_6WN_4 as a potential precursor high experiments in a laser-heated diamond anvil cell (LH-DAC), we then investigate potential high-pressure phases with composition $Li_6WN_{(2\cdot n)}$ (n=4-11) in the next step. Thereafter, we will address the thermodynamic stability of ternary Li–W–N compounds by comparing them to possible mixtures of binary W–N and Li–N compounds. This work results in a ternary Li–W–N pressure-temperature phase diagram that displays thermodynamically stable Li_3WN_3, $LiWN_3$, Li_2WN_4, Li_3WN_5, Li_4WN_6, and Li_5WN_7 as

well as binary phases together with their respective stability fields. We also provide slices through this Li–W–N phase diagram at constant pressure and at constant temperature, respectively, to guide experimentalists to locate conditions of maximum driving force to synthesis $LiWN_3$.

Computational method:

Calculations of total energy are performed within Density Functional Theory (DFT) as implemented in Vienna Ab-initio Simulation Package (VASP).[28-31] We use pseudopotentials based on the projector-augmented-wave (PAW) method.[32-33] We apply strongly constrained and appropriately normed semilocal density functional (SCAN).[34] The Brillouin zone of each structure is sampled by k-point meshes with grid sizes smaller than 0.03 $Å^{-1}$. All calculations depend on well forces converged to better than 1 meV/Å with a plane wave cut-off energy of (500 eV) which yields energy and enthalpy differences between structures converged to better than 1 meV per atom.

For structural collection we first computed structures previously reported for each system. We then used , Universal Structure Predictor: Evolutionary Xtallography (USPEX)[35] code to identify known and new polymorphs.

Enthalpy-pressure data of every structure is acquired using standard techniques described earlier.[36] In brief: total energy E for every structure calculated as function of volume V, reducing V stepwise to simulate higher densities and pressures. The resulting E–V data yields pressure p by numerical differentiation, $p = -\partial E/\partial V$, and enthalpy $H = E + pV$. For all reaction involving solid state structures the enthalpy of reaction ΔH is equated to reaction Gibbs energies ΔG, because entropy changes that contribute to ΔG are much smaller than changes of ΔH within a few GPa of pressure. For reaction involving nitrogen, we augment reaction Gibbs energies ΔG with chemical potential changes of nitrogen, $\Delta\mu(p,T)$, as outlined in previous studies.[10, 37] Experimental data of

$\Delta\mu$(p,T) for nitrogen is available for low pressures from the freezing point to 4000K.[38] The data is extrapolated to high pressure and high temperature using the "moderate extrapolation" for fugacity of nitrogen.[10] As result we obtain quantitative data of chemical potential for every phase system and can compare reaction Gibbs energies at high pressure and high temperature conditions. The approach has shown good agreement between experiment and calculations for several systems to at least 200 GPa.[37, 39]

Advance in tungsten–nitrogen compounds

Several new tungsten nitrides were synthesized in a multi-anvil press through solid-state reactions between Na_2WO_4 and hexagonal BN. Both a hexagonal (*$P6_3/mmc$* (no. 194)) and a rhombohedral (*R3* (no.146)) structure of W_2N_3 were observed at 5 GPa and 880-1770 K. Increasing temperature above 2000 K caused loss of nitrogen in hexagonal W_2N_3 and observation of a cubic compound, which was assigned c-W_3N_4 (*Pm-3m* (no. 221)), together with WN with WC-type structure (*P-6m2* (no. 187)). at 5 GPa and 2273-2570 K.[7] Subsequently, elastic and some thermodynamic properties of c-W_3N_4 were studied in first principle calculations.[8] Different structures of tungsten mononitride (WN) were investigated theoretically, but also observed in experimental work. NiAs-type WN (*$P6_3/mmc$* (no. 194)) and MnP-type WN (*Pm-3m* (no. 221)) were investigated.[9-10] NaCl-type δ-WN (*Fm-3m* (no. 225)) was synthesized at 5.2 GPa and 2073 K in cubic anvil apparatus using W_2N_3 powder and melamine as starting materials.[11] MoC-type WN (*$P6_3/mmc$* (no. 194)), NaCl-type δ-WN, and WC-type WN were all synthesized via nitridation at 6 GPa and 1000-1200°C in a multi-anvil press.[12] WC-type WN as well as $W_{2.25}N_3$ were obtained via solid-state reaction between at 7.7 GPa and 1373-1973 K using a large volume press.[13]

Mechanical and dynamical stabilities of various polymorphs of W_2N_3 were investigated by density functional theory.[14] A later study augmented the collection of structures by a new polymorph η-W_2N_3 space group (*Pnma* (no. 62)).[15] Structures of WN_2

with space group (*P6$_3$/mmc* (no. 194)) and (*P-6m2* (no. 187)) were proposed to be stable at 0 GPa and up to 60 GPa.[16] Another candidate of WN_2 with space group *Pa-3* (no. 205) was proposed.[17] Physical properties of several WN_2 structures were investigated by first principle calculations.[40] Further studies of the structural, elastic, electronic properties, and hardness of a tetragonal WN_2 space group (*P4/mmm* (no. 123)) followed.[41] More potential W–N phases were investigated, including a NbO-type WN, yet another WN_2 (*P6m2*, (no. 187)), W_5N_6 (*P6$_3$/mcm* (no. 193)), in anology to Ta_5N_6, and W_3N_2 (*R-3m* (no. 166)), analogous to Ag_2NiO_2.[18] More work about W-N structures including WC-type WN, WN_2 (*P21/c,* (no. 14)), analogous to IrN_2, WN_3 (*Pnma* (no. 62)), analogous to TcP_3 followed for pressures up to 100 GPa.[19] Finally, W–N structures including NiAs-type WN, WN_2 (*P4/mbm* (no. 127)), WN_6 (*R32m* (no. 166)), and WN_{10} (*Immm* (no. 177)) were studied to identify W–N compounds stable up to 100 GPa.[20-23] It is worthy to note that subsequently WN_8-N_2 was synthesized at 105 GPa and above 2000 K, while WN_6 was synthesized at 126-165 GPa for temperatures up to 3500 K.[24-25]

Results:

Phase Diagram of tungsten–nitrogen at high pressure and high temperature

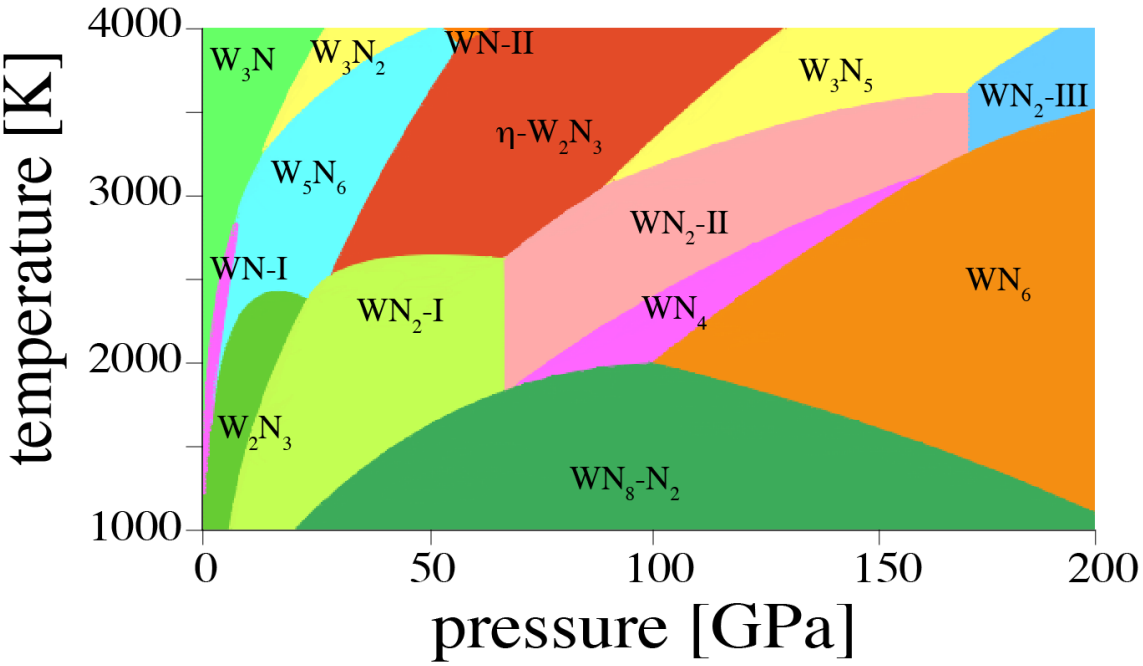

Figure 1: The tungsten–nitrogen pressure-temperature phase diagram computed by combining of first principles (SCAN functional) and thermodynamic calculations. The pressure scale refers to partial pressure of nitrogen in the experiment.

Combining first-principles computations with thermodynamic calculations we compute the pressure–temperature (*p*,*T*) phase diagram for the tungsten–nitrogen system using the moderate approximation for the chemical potential of nitrogen shown in Figure 1. Taking into account all published structures and including results of our own structure searches we present the thermodynamically stable W–N phases at given p,T-conditions in the presence of excess nitrogen. At low pressure and low temperature we find W_2N_3-I, the monoclinic polymorph of W_2N_3 with space group symmetry (*C1m1* (no. 8)). At slightly higher temperature NbO-type WN emerges,[9, 18], and above 2500K we find monoclinic structure W_3N (*P21* (no. 4)). Keeping the temperature above 2500K, we then find with increasing pressure the phases W_5N_6, analogous to Ta_5N_6, W_3N_2, analogous to Ag_2NiO_2,

the NiAs-type WN,[18] and η-W_2N_3.[15] A substantial part of the phase diagram is then occupied by three WN_2 polymorphs. Hexagonal WN_2-I (*P6m2)*,[16] will transform to monoclinic WN_2-II (*C2/m)* at 66 GPa, which is followed by WN_2-III (*P4/mbm)* at 120 GPa.[20] WN_2-I comprises the pernitride anion, while WN_2-II and WN_2-III structures are mixed nitride-pernitride structures, WN_2 == $W_2N_2(N_2)$. Three more phases with high nitrogen content appear at high pressures and lower temperatures. Monoclinic WN_4 ($P2_1/n$) is isostructural to the recently synthesized TaN_4.[42] It exhibits short chains of nitrogen that are best described as teraz-1-enide anions $[N\text{-}N\text{-}N{=}N]^{4-}$. WN_6 (*R32m*) displays a cyclo-hexane analogue of nitrogen atoms forming a six-membered ring anion, N_6^{6-}.[20] This structure has been synthesized at 126-165 GPa and temperatures up to 3500 K.[25] Finally, orthorhombic WN_8-N_2 (*Immm*) emerges at temperatures below 2000 K. This phase is isostructural to $ReN_8{\cdot}N_2$,[43] and comprises embedded molecular N_2 besides infinite chains of poly-diazenediyl, $[N_4]_\infty^{2-}$.

Advance in lithium–nitrogen compounds

Many crystalline Li–N structures have been investigated by first principle calculations, including $Li_{13}N$, Li_5N, α,β,γ-Li_3N, Li_2N_2, LiN, Li_3N_2, LiN_2, LiN_3, and LiN_5.[44-46] Lithium diazenide, Li_2N_2 (*Immm* (no. 71)) was synthesized in a in multi-anvil cell by decomposition of lithium azide LiN_3 at 9 GPa and 750 K.[47] Several more nitrogen-rich compounds with lithium were subsequently realized, including a new high-pressure phase of Li_3N, Li_2N_2, LiN_2, LiN_3, and LiN_5. Laniel et al. preformed LH-DAC experiments to synthesize Li–N compounds.[48] Below 20 GPa laser-heating was limited to temperatures up to 1500 K, while above 20 GPa temperatures of ~2500 K were possible. Reaction between Li and N yielded β-Li_3N (*P6/mmc* (no. 41)), and further heating of β-Li_3N yield only β-Li_3N at 3.5 GPa but no detection of γ-Li_3N (*Fm-3m* (no. 225)). Above 25.2 and up to 73.6 GPa synthesis of LiN (*Cmcm* (no. 63)) occurred jointly with LiN_2 ($P6_3/mmc$ (no. 194)) and LiN_5 ($P2_1$ (no. 4)). Laser heating of either β-Li_3N or LiN in excess of nitrogen

yields LiN_2 at 10.5 GPa. LiN_5 was synthesized by laser heated of either β-Li_3N or LiN_2 in excess nitrogen between 46.5 GPa and 73.6 GPa. LiN_5 was also synthesized by compressing lithium azide, LiN_3, in excess nitrogen at 40 GPa.[49] Later, Laniel et al. recovered LiN_5 to ambient conditions and supported presence of the pentazolate anion in the sample.[50] Further LiN_5 structures were predicted computed.[51]

Results:

Phase Diagram of lithium–nitrogen at high pressure and high temperature

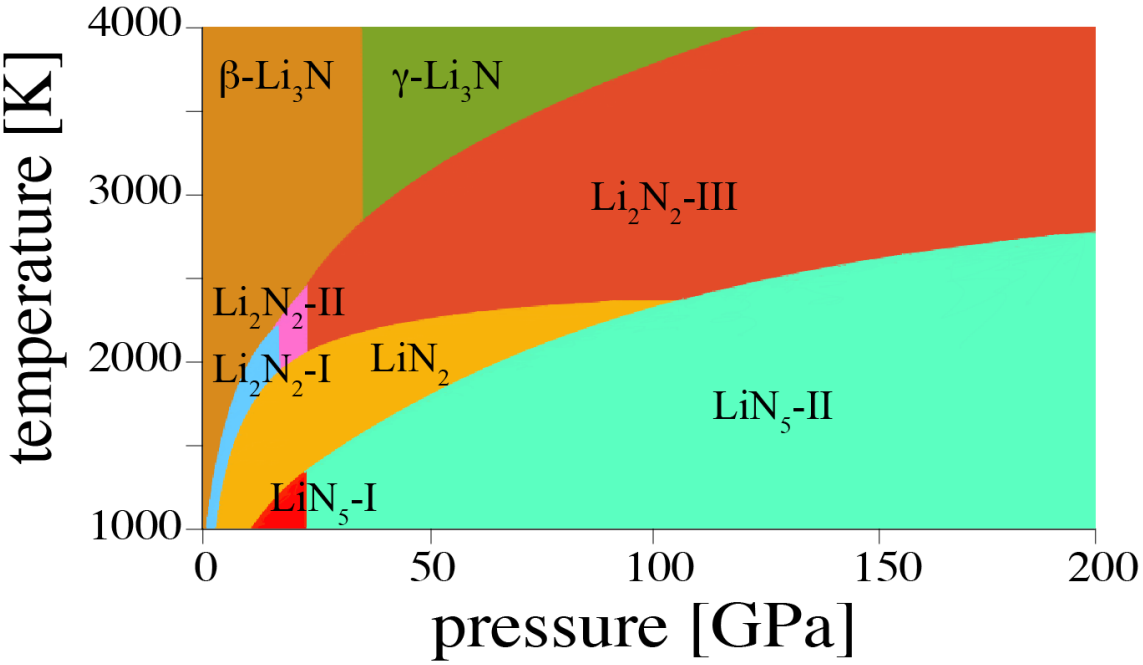

Figure 2: The lithium–nitrogen pressure-temperature phase diagram computed by combining of first principles (SCAN functional) and thermodynamic calculations.

We compute the pressure–temperature (p,T) phase diagram for the lithium–nitrogen system combining first-principles computations with thermodynamic calculations shown in Figure 2. We use the moderate extrapolation to account the change of the chemical potential of nitrogen. The diagram displays the thermodynamically most stable Li-N phase at given *p*,*T*-conditions in the presence of excess nitrogen. At low pressure we find

β-Li_3N. In agreement with early prediction of Li–N phase diagram,[44-45] the lowest energy hexagonal polymorph of α-Li_3N with space group symmetry (*P6/mmm* (no. 191)) shows stability up to 0.5 GPa. However, since β-Li_3N has the more favorable pressure behavior, it is the only Li_3N structure stable at low pressure. Synthesis of β-Li_3N at 3.5 GPa and below 1500 K[48] is well reflected in the computed phase diagram. At higher temperature and higher pressure we locate γ-Li_3N. This phase has not been observed experimentally. A significant part of the phase diagram is occupied by Li_2N_2. Li_2N_2-I (*Immm* (no. 71)), synthesized at 9 GPa and 750 K, will transfer to Li_2N_2-II (*I4mm* (no. 107)) at 16 GPa. This compound will further transform to Li_2N_2-III (*Cmcm* (no. 63)) at 22 GPa. The latter phase, Li_2N_2-III, was attained at 25.2 GPa and up to 73.6 GPa at temperatures below 2500 K.[48] The compound LiN_2 (*$P6_3/mmc$* (no. 194)) shows a remarkably large stability field between 5 and 100 GPa and moderate temperatures. This phase was experimentally realized at 10.5 GPa below 1500 K. At higher pressures we locate LiN_5 (*$P2_1$* (no. 4)). This phase was synthesized between 46.5 GPa and 73.6 GPa and below 2500 K. Synthesis of LiN_5 was accompanied with synthesis of LiN and LiN_2 at 25.2 GPa and up to 73 GPa. Small portion of the phase diagram are occupied by a low-pressure form of LiN_5 (*$P2_1/m$* (no. 11)), and by LiN_3 (*C2/m* (no. 12)).

Ternary lithium–tungsten–nitrogen

Li_6WN_4 with tetragonal structure (*P42/nmc* (no. 128)) is the only known ternary Li–W–N compound so far. W^{6+} cations are approximately tetrahedrally connected to nitrogen, and those complex $[WN_4]^{6-}$ ions are embedded in a sea of Li^+ cations. Li_6WN_4 was synthesized by reacting Li_3N and W in nitrogen atmosphere at 1123 K.[26] The compound decomposes at 1273 K, and among the residue only elemental tungsten was characterized. To address decomposition of Li_6WN_4 we followed various reaction paths at ambient pressure. A first path is a decomposition into the starting materials, hence, $Li_6WN_4 \rightarrow 2\alpha\text{-}Li_3N + W + N_2$. We obtain an enthalpy of reaction (at 0 GPa and 0 K) of

$\Delta H = + 6.45$ eV/Li_6WN_4, indicating a significant thermodynamic stability of Li_6WN_4 at these conditions. Since the reaction evolves nitrogen, we augment the chemical potential of nitrogen to access the Gibbs energy of the reaction. Using the available NIST data,[38] we get $\Delta G = + 2.00$ eV/Li_6WN_4 at 2500 K and $\Delta G = - 0.02$ eV/Li_6WN_4 at 3416 K. Thus, we find that Li_6WN_4 will decompose at higher temperature and estimate the limit of its high-temperature stability to 3416 K. Furthermore, we investigated decomposition of Li_6WN_4 into binary Li–N and W–N compounds as well as nitrogen. Based on the computed Li–N and W–N phase diagrams (Fig.1&2 above), we find – for temperatures above 1000 K, W_3N and α-Li_3N to be preferred. For the reaction $Li_6WN_4 \rightarrow 1/3(W_3N + 6Li_3N + 5/2N_2)$ we obtain $\Delta H = + 4.371$ eV/Li_6WN_4, and augmenting the chemical potential of nitrogen again we obtain $\Delta G = + 2.69$ eV/Li_6WN_4 at 2500 K and $\Delta G = - 0.00$ eV/Li_6WN_4 at 3970 K. Thus, Li_6WN_4 appears to be stable against decomposition to binary Li-N and W-N compounds up to 3970 K. A third pathway addresses loss of nitrogen of Li_6WN_4 at elevated temperature. We approximated nitrogen-deficient Li_6WN_{4-x} by forming nitrogen vacancy in super-cells of the Li_6WN_4 structure. This way, we obtained crystalline approximants for Li_6WN_3, $Li_6WN_{3.5}$, $Li_6WN_{3.75}$, $Li_6WN_{3.875}$, and $Li_6WN_{3.9375}$. Respective decomposition reactions are:

$$Li_6WN_4 \rightarrow Li_6WN_3 + \tfrac{1}{2}\ N_2, \qquad Li_6WN_4 \rightarrow Li_6WN_{3.5} + \tfrac{1}{4}\ N_2,$$

$$Li_6WN_4 \rightarrow Li_6WN_{3.75} + 1/8\ N_2, \qquad Li_6WN_4 \rightarrow Li_6WN_{3.875} + 1/16\ N_2,$$

$$\text{and } Li_6WN_4 \rightarrow Li_6WN_{3.9375} + 1/32\ N_2.$$

Approximating $Li_6WN_{3.9375}$ requires computing a model of $Li_{96}W_{16}N_{63}$. Since vacancies may appear in different patterns, we estimated the configurational entropy through an (ideal) mixing term within the anion sub-lattice. We then obtain[52-53]

$$S_{mix} = S_{mix}^{an} = R.[M_{an}\left(x_N\ .\ ln_{x_N} + x_V\ .ln_{x_{NV}}\right)]$$

In this equation, R is the universal gas constant (8.314 $JK^{-1}mol^{-1}$). X_N and X_v are fractions of N and vacancies, respectively. M_{an} accounts for the number (mol) of available anion sites. Combining computations of reaction enthalpies with mixing entropies, and

augmenting the result with data of chemical potential change of nitrogen at elevated temperatures yields estimates for reaction Gibbs energies. Results for decomposition pathways are collected in Figure 3 together with results for decompositions into starting materials and into binary nitrides.

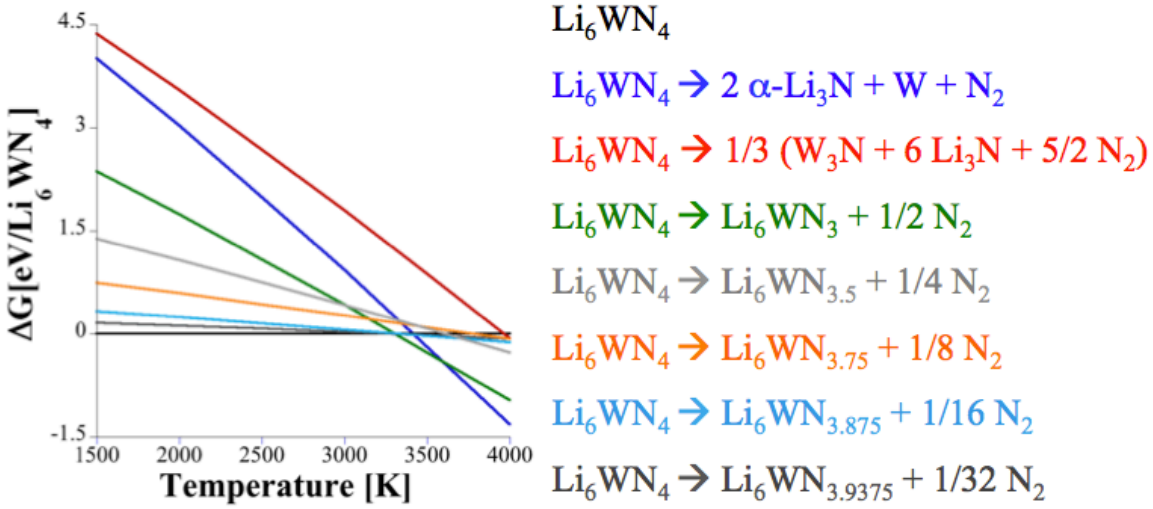

Figure 3: Relative Gibbs energy versus temperature, Δ*G*-*T*, of lithium–tungsten–nitrogen phases in excess nitrogen at 0 K using pure NIST data.

According to the diagram, the preferred – or initial – decomposition pathway of Li_6WN_4 is a loss of nitrogen at elevated temperature. This loss goes along with a (partial) reduction of W and an increasing amount of nitrogen vacancies. The two other pathways – both with complete structure transformations – appear less preferred. We note, however, that the uncertainty of this assessment is considerable.

We discovered through structure searches two high-pressure polymorphs of Li_6WN_4. At 48 GPa tetragonal Li_6WN_4, which we designate as Li_6WN_4-I, will transfer to orthorhombic Li_6WN_4-II (*Cmc21,* (no. 36)). It comprises edge-sharing WN_6-octahedra. Yet another structure, monoclinic Li_6WN_4-III (*C2* (no. 5)) – also comprises edge–sharing octahedral WN_6 – may have a kinetic advantage to form. Serendipitously, we observed a smooth transformation from Li_6WN_4-III to Li_6WN_4-I upon decompression. This is

illustrated in Figure 4. Starting at 20 GPa, the (infinite) chains of edge–sharing WN_6 are still present. Towards 10 GPa the structure has expanded and one W–N bond is lost, leaving behind WN_5 polyhedra. Further expansion down to 5 GPa yields WN_4–tetrahedra only – and a final optimization at 0 GPa allows identification with Li_6WN_4-I. While we were not able to follow the same path during compression, we still think that this continuous transformation path may have its impact on high-pressure transformations of Li_6WN_4-I.

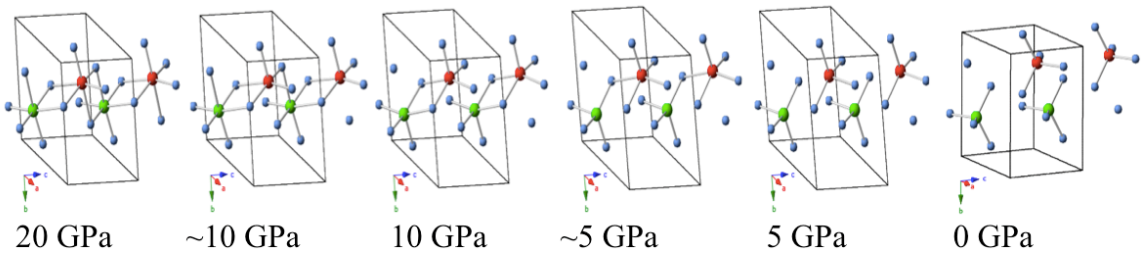

Figure 4. Continuous transformation path from Li_6WN_4-III to Li_6WN_4-I. Green and red atoms are tungsten; blue atoms are nitrogen.

A typical high pressure synthesis experiment in a diamond anvil cell (DAC) sees a compound, often elemental metals, being inserted and the apparatus loaded with nitrogen. Nitrogen acts both as pressure transmitting medium as well as reactant. Once the sample is compressed to a desired pressure it is heated by a laser. High temperatures enable reactions with nitrogen at high pressures by overcoming activation barriers. We have this experimental approach in mind when considering Li_6WN_4-I as starting material to explore ternary Li–W–N compounds. Since the full ternary phase diagram quickly becomes very complex, we first consider only single phases that retain the ratio Li:W=6:1 but exhibit high nitrogen content. Hence, we initially address only $Li_6WN_{(2\cdot n)}$, with n=4 to 11. After structure searches, we combine our results from Density Functional Theory with thermodynamic calculations to attain the p-T phase diagram of $Li_6WN_{(2\cdot n)}$ Figure 5. We only use the moderate approximation for the chemical potential of nitrogen, which has shown the best correspondence to experiment.[10, 37, 39]

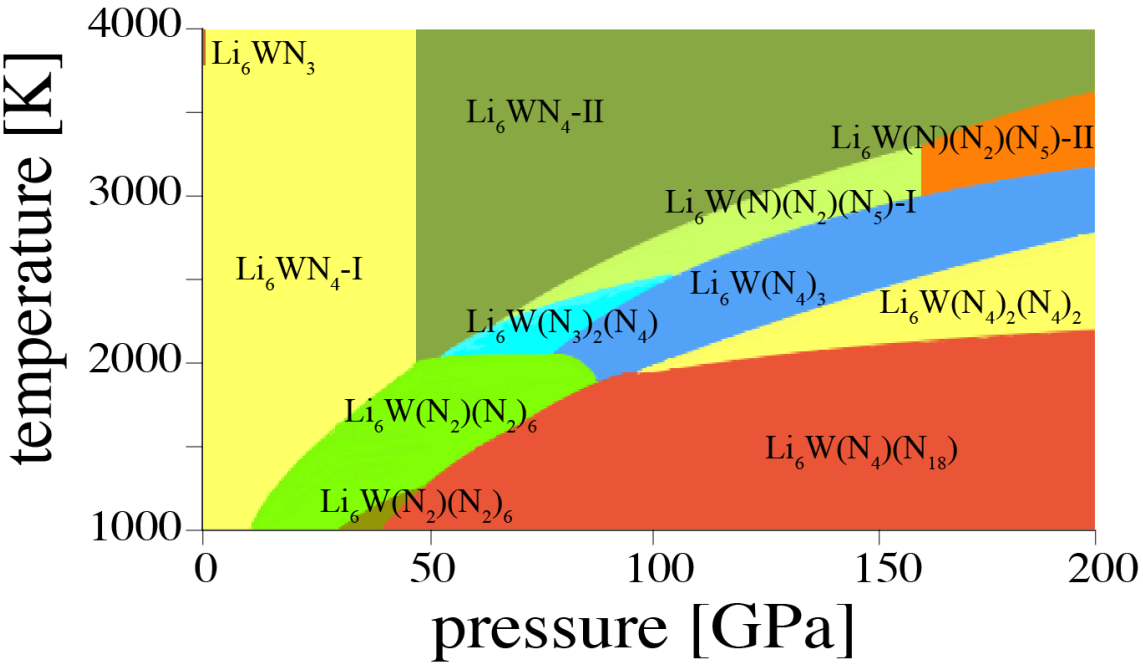

Figure 5: The $Li_6WN_{(2-n)}$ pressure-temperature phase diagram computed by combining of first principles (SCAN functional) and thermodynamic calculations.

At low pressure the computed $Li_6WN_{(2-n)}$ phase diagram displays, as expected, Li_6WN_4-I (*P42/nmc* (128)). As shown before, above 3500 K tetragonal Li_6WN_3 (*P42/nmc* (no. 128)) emerges. Increasing pressure yields orthorhombic Li_6WN_4-II (*Cmc21* (no. 36)) at 48 GPa. Li_6WN_4-II is rivaled by Li_6WN_4-III (*C2* (no. 5)) as outlined earlier. Both structures show edge-sharing WN_6-octahedra, comprise nitride anions $[N]^{3-}$ and tungsten in oxidation state of W^{6+}. These two structures appear – in this limited $Li_6WN_{(2-n)}$ phase diagram – at high temperatures. At lower temperatures structures with high nitrogen content appear. These structures display not only pernitride $[N_2]^{4-}$ anions, but a multitude of possible poly-nitrogen arrangements.

Two triclinic structures of Li_6WN_8 (*P1* (no. 1)) emerge. The display nitride $[N]^{3-}$, pernitride $[N_2]^{4-}$, and branched nitrogen chain $[N_5]^{5-}$. Hence, the description $Li_6W(N)(N_2)(N_5)$. The coordination environment of W is irregular, but best described as 8-fold coordination to N. A triclinic Li_6WN_{10} (*P1* (no. 1)) emerges comprising poly-

atomic anions $2[N_3]^{5-}$ and $[N_4]^{2-}$, hence, $Li_6W(N_3)_2(N_4)$. W in this structure adopts 9-fold coordination to nitrogen.

A triclinic Li_6WN_{12} (*P1* (no. 1)) is found at 80 GPa between 2000 K-2500 K. With W in 8-fold coordination to N, it comprises two $[N_6]^{6-}$ chains, hence $Li_6W(N_6)_2$. At lower temperatures rhombohedral Li_6WN_{14} (*R-3* (no. 148)) appears. The structure comprises WN_6-polyhedra and diazenide $[N_2]^{2-}$ anions, and is stabilized by an additional nitrogen molecule $[N_2]$. Thus $Li_6W(N_2)(N_2)_6$. Above 100 GPa we find triclinic Li_6WN_{16} (*P-1* (no. 2)), with 8-fold coordinated W and polyatomic nitrogen anions, $2[N_4]^{4-}$ and $2[N_4]^{2-}$. Hence, $Li_6W(N_4)_2(N_4)_2$. Two more compounds with high nitrogen content appear. A tetragonal Li_6WN_{18} (*P4/m* (no. 83)) with very small stability range. It contains W in 8-fold coordination to N together with diazenide $5[N_2]^{2-}$ anions, plus molecular nitrogen $4[N_2]$. Thus $Li_6W(N_2)_5(N_2)_4$. At even higher pressures we observe triclinic Li_6WN_{22} (*P-1* (no. 2)). W is in 8-fold coordination to N. Besides infinite chain ofthe polyatomic $[N_4]^{4-}$, the structure displays an unprecedented $[N_{18}]^{8-}$ anion, which resembles 18-crown-6 ether.

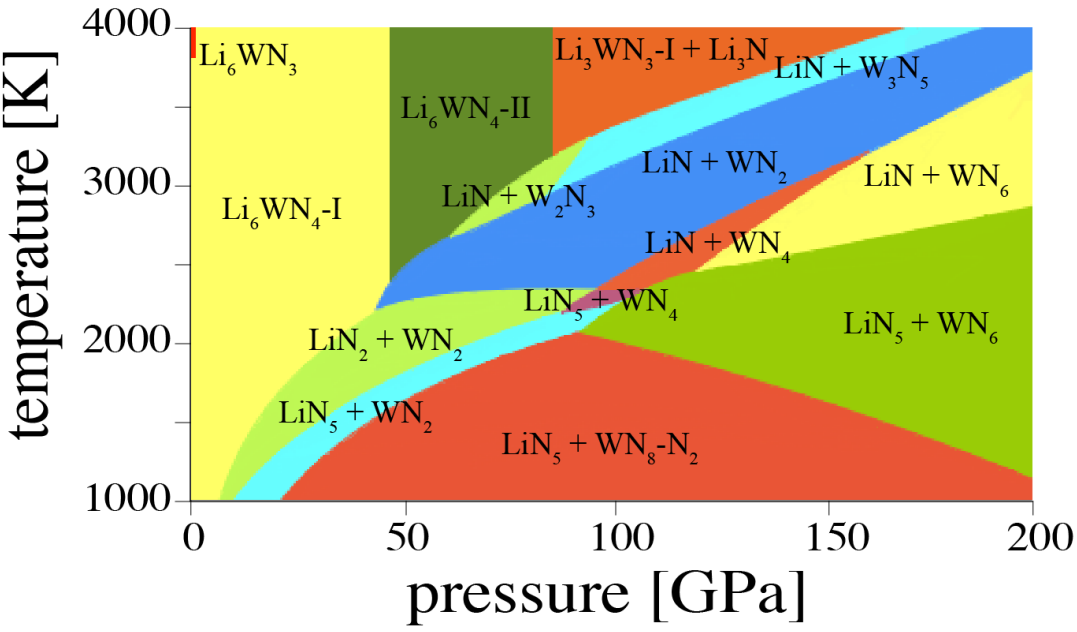

Figure 6: Partial pressure-temperature phase diagram of lithium–tungsten–nitrogen, limited to Li:W = 6:1.

Once the (restricted or limited) $Li_6WN_{(2-n)}$ phase diagram is available, we consider decomposition of each ternary compound found in it into a mixture of binary W–N and Li–N plus nitrogen. The proper choice of binary W–N and Li–N compounds is determined by their respective phase diagrams, and the amount of nitrogen accordingly. Again we use the moderate approximation for the chemical potential of nitrogen. It turns out – the result is shown in Figure 6 – that all high nitrogen content $Li_6WN_{(2-n)}$ phases are unstable against decomposition, and only Li_6WN_4-I and Li_6WN_4-II appear. We have included ternary Li_3WN_3, as it was considered previously as decomposition product of Li_6WN_4. Li_6WN_4-II decomposes to Li_3WN_3 and Li_3N above 80 GPa, and is found in the phase diagram above 3000 K. Overall, the phase diagram appears dominated by binary W–N and Li–N phases.

After considering ternary $Li_6WN_{(2-n)}$ and binary W–N and Li–N, we include ternary $Li_nW_kN_m$ compounds as well. We restricted the search to models with k=1 and l>k. Hence, always more Li than W cations in a structure. Furthermore, we focus on the pressure range between 50 and 100 GPa at temperatures between 2000 K and 3000 K, since these are conditions available in concurrent LH-DAC experiments. Referring to Figure 6, we notice that the two binary phases LiN and WN_2 dominated this region — and we look into possible solid-state reactions of these binaries into ternary Li–W–N: $LiWN_3$, Li_2WN_4, Li_3WN_5, Li_4WN_6, and Li_5WN_7 according to reactions:

$$LiN + WN_2 \rightarrow LiWN_3 \qquad 2LiN + WN_2 \rightarrow Li_2WN_4$$

$$3LiN + WN_2 \rightarrow Li_3WN_5 \qquad 4LiN + WN_2 \rightarrow Li_4WN_6$$

$$5LiN + WN_2 \rightarrow Li_5WN_7$$

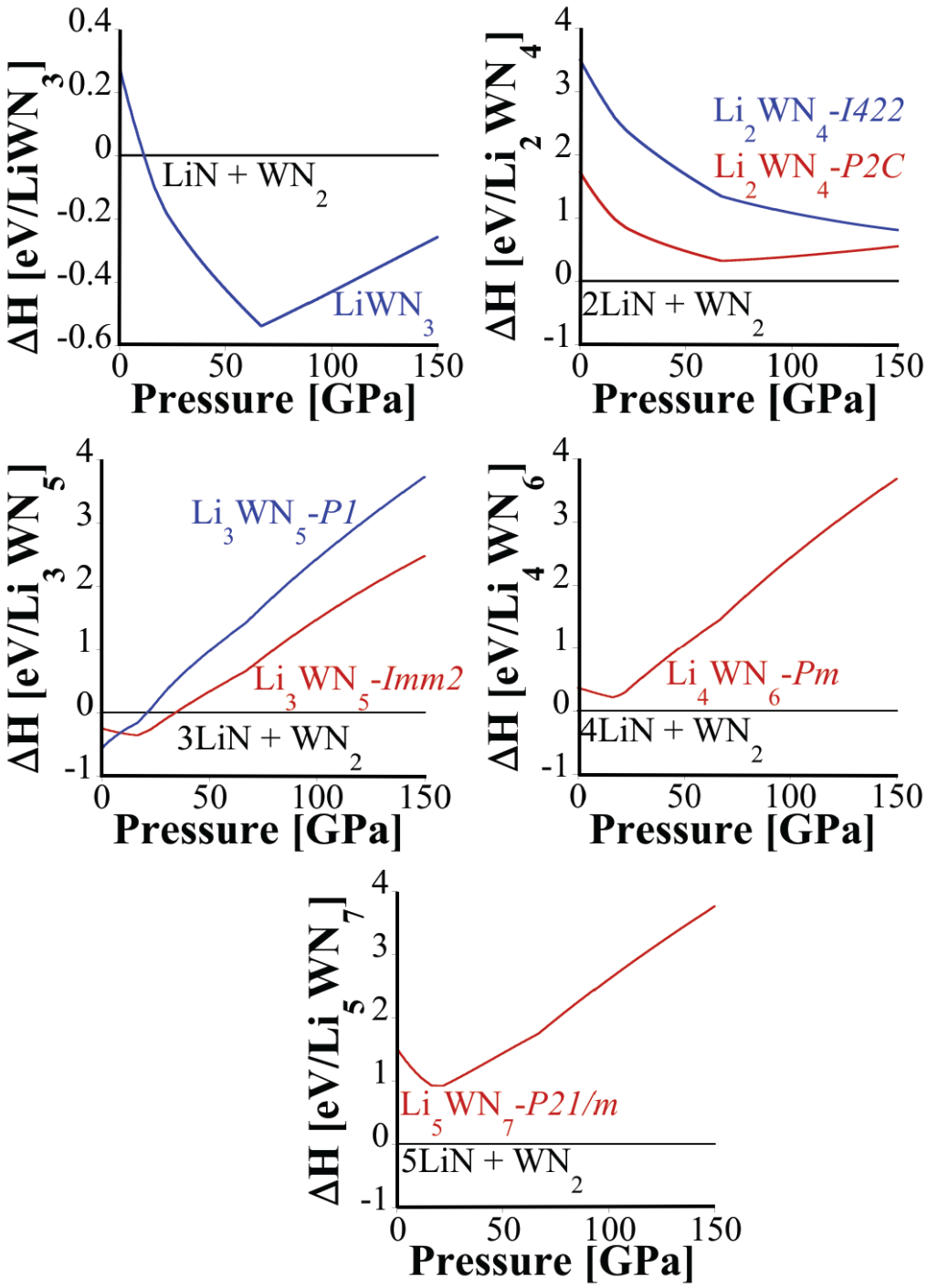

Figure 7: The Enthalpy-pressure (ΔH-p) of $LiWN_3$, Li_2WN_4, Li_3WN_5, and Li_5WN_7 computed using the SCAN functional.

After structure search we computed relative enthalpy pressure diagrams for each composition relative to a phase assembly of LiN and WN_2. The results are shown in Figure 7. Note that kinks in these diagrams appear because phase transitions to structure with the same composition (binary or ternary subsystems) occur. We find that $LiWN_3$ and Li_3WN_5 are candidates to consider as stable ternary Li–W–N compounds, since they are energetically favored over a combination of LiN and WN_2. Adding $LiWN_3$ and Li_3WN_5, and additionally Li_3WN_3 to the data shown in Figure 6 requires to add the appropriate amount of Li–N compounds, the choice depends on pressure and temperature) as well as of nitrogen. Examples are:

$$Li_6WN_4 + 18N_2 \rightarrow LiWN_3 + 5LiN + 16N_2$$

$$Li_6WN_4 + 18N_2 \rightarrow Li_3WN_5 + 3LiN + 16N_2$$

$$Li_6WN_4 + 18N_2 \rightarrow Li_3WN_3 + 3LiN + 17N_2$$

Doing so we receive a ternary Li–W–N p-T phase diagram, shown in Figure 8. It is simplified in so far as that it considers compositions with Li:W = n:1, with n=1–6 only. Thus, it may contain additional ternary phases that we didn't consider in our study.

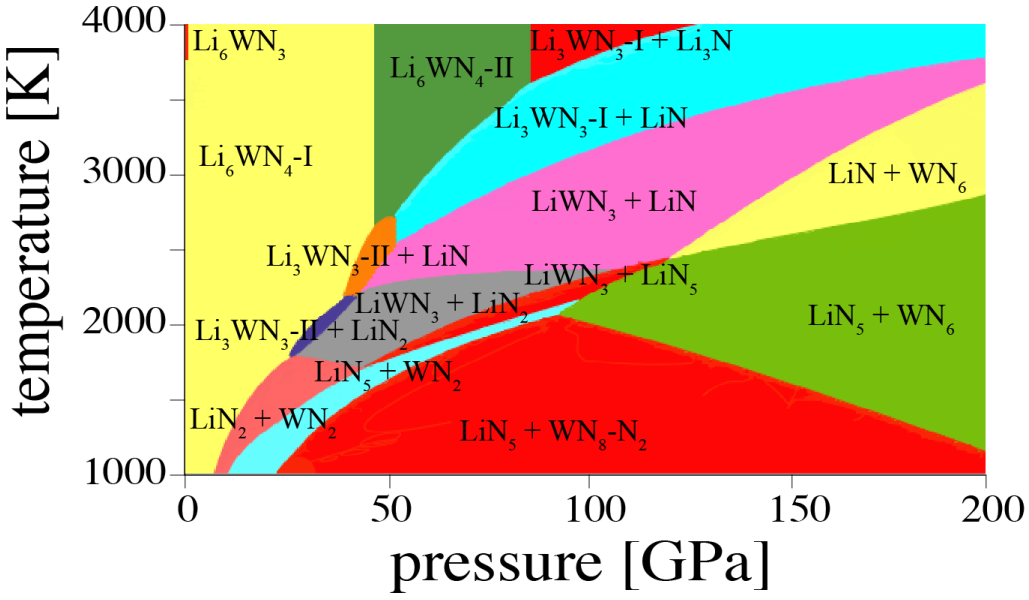

Figure 8: Ternary lithium–tungsten–nitrogen pressure-temperature phase diagram computed by combining of first principles (SCAN functional) and thermodynamic calculations. Only ternary phases with Li:W = n:1 (n=1–6) have been included.

As expected we find Li_6WN_4-I again at low pressures and low temperatures while at higher temperature tetragonal Li_6WN_3 emerges. Above 48 GPa and temperatures over 2500 K Li_6WN_4-II is favored. It turns out that in comparison to Figure 8, which didn't contain ternary Li–W–N compounds except those mentioned so far, the a wide experimentally accessible temperature–pressure field is now populated with ternary Li–W–N compounds that will form under such Li–rich conditions. A first interesting compound accessible at higher temperatures above 60 GPa is orthorhombic Li_3WN_3-I (*Pmn2*$_1$ (no. 31)). It comprises octahedrally coordinated W, and nitrogen as nitride and pernitride. Accordingly, Li_3WN_3-I can be viewed as $Li_3W(N)(N_2)$. As small field just below 60 GPa is occupied by triclinic Li_3WN_3-II (*P1* (no. 1)), which is a simple nitride compound. We note that the low-pressure form of Li_3WN_3-II exhibits W in oxidation state +6, hence W^{+6}, while the high-pressure form Li_3WN_3-I comprises W^{+4}. At even

lower pressure, starting at 30 GPa, orthorhombic $LiWN_3$ (*Pmmn* (no. 59)) becomes accessible. It is a mixed nitride-pernitride $LiW(N)(N_2)$ with W^{+6} cations in 8-fold coordination to N. Overall, we find there are three new ternary Li–W–N compounds attainable in high-pressure experiments.

To provide some guidance to experimentalists, we strive to locate temperature-pressure conditions that provide the largest driving force (ΔG) to attain a certain phase. As phase diagrams such as shown in Figure 8 show only the one single phase with minimum Gibbs energy at a given *p,T*-condition, we are typically unaware of competitors. If we know more about the energy difference to competing phases, we can also address uncertainties of the method in general much better. Therefore, we provide relative Gibbs energy versus temperature data (ΔG-T) and relative Gibbs energy versus pressure data (ΔG-p) for Li–W–N phases. These are "slices" cut through the manifold of G(p,T) data of all structures at constant p or at constant T, respectively. ΔG-T data at constant pressure also relates to experiments, since often a desired pressure is set before heating of the sample is provided to reach desired temperatures.

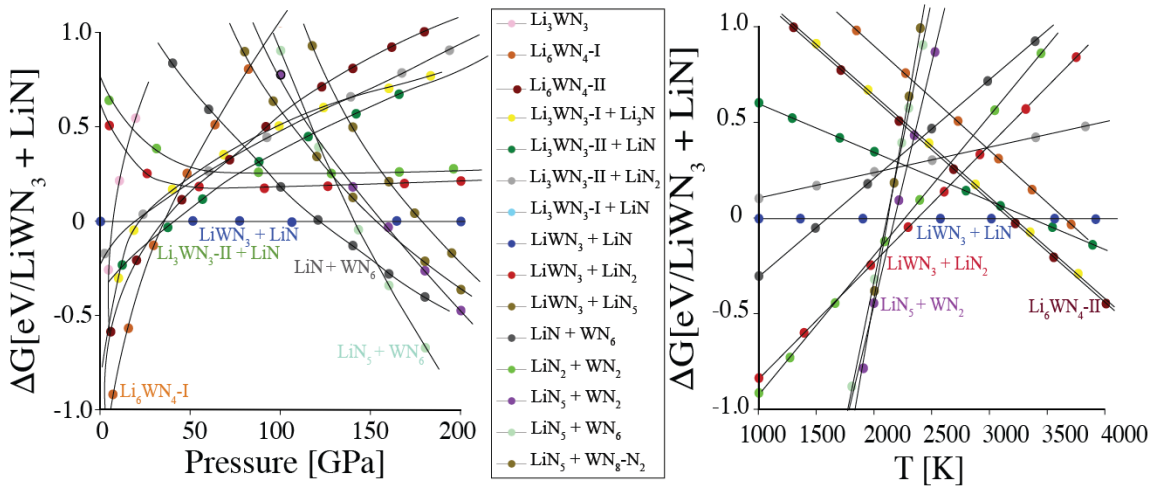

Figure 9: (Left side of legend) Relative Gibbs energy versus pressure, Δ*G*-*p*, of Li–W–N phases in excess nitrogen at 2600 K. (Right side of legend) Relative Gibbs energy versus temperature, Δ*G*-*T*, of Li–W–N phases in excess nitrogen at 80 GPa. Symbols in the respective diagrams refer to structures listed in the boxed legend. Note that in each diagram energy refers to an overall composition $LiWN_3 + LiN$.

In Figure 9 (right) we present ΔG-T of Li–W–N compounds at 80 GPa. Each line represents the Gibbs energy relative to $LiWN_3 + LiN$ for a system comprised of a structure with given composition plus appropriate amounts of nitrogen. The sequence of structures computed at 80 GPa then is $LiN_5 + WN_2 \xrightarrow{2100\ K} LiWN_3 + LiN_2 \xrightarrow{2360\ K} LiWN_3 + LiN \xrightarrow{3235\ K} Li_6WN_4 - II$ with the temperature of transition indicated above the arrow. Hence, computed data suggested that $LiWN_3 + LiN$ structures will be favorable between 2100 and 3235 K. The maximum driving force ΔG to attain the structure is at 2600 K, when it is favored by about 0.192 eV/($LiWN_3 + LiN$) over its closest competitor Li_6WN_4-II. Likewise, Figure 3 (left) shows ΔG-p of Fe–N compounds at 2380 K. We find the sequence of $Li_6WN_4 - I \xrightarrow{30\ GPa} Li_3WN_3 - II + LiN \xrightarrow{40\ GPa} LiWN_3 + LiN \xrightarrow{122\ GPa} LiN + WN_6$. The thermodynamic stability of $LiWN_3 + LiN$ at 2380 K ranges from 30 to 122 GPa, with

maximum ΔG of about 0.3 eV/ $LiWN_3$ + LiN relative to its competitor LiN + WN_6 found at 86 GPa.

Discussion

Our assessment of the Li-W-N phase diagram at high-temperature and high-pressure targets chemical synthesis of new compounds. These are accessible in laser-heated diamond anvil experiments when nitrogen acts as reactant and as pressure medium. The approach augments quantum-chemical calculations with thermochemical data and provides a practical guide for experimentalists. For every phase system we provide a Gibbs energy surface in pressure-temperature space, valid under the condition of excess nitrogen. This information is most helpful assuming ideal conditions. However, in a real experiment, conditions vary at different location of the reaction zone, for example at the edge of the laser beam, and alternative structures may form as well. Therefore, appropriate "slices" into the phase diagram made at constant pressure or at constant temperature are beneficial, since they identify competing phases. Gibbs energy differences may then be interpreted similar to a statistical weight, indicating the likelihood of a structure to emerge. Also, it offers the optimum experimental conditions to realize a certain structure in its stability field. A major outcome of this study is that two new ternary Li–W–N compounds with compositions Li_3WN_3 and $LiWN_3$ are attainable in high-pressure experiments. $LiWN_3$ exhibits a particularly large stability field in the *p*,*T*-phase diagram, and we propose to choose 2500 K and 80 GPa for its synthesis. Such pressures and temperatures are not uncommon.

Conclusion:

Combining Density Functional Theory computations with thermodynamic calculations that include an assessment of the chemical potential change of nitrogen at high pressure and high temperature we provide a comprehensive computation of the pressure-

temperature phase diagram of the Li–N, W–N, and Li–W–N system for pressures up to 200 GPa and temperatures up to 4000 K. We identify stability fields of Li–N, W–N, and Li–W–N structures in the presence of excess nitrogen under conditions of typical DAC experiments. We made "slices" of the phase diagram at constant pressure or at constant temperature to determine maximum driving force to locate optimum pressure temperature to synthesized ternary $LiWN_3$.

Acknowledgement

This work was supported by the National Science Foundation (NSF) through award OISE-1743701. The computational work was made possible through generous grants by the Texas Advance Computing Center in Austin, TACC, Texas, and by the High Performance Computing facilities at UTA. H.A. acknowledges support by the Saudi Arabian Cultural Mission.

References:

1. Uhlein, E., *Cotton,Fa - Advanced Inorganic Chemistry*, 1967; Vol. 218, p 66-&.
2. Mailhiot, C.; Yang, L. H.; Mcmahan, A. K., Polymeric Nitrogen. *Phys Rev B* **1992**, *46*, 14419-14435.
3. Nordlund, K.; Krasheninnikov, A.; Juslin, N.; Nord, J.; Albe, K., Structure and Stability of Non-Molecular Nitrogen at Ambient Pressure. *Europhysics Letters* **2004**, *65*, 400-406.
4. Eremets, M. I.; Gavriliuk, A. G.; Trojan, I. A.; Dzivenko, D. A.; Boehler, R., Single-Bonded Cubic Form of Nitrogen. *Nat. Mater.* **2004**, *3*, 558-563.
5. Yao, Y. S.; Adeniyi, A. O., Solid Nitrogen and Nitrogen-Rich Compounds as High-Energy-Density Materials. *Physica Status Solidi B-Basic Solid State Physics* **2021**, *258*.
6. Bartlett, R. J., Exploding the Mysteries of Nitrogen. *Chemistry & Industry* **2000**, 140-143.
7. Wang, S. M., et al., Synthesis, Crystal Structure, and Elastic Properties of Novel Tungsten Nitrides. *Chemistry of Materials* **2012**, *24*, 3023-3028.
8. Liu, K.; Wang, S. M.; Zhou, X. L.; Chang, J., Theoretical Calculations for Structural, Elastic, and Thermodynamic Properties of C-W3n4 under High Pressure. *Journal of Applied Physics* **2013**, *114*.
9. Xing, W. D.; Miao, X. J.; Meng, F. Y.; Yu, R., Crystal Structure of and Displacive Phase Transition in Tungsten Nitride Wn. *Journal of Alloys and Compounds* **2017**, *722*, 517-524.
10. Kroll, P.; Schroter, T.; Peters, M., Prediction of Novel Phases of Tantalum(V) Nitride and Tungsten(Vi) Nitride That Can Be Synthesized under High Pressure and High Temperature. *Angew. Chem.-Int. Edit.* **2005**, *44*, 4249-4254.
11. Wang, C. C.; Tao, Q.; Dong, S. S.; Wang, X.; Zhu, P. W., Synthesis and Mechanical Character of Hexagonal Phase Delta-Wn. *Inorganic Chemistry* **2017**, *56*, 3970-3975.
12. Sasaki, T.; Ikoma, T.; Sago, K.; Liu, Z.; Niwa, K.; Ohsuna, T.; Hasegawa, M., High-Pressure Synthesis and Crystal Structure of Moc-Type Tungsten Nitride by Nitridation with Ammonium Chloride. *Inorganic Chemistry* **2019**, *58*, 16379-16386.
13. Kawamura, F.; Yusa, H.; Taniguchi, T., Synthesis of Hexagonal Phases of Wn and W2.25n3 by High-Pressure Metathesis Reaction. *Journal of the American Ceramic Society* **2018**, *101*, 949-956.
14. Wang, Y. T.; Zhao, E. J.; Zhao, J. D.; Fu, L.; Ying, C.; Lin, L., Prediction of Novel Ground State and High Pressure Phases for W2n3: First-Principles. *Computational Materials Science* **2019**, *156*, 215-223.
15. Zhang, J. D.; Cheng, X. L., Theoretical Investigations of Structural, Elastic and Electronic Properties of M_2N_3 (M = Zr, Hf, W and Re) with U2s3 Structure. *Computational Materials Science* **2015**, *99*, 43-46.
16. Wang, H.; Li, Q.; Li, Y. E.; Xu, Y.; Cui, T.; Oganov, A. R.; Ma, Y. M., Ultra-Incompressible Phases of Tungsten Dinitride Predicted from First Principles. *Physical Review B* **2009**, *79*.
17. Soto, G., Computational Study of Hf, Ta, W, Re, Ir, Os and Pt Pernitrides. *Computational Materials Science* **2012**, *61*, 1-5.

18. Zhao, Z. L.; Bao, K.; Duan, D. F.; Tian, F. B.; Huang, Y. P.; Yu, H. Y.; Liu, Y. X.; Liu, B. B.; Cui, T., The Low Coordination Number of Nitrogen in Hard Tungsten Nitrides: A First-Principles Study. *Physical Chemistry Chemical Physics* **2015**, *17*, 13397-13402.
19. Song, L.; Wang, Y. X., First-Principles Study of W, WN, WN_2, and WN_3. *Physica Status Solidi B-Basic Solid State Physics* **2010**, *247*, 54-58.
20. Li, Q.; Sha, L.; Zhu, C.; Yao, Y., New Multifunctional Tungsten Nitride with Energetic N-6 and Extreme Hardness Predicted from First Principles. *Epl* **2017**, *118*.
21. Xia, K.; Gao, H.; Liu, C.; Yuan, J. N.; Sun, J.; Wang, H. T.; Xing, D. Y., A Novel Superhard Tungsten Nitride Predicted by Machine-Learning Accelerated Crystal Structure Search. *Science Bulletin* **2018**, *63*, 817-824.
22. Kang, Z. X.; He, H. Y.; Ding, R.; Chen, J. L.; Pan, B. C., Structures of W_xN_y Crystals and Their Intrinsic Properties: First Principles Calculations. *Crystal Growth & Design* **2018**, *18*, 2270-2278.
23. Mehl, M. J.; Finkenstadt, D.; Dane, C.; Hart, G. L. W.; Curtarolo, S., Finding the Stable Structures of $N_{1-X}W_x$ with an Ab Initio High-Throughput Approach. *Physical Review B* **2015**, *91*.
24. Bykov, M., et al., High-Pressure Synthesis of Metal-Inorganic Frameworks $Hf_4N_{20}.N_2$, $WN_8.N_2$, and $Os_5N_{28}.3N_2$ with Polymeric Nitrogen Linkers. *Angewandte Chemie-International Edition*, 7.
25. Salke, N. P.; Xia, K.; Fu, S. Y.; Zhang, Y. J.; Greenberg, E.; Prakapenka, V. B.; Liu, J.; Sun, J.; Lin, J. F., Tungsten Hexanitride with Single-Bonded Armchairlike Hexazine Structure at High Pressure. *Physical Review Letters* **2021**, *126*.
26. Yuan, W. X.; Hu, J. W.; Song, Y. T.; Wang, W. J.; Xu, Y. P., Synthesis and Structure of the Ternary Nitride Li_6WN_4. *Powder Diffraction* **2005**, *20*, 18-21.
27. Sun, W. H., et al., A Map of the Inorganic Ternary Metal Nitrides. *Nature Materials* **2019**, *18*, 732-+.
28. Hohenberg, P.; Kohn, W., Inhomogeneous Electron Gas. *Phys Rev B* **1964**, *136*, B864-+.
29. Kresse, G., Ab-Initio Molecular-Dynamics for Liquid-Metals. *J Non-Cryst Solids* **1995**, *193*, 222-229.
30. Kresse, G.; Hafner, J., Ab-Initio Molecular-Dynamics Simulation of the Liquid-Metal Amorphous-Semiconductor Transition in Germanium. *Phys Rev B* **1994**, *49*, 14251-14269.
31. Kresse, G.; Furthmuller, J., Efficiency of Ab-Initio Total Energy Calculations for Metals and Semiconductors Using a Plane-Wave Basis Set. *Comp Mater Sci* **1996**, *6*, 15-50.
32. Blochl, P. E.; Forst, C. J.; Schimpl, J., Projector Augmented Wave Method: Ab Initio Molecular Dynamics with Full Wave Functions. *Bulletin of Materials Science* **2003**, *26*, 33-41.
33. Kresse, G.; Joubert, D., From Ultrasoft Pseudopotentials to the Projector Augmented-Wave Method. *Phys Rev B* **1999**, *59*, 1758-1775.
34. Sun, J. W.; Ruzsinszky, A.; Perdew, J. P., Strongly Constrained and Appropriately Normed Semilocal Density Functional. *Physical Review Letters* **2015**, *115*.
35. Oganov, A. R.; Ma, Y. M.; Lyakhov, A. O.; Valle, M.; Gatti, C., Evolutionary Crystal Structure Prediction as a Method for the Discovery of Minerals and Materials. In

Theoretical and Computational Methods in Mineral Physics: Geophysical Applications, Wentzcovitch, R.; Stixrude, L., Eds. 2010; Vol. 71, pp 271-298.
36. Kroll, P., Pathways to Metastable Nitride Structures. *J. Solid State Chem.* **2003**, *176*, 530-537.
37. Alkhaldi, H.; Kroll, P., Chemical Potential of Nitrogen at High Pressure and High Temperature: Application to Nitrogen and Nitrogen-Rich Phase Diagram Calculations. *Journal of Physical Chemistry C* **2019**, *123*, 7054-7060.
38. Jacobsen, R. T.; Stewart, R. B.; Jahangiri, M., Thermodynamic Properties of Nitrogen from the Freezing Line to 2000-K at Pressures to 1000-Mpa. *Journal of Physical and Chemical Reference Data* **1986**, *15*, 735-909.
39. Alkhaldi, H.; Kroll, P., Computing the Tantalum-Nitrogen Phase Diagram at High Pressure and High Temperature. *Journal of Physical Chemistry C* **2020**, *124*, 22221-22227.
40. Li, X. F.; Liu, Z. L.; Ding, C. L.; Fu, H. Z.; Ji, G. F., First-Principles Investigations on Mechanical Stability and Elastic Properties of Hexagonal Tungsten Dinitride under Pressure. *Materials Chemistry and Physics* **2011**, *130*, 14-19.
41. Du, X. P.; Wang, Y. X.; Lo, V. C., Investigation of Tetragonal Ren2 and Wn2 with High Shear Moduli from First-Principles Calculations. *Physics Letters A* **2010**, *374*, 2569-2574.
42. Bykov, M.; Bykova, E.; Ponomareva, A. V.; Abrikosov, I. A.; Chariton, S.; Prakapenka, V. B.; Mahmood, M. F.; Dubrovinsky, L.; Goncharov, A. F., Stabilization of Polynitrogen Anions in Tantalum-Nitrogen Compounds at High Pressure. *Angewandte Chemie-International Edition* **2021**, *60*, 9003-9008.
43. Bykov, M., et al., High-Pressure Synthesis of a Nitrogen-Rich Inclusion Compound Ren(8)Xn(2) with Conjugated Polymeric Nitrogen Chains. *Angew. Chem.-Int. Edit.* **2018**, *57*, 9048-9053.
44. Shen, Y. Q.; Oganov, A. R.; Qian, G. R.; Zhang, J.; Dong, H. F.; Zhu, Q.; Zhou, Z. X., Novel Lithium-Nitrogen Compounds at Ambient and High Pressures. *Scientific Reports* **2015**, *5*.
45. Peng, F.; Yao, Y. S.; Liu, H. Y.; Ma, Y. M., Crystalline Lin5 Predicted from First-Principles as a Possible High-Energy Material. *Journal of Physical Chemistry Letters* **2015**, *6*, 2363-2366.
46. Zhang, J.; Wang, X. L.; Yang, K. S.; Cheng, Y.; Zeng, Z., The Polymerization of Nitrogen in Li2n2 at High Pressures. *Scientific Reports* **2018**, *8*.
47. Schneider, S. B.; Frankovsky, R.; Schnick, W., High-Pressure Synthesis and Characterization of the Alkali Diazenide Li_2N_2. *Angewandte Chemie-International Edition* **2012**, *51*, 1873-1875.
48. Laniel, D.; Weck, G.; Loubeyre, P., Direct Reaction of Nitrogen and Lithium up to 75 Gpa: Synthesis of the Li_3N, LiN, LiN_2, and LiN_5 Compounds. *Inorganic Chemistry* **2018**, *57*, 10685-10693.
49. Zhou, M.; Sui, M. H.; Shi, X. H.; Zhao, Z. T.; Guo, L. L.; Liu, B.; Liu, R.; Wang, P.; Liu, B. B., Lithium Pentazolate Synthesized by Laser Heating-Compressed Lithium Azide and Nitrogen. *Journal of Physical Chemistry C* **2020**, *124*, 11825-11830.
50. Laniel, D.; Weck, G.; Gaiffe, G.; Garbarino, G.; Loubeyre, P., High-Pressure Synthesized Lithium Pentazolate Compound Metastable under Ambient Conditions. *Journal of Physical Chemistry Letters* **2018**, *9*, 1600-+.

51. Yi, W. C.; Jiang, X. G.; Yang, T.; Yang, B. C.; Liu, Z.; Liu, X. B., Crystalline Structures and Energetic Properties of Lithium Pentazolate under Ambient Conditions. *Acs Omega* **2020**, *5*, 24946-24953.
52. Kroll, P.; Milko, M., Theoretical Investigation of the Solid State Reaction of Silicon Nitride and Silicon Dioxide Forming Silicon Oxynitride (Si_2N_2O) under Pressure. *Zeitschrift Fur Anorganische Und Allgemeine Chemie* **2003**, *629*, 1737-1750.
53. Kroll, P., Spinel-Type Gallium Oxynitrides Attainable at High Pressure and High Temperature. *Physical Review B* **2005**, *72*.

CONCLUSION

The computational materials research presented here addresses the foundation as well as the application of a combination of thermodynamical and quantum chemical calculations. The first part demonstrates and validates the significant role of the chemical potential change of nitrogen at high-pressure and high-temperature for the location of phase boundaries in temperature-pressure phase diagrams of nitrogen-rich compounds. The second part then applies the approaches to several complex binary metal–nitrogen systems, culminating with the first computed ternary metal–nitrogen phase diagram.

In Chapter 1 the work concentrates on validation of the approach by comparing computed phase boundaries to available experimental data. Since detailed experimental assessments of phase boundaries are scares, and only few data points for different systems are available, the validity of the approach is demonstrated for three simple characteristic systems: pure nitrogen, and nitrogen-rich Si-N and Ti-N phases. Overall, the accounting of the chemical potential change of nitrogen at high-pressure and high-temperature is in good agreement with experimental data. This shows that the estimates of fugacity of nitrogen at high-pressure and high-temperature have merit. In particular, the moderate extrapolation yields best agreement with experimental data – which is why it is used further as the primary tool to explore new high pressure nitrogen-rich compounds.

In Part II Chapter 1, we apply the approach – the combination of Density Functional Theory computations and thermodynamic calculations – to the tantalum–nitrogen system to investigate its pressure-temperature phase diagram. To augment the calculations with more suitable tools for experimentalists, we provide slices through the phase diagram at constant pressure or constant temperature. This allows locating optimum pressure and

temperature conditions for the synthesis of a specific compound, and thus provides a strategy for syntheses of new nitrogen-rich compounds.

In Chapter 2 we continue our research, focusing on the iron–nitrogen phase diagram at high-pressure/high-temperature. This work targets the science relevant to earth's interior and connects to ongoing research with diamond-anvil-cell (DAC) experiments.

In Chapter 3 the work culminates in a comprehensive study that explores whether and how it is possible to attain tungsten in high oxidation states. Taking into consideration a potential decomposition of ternary phases into binaries, this project includes full calculations of both ternary metal–nitrogen systems before the ternary system is addressed. The choice of the ternary lithium–tungsten–nitrogen originated in availability of ternary Li_6WN_4 for experimental research. We compute the Li–W–N phase diagram at high-pressure/high-temperature and identify new ternary compounds with W in its highest oxidation state. In particular, we predict $LiWN_3$ to be accessible in LH-DAC experiments. $LiWN_3$ is a mixed nitride-pernitride compound with tungsten in its highest oxidation state, W^{+6}.

Future Work

The work presented here establishes and validates a method to compute temperature–pressure phase diagrams relevant to experimentalists: which temperature and which pressure to choose to synthesize a new compound. Now the time has come to collect the multitude computational work of metal–nitrogen structures that comprise nitrides, diazenides, pernitrides, mixed nitride-pernitrides, compounds comprising complex polyatomic nitrogen anions, and compounds with extended anionic nitrogen chains — and make them desirable objects of experimental research. It is fundamental work – available at the finger-tips – to investigate further binary and ternary nitrogen compounds, explore their range of stability and locate best conditions for their synthesis.

APPENDIX

Nitrogen Compounds

Compounds	P [GPa]	Space group	Lattice parameters [Å]	Atom	x	y	z
ε-N_2	0	R-3c (167)	a = 9.05 b = 9.05 c = 12.39 α= 90.00 β= 90.00 γ= 120.00	N1 N2	-0.2754 0.0000	-0.3966 0.0000	0.0577 -0.4553
cg-N	100	$I2_13$ (199)	a = 3.48 b = 3.48 c = 3.48 α= 90.00 β= 90.00 γ= 90.00	N1	0.1770	0.1770	0.1770

Silicon-Nitrogen Compounds

Compounds	P [GPa]	Space group	Lattice parameters [Å]	Atom	x	y	z
γ-Si_3N_4	29	Fd-3m (227)	a = 7.52 b = 7.52 c = 7.52 α= 90.00 β= 90.00 γ= 90.00	Si1 Si2 N1	0.3750 0.0000 0.2430	0.3750 0.0000 0.2430	0.3750 0.0000 0.2430

SiN_2	64	Pa-3 (205)	a = 4.23 b = 4.23 c = 4.23 α= 90.00 β= 90.00 γ= 90.00	Si1 N1	0.5000 -0.0971	0.5000 -0.0971	0.5000 -0.0971
SiN_4	108	R-3c (167)	a = 4.12 b = 4.12 c = 11.91 α= 90.00 β= 90.00 γ= 120.00	Si1 N1 N2	0.0000 0.3055 0.0000	0.0000 0.0000 0.0000	0.0000 0.2500 0.2500

Titanium-Nitrogen Compounds

Compounds	P [GPa]	Space group	Lattice parameters [A°]	Atom	x	y	z
TiN	0	Fm-3m (225)	a = 4.25 b = 4.25 c = 4.25 α= 90.00 β= 90.00 γ= 90.00	Ti1 N1	0.0000 0.5000	0.0000 0.5000	0.0000 0.5000
TiN_2	78	I4/mcm (140)	a = 4.10 b = 4.10 c = 4.10 α= 90.00 β= 90.00	Ti1 N1	0.0000 -0.3843	0.0000 0.1156	0.2500 0.0000

			γ= 90.00				
Ti_3N_4	76	I-43d (220)	a = 5.93 b = 5.93 c = 5.93 α= 90.00 β= 90.00 γ= 90.00	Ti1 N1	0.8750 0.1738	0.0000 0.17386	0.2500 0.17386

Tantalum-Nitrogen Compounds

Compounds	P [GPa]	Space group	Lattice parameters [A°]	Atom	x	y	z
β-Ta_2N	0	P31m (157)	a = 5.26 b = 5.26 c = 4.90 α= 90.00 β= 90.00 γ= 120.00	Ta1 N1 N2	0.3338 0.3333 0.0000	0.0000 0.6666 0.0000	-0.2458 0.5000 0.0000
ϑ-TaN	0	P-6m2 (187)	a = 2.92 b = 2.92 c = 2.92 α= 90.00 β= 90.00 γ= 120.00	Ta1 N1	0.6666 0.0000	0.3333 0.0000	0.5000 0.0000
η-Ta_2N_3	11	Pnma (62)	a = 8.11 b = 2.93 c = 8.03 α= 90.00	Ta1 Ta2 N1 N2	0.0218 -0.3058 -0.0461 0.1216	0.25000 0.25000 0.25000 0.25000	0.1867 -0.0048 -0.3757 -0.0490

			β= 90.00 γ= 90.00	N3	-0.2201	0.25000	0.2981
Ta_2N_3	0	P-4m2 (115)	a = 2.96 b = 2.96 c = 2.96 α= 90.00 b= 90.00 γ= 90.00	Ta1 N1 N2	0.0000 0.0000 0.5000	0.5000 0.5000 0.5000	0.2563 -0.3599 0.0000
Ta_3N_5-I	0	Cmcm (63)	a = 3.86 b = 10.23 c = 10.26 α= 90.00 β= 90.00 γ= 90.00	Ta1 Ta2 N1 N2 N3	0.0000 0.0000 0.0000 0.0000 0.0000	0.1974 -0.1329 -0.2368 -0.0472 -0.3081	0.2500 0.0599 0.2500 -0.3813 -0.4257
Ta_3N_5-II	81	Pnma (62)	a = 10.33 b = 2.79 c = 9.05 α= 90.00 β= 90.00 γ= 90.00	Ta1 Ta2 Ta3 N1 N2 N3 N4 N5	0.3742 0.1340 0.1193 0.4746 0.4325 0.2349 0.2158 -0.0739	0.2500 0.2500 0.2500 0.2500 0.2500 0.2500 0.2500 0.2500	0.0892 -0.0744 0.2487 -0.1108 0.2957 -0.2810 0.4518 -0.0812
Ta_3N_5-III	50	Pmmn (59)	a = 2.87 b = 8.72 c = 5.61 α= 90.00	Ta1 Ta2 N1 N2	0.2500 0.2500 0.2500 0.2500	0.7500 0.0785 0.7500 0.4138	0.2723 0.2489 -0.3471 -0.3700

			β= 90.00 γ= 90.00	N3	0.2500	-0.1060	0.0058
TaN_2	112	$P2_1/c$ (14)	a = 6.18 b = 2.84 c = 5.64 α= 90.00 β= 115.10 γ= 90.00	Ta1 N1 N2	0.2668 0.0003 0.3710	-0.2005 -0.3457 0.2587	-0.2296 0.4035 0.0636
TaN_2	84	Cmca (64)	a = 11.59 b = 3.95 c = 3.95 α= 90.00 β= 90.00 γ= 90.00	Ta1 N1 N2	0.3696 0.0000 0.1915	0.0000 -0.1193 0.0000	0.0000 -0.1193 0.0000
TaN_4	100	P-1 (2)	a = 4.32 b = 4.51 c = 3.61 α= 96.10 γ= 68.71 γ= 87.15	Ta1 N1 N2 N3 N4	0.2205 -0.2786 0.2713 -0.0169 0.4425	0.2566 0.1401 -0.1467 0.3138 -0.4263	0.0799 -0.3011 -0.3216 -0.2995 -0.3098
TaN_{10}	140	Immm (71)	a = 5.99 b = 6.64 c = 3.46 α= 90.00 β= 90.00 γ= 90.00	Ta1 N1 N2	0.0000 -0.1909 0.5000	0.0000 0.1786 0.0000	0.0000 0.3206 -0.1607

Iron-Nitrogen Compounds

Compounds	P [GPa]	Space group	Lattice parameters [Å]	Atom	x	y	z
γ'-Fe_4N	0	P m-3m (221)	a = 3.63 b = 3.63 c = 3.63 α= 90.00 β= 90.00 γ= 90.00	Fe1 Fe2 N1	0.5000 0.5000 0.0000	0.0000 0.5000 0.0000	0.0000 0.5000 0.0000
ζ-Fe_2N	0	Pbcn (60)	a = 4.38 b = 5.20 c = 4.60 α= 90.00 β= 90.00 γ= 90.00	Fe1 N1	0.2447 -0.0000	0.1097 -0.3546	-0.4208 0.2500
Fe_3N_2-I	24	Pnma (62)	a = 5.80 b = 2.55 c = 10.37 α= 90.00 β= 90.00 γ= 90.00	Fe1 Fe2 Fe3 N1 N2	-0.0742 -0.3650 -0.1471 -0.2035 -0.0984	0.2500 0.2500 0.2500 0.2500 0.2500	-0.4117 0.4245 0.2345 0.0561 -0.2202
Fe_3N_2-II		Fdd2 (43)	a = 6.94 b = 6.08 c = 6.76 α= 90.00 β= 90.00	Fe1 N1 N2	0.0000 -0.1674 0.3048	0.0000 0.0624 0.0299	-0.2239 0.2292 0.4493

			γ= 90.00				
Fe_4N_3	33	Imm2 (44)	a = 2.49 b = 6.28 c = 6.59 α= 90.00 β= 90.00 γ= 90.00	Fe1 Fe2 Fe3 N1 N2	0.0000 0.0000 0.0000 0.0000 0.0000	0.2016 0.0000 0.0000 0.5000 -0.2988	-0.0272 -0.3432 0.2973 -0.4183 0.2470
FeN	54	P63/mmc (194)	a = 2.67 b = 2.67 c = 4.50 α= 90.00 β= 90.00 γ= 120.00	Fe1 N1	0.0000 0.3333	0.0000 0.6666	0.0000 0.2500
FeN_2	58	Pnmm (194)	a = 4.43 b = 3.70 c = 2.40 α= 90.00 β= 90.00 γ= 90.00	Fe1 N1	0.0000 0.0983	0.0000 -0.3685	0.0000 0.0000
FeN_4	119	P-1 (2)	a = 3.55 b = 3.53 c = 2.54 α= 87.89 β= 69.13 γ= 104.66	Fe1 N1 N2	0.0000 -0.4904 0.1379	0.0000 -0.3452 -0.3107	0.5000 -0.1504 -0.0672
FeN_6	31	C 2/m	a = 5.68	Fe1	0.0000	0.0000	0.0000

		(12)	b = 4.90 c = 4.38 α= 90.00 β= 90.00 γ= 90.00	N1 N2	-0.2307 0.2864	0.0000 0.2372	-0.2232 0.3366
FeN_8	100	P-1 (2)	a = 4.14 b = 4.31 c = 3.44 α= 110.70 β= 83.43 γ= 72.25	Fe1 N1 N2 N3 N4	0.0000 -0.1317 -0.0346 -0.4423 0.4097	0.0000 -0.2309 0.3636 0.1252 0.2941	0.0000 -0.2288 -0.0033 0.4892 0.2798
FeN_8-N_2	102	Immm (71)	a = 3.46 b = 6.38 c = 5.87 α= 90.00 β= 90.00 γ= 90.00	Fe1 N1 N2	0.0000 0.1807 -0.3399	0.0000 -0.3234 0.50000	0.0000 0.3121 0.0000

Lithium-Nitrogen Compounds

Compounds	P [GPa]	Space group	Lattice parameters [A°]	Atom	x	y	z
β-Li_3N	0	P6/mmc (41)	a = 3.51 b = 3.51 c = 6.26 α= 90.00 β= 90.00 γ= 120.00	Li1 Li2 N1	0.0000 0.3333 0.3333	0.0000 0.6666 0.6666	0.2500 -0.0773 0.2500

γ-Li_3N	0	Fm-3m (225)	a = 4.95 b = 4.95 c = 4.95 α= 90.00 β= 90.00 γ= 90.00	Li1 Li2 N1	0.5000 0.2500 0.0000	0.5000 0.2500 0.0000	0.5000 0.2500 0.0000
Li_2N_2	10	Cmcm (63)	a = 4.19 b = 6.87 c = 3.94 α= 90.00 β= 90.00 γ= 90.00	Li1 Li2 N1	0.0000 0.0000 0.3487	-0.4095 0.1745 0.3839	0.2500 0.2500 0.2500
Li_2N_2	10	Immm (71)	a = 10.26 b = 4.27 c = 2.87 α= 90.00 β= 90.00 γ= 90.00	Li1 Li2 Li3 N1	0.0000 0.0000 -0.2458 0.1231	0.0000 0.5000 0.0000 -0.3525	0.0000 0.5000 0.0000 0.0000
Li_2N_2	5	I4mm (107)	a = 2.82 b = 2.82 c = 7.66 α= 90.00 β= 90.00 γ= 90.00	Li1 N1	0.0000 0.0000	0.0000 0.0000	0.3388 -0.0822
LiN_2	47	$P6_3$/mmc (194)	a = 2.47 b = 2.47	Li1 N1	0.0000 0.3333	0.0000 0.6666	0.0000 -0.3281

			c = 7.34 α= 90.00 β= 90.00 γ= 120.00				
LiN_5-I	50	$P2_1/m$ (11)	a = 3.84 b = 7.68 c = 2.71 α= 90.00 β= 80.67 γ= 90.00	Li1 N1 N2 N3	0.0000 0.4096 -0.2892 -0.1054	0.0000 0.1664 0.3854 0.2500	0.0000 0.3391 0.0914 -0.0561
LiN_5-II	70	$P2_1$ (4)	a = 4.17 b = 8.36 c = 3.11 α= 90.00 β= 78.36 γ= 90.00	Li1 N1 N2 N3 N4 N5	0.0029 0.4149 -0.2923 -0.4179 -0.1199 0.2972	0.1729 -0.1551 0.0496 -0.4993 -0.0767 0.2963	-0.4961 0.3208 0.1143 -0.3319 -0.0308 -0.0956

Tungsten-Nitrogen Compounds

Compounds	P [GPa]	Space group	Lattice parameters [Å]	Atom	x	y	z
W_3N	0	P21 (4)	a = 7.19 b = 2.86 c = 5.15 α= 90.00 β= 103.00 γ= 90.00	W1 W2 W3 N1	0.1615 0.1615 0.4937 0.3321	0.3815 -0.1182 -0.1183 -0.1185	-0.4975 -0.0238 -0.2249 0.3633

W_3N_2	0	R-3m (166)	a = 2.82 b = 2.82 c = 24.09 α= 90.00 β= 90.00 γ= 120.00	W1 W2 N1	0.0000 0.0000 0.0000	0.0000 0.0000 0.0000	-0.1192 0.0000 0.2718
W_2N_3	0	C1m1 (8)	a = 4.97 b = 8.56 c = 5.31 α= 90.00 β= 108.31 γ= 90.00	W1 W2 W3 N1 N2 N3 N4	0.0006 0.1851 0.1708 0.4130 -0.3985 0.4297 -0.4122	0.0000 0.0000 0.3316 0.0000 0.0000 0.3412 0.3327	0.0009 -0.4624 -0.4855 0.2693 -0.2260 0.2716 -0.2234
η-W_2N_3	11	Pnma (62)	a = 7.50 b = 2.69 c = 7.74 α= 90.00 β= 90.00 γ= 90.00	W1 W2 N1 N2 N3	-0.4699 0.2009 0.4502 -0.3819 0.2892	0.2500 0.2500 0.2500 0.2500 0.2500	-0.3132 0.4789 0.1217 0.4463 -0.2053
W_5N_6	0	$P6_3$/mcm (193)	a = 4.85 b = 4.85 c = 11.20 α= 90.00 β= 90.00 γ= 120.00	W1 W2 W3 N1	0.0000 0.3333 0.3333 0.3322	0.0000 0.6666 0.6666 0.0000	0.2500 0.2500 0.0000 -0.1306
WN-I	0	Pm-3m	a = 4.08	W1	0.0000	0.5000	0.5000

		(221)	b = 4.08 c = 4.08 α= 90.00 β= 90.00 γ= 90.00	N1	0.5000	0.0000	0.0000
WN-II	0	$P6_3/mmc$ (194)	a = 2.81 b = 2.81 c = 5.79 α= 90.00 β= 90.00 γ= 120.00	W1 N1	0.0000 0.3333	0.0000 0.6666	0.0000 0.2500
WN_2-I	42	P-6m2 (187)	a = 2.79 b = 2.79 c = 3.82 α= 90.00 β= 90.00 γ= 120.00	W1 N1	0.6666 0.0000	0.3333 0.0000	0.0000 0.3214
WN_2-II	78	C2/m (12)	a = 11.72 b = 2.79 c = 7.53 α= 90.00 β= 48.03 γ= 90.00	W1 W2 N1 N2 N3 N4	-0.4287 0.2728 0.0377 -0.2248 -0.3522 0.0613	0.0000 0.0000 0.0000 0.0000 0.0000 0.0000	0.1748 0.2910 -0.1186 0.0917 -0.4599 0.3823
WN_2-III	168	P4/mbm (127)	a = 3.96 b = 3.96 c = 2.54	W1 N1	0.0000 -0.3825	0.0000 0.1174	0.0000 0.5000

			α= 90.00 β= 90.00 γ= 90.00				
WN_4	100	$P2_1/n$ (14)	a = 4.51 b = 5.44 c = 6.41 α= 90.00 β= 54.86 γ= 90.00	W1 N1 N2 N3 N3	-0.1449 0.2771 -0.3799 -0.3031 0.1626	0.1817 -0.0560 0.0264 -0.1703 0.3292	0.3819 0.2731 0.1386 0.4245 0.4896
WN_6	125	R32m (166)	a = 5.67 b = 5.67 c = 4.21 α= 90.00 β= 90.00 γ= 120.00	W1 N1	0.0000 0.4560	0.0000 -0.4560	0.0000 0.2475
WN_8-N_2	105	Immm (177)	a = 3.65 b = 6.98 c = 6.83 a= 90.00 β= 90.00 γ= 90.00	W1 N1 N2	0.0000 0.1798 -0.3485	0.0000 -0.3155 0.5000	0.0000 0.3118 0.0000

Lithium-Tungsten-Nitrogen Compounds

Compounds	P [GPa]	Space group	Lattice parameters [A°]	Atom	x	y	z
Li_6WN_4-I	0	P42/nmc (128)	a = 6.63 b = 6.63	Li1 Li2	0.7131 0.7869	0.2869 0.7869	0.5000 0.0000

			c = 4.88	Li3	0.2131	0.2131	0.0000
			α= 90.00	Li4	0.2869	0.7131	0.5000
			β= 90.00	Li5	0.7869	0.2131	0.0000
			γ= 90.00	Li6	0.7131	0.7131	0.5000
				Li7	0.2869	0.2869	0.5000
				Li8	0.2131	0.7869	0.0000
				Li9	0.5000	0.0000	0.9222
				Li10	0.5000	0.0000	0.4222
				Li11	0.0000	0.5000	0.0778
				Li12	0.0000	0.5000	0.5778
				W1	0.0000	0.0000	0.5000
				W2	0.5000	0.5000	0.0000
				N1	0.5000	0.2583	0.2002
				N2	0.5000	0.7417	0.2002
				N3	0.2417	0.0000	0.7002
				N4	0.7583	0.0000	0.7002
				N5	0.2583	0.5000	0.7998
				N6	0.0000	0.2417	0.2998
				N7	0.0000	0.7583	0.2998
				N8	0.7417	0.5000	0.7998
Li_6WN_4-II	80	Cmc21	a = 2.82	Li1	0.0000	0.0057	0.3263
		(36)	b = 10.39	Li2	0.0000	0.2169	-0.2127
			c = 8.94	Li3	0.0000	0.4027	0.2107
			α= 90.00	Li4	0.0000	-0.1156	-0.4873
			β= 90.00	Li5	0.0000	0.3914	-0.3236
			γ= 90.00	Li6	0.0000	0.4947	0.0037

				W1	0.0000	-0.1959	0.0036
				N1	0.0000	0.3580	0.4014
				N2	0.0000	-0.3749	0.3728
				N3	0.0000	0.2422	0.1382
				N4	0.0000	0.0285	-0.3772
Li_6WN_4-III	80	C2	a = 9.04	Li1	-0.1815	0.4480	0.1700
		(5)	b = 5.61	Li2	0.3149	0.4478	0.2244
			c = 4.83	Li3	0.0000	-0.3008	0.0000
			α= 90.00	Li4	-0.3167	0.2232	0.3496
			β= 89.55	Li5	0.0000	-0.0536	0.5000
			γ= 90.00	Li6	-0.2701	0.1994	-0.0024
				Li7	0.1862	0.1813	0.3559
				W1	0.0000	0.4753	0.5000
				W2	0.0000	0.1691	0.0000
				N1	-0.3734	0.4516	0.1447
				N2	0.1170	0.2049	-0.3289
				N3	-0.3843	0.1928	-0.3265
				N4	0.1251	0.4450	0.1713
Li_6WN_8-I	120	P1	a = 2.82	Li1	-0.4815	-0.0445	0.2385
		(1)	b =10.39	Li2	0.0557	0.1456	0.0554
			c = 8.94	Li3	-0.1722	-0.3207	-0.3150
			α= 90.00	Li4	-0.4285	0.4584	0.1916
			β= 90.00	Li5	0.4467	-0.0918	-0.2441
			γ= 90.00	Li6	0.3001	-0.3786	-0.0796
				W1	0.1120	0.2646	-0.4301
				N1	-0.420	0.1960	-0.1600

				N2	-0.4067	0.2271	0.3048
				N3	-0.0659	-0.1543	0.0169
				N4	-0.0539	-0.0802	-0.4949
				N5	-0.3097	0.4198	-0.1602
				N6	-0.0251	-0.2094	0.2678
				N7	0.1522	-0.3834	0.2725
				N8	0.2839	-0.4150	-0.4844
Li_6WN_8-II	80	P1	a = 3.90	Li1	-0.2568	-0.4239	0.0286
		(1)	b= 4.87	Li2	0.0702	-0.4512	-0.2309
			c = 5.35	Li3	0.1594	0.0560	0.4611
			α= 109.76	Li4	0.2511	0.1622	-0.0724
			β= 106.40	Li5	-0.1645	-0.2035	0.4634
			γ= 70.61	Li6	-0.2003	0.0723	-0.0163
				W1	0.4923	0.3960	0.3951
				N1	-0.0568	0.3712	0.2875
				N2	-0.1751	0.2661	-0.2832
				N3	-0.3949	-0.2228	-0.2896
				N4	0.2789	-0.2356	-0.3238
				N5	0.2321	-0.3536	0.1469
				N6	-0.4356	-0.0258	0.1994
				N7	0.4947	0.2610	-0.2826
				N8	0.2569	-0.1206	0.1023
Li_6WN_{10}	80	P1	a = 6.11	Li1	-0.0015	-0.4825	0.4685
		(1)	b = 5.16	Li2	-0.4915	0.0332	-0.4940
			c = 3.66	Li3	0.2472	-0.0498	0.2505
			α= 75.58	Li4	0.0128	-0.2151	-0.0679

			β= 76.39	Li5	-0.2920	-0.0626	-0.1161
			γ= 107.48	Li6	0.0037	0.2749	0.0322
				W1	-0.4855	0.4825	-0.4185
				N1	0.2526	-0.3462	-0.3260
				N2	0.4443	-0.4128	0.0729
				N3	-0.2259	0.4403	0.2051
				N4	-0.4609	0.1544	-0.0407
				N5	-0.2502	-0.0969	0.3677
				N6	0.0422	0.1566	-0.4479
				N7	0.2238	0.1485	-0.3220
				N8	-0.0533	-0.0864	0.4533
				N9	0.2668	-0.3389	0.0232
				N10	-0.2608	0.3754	-0.1087
Li_6WN_{12}	80	P1	a = 3.82	Li1	0.0569	0.2819	0.1084
		(1)	b = 5.99	Li2	0.0163	0.4827	-0.2367
			c = 5.11	Li3	-0.3598	-0.4975	0.0311
			α= 84.27	Li4	-0.0352	-0.3474	0.3937
			β= 96.97	Li5	0.3936	0.4764	0.4752
			γ= 107.53	Li6	-0.0266	-0.1450	0.0016
				W1	0.0123	0.0504	-0.4442
				N1	0.4511	0.2400	0.3242
				N2	0.4011	-0.2911	-0.3342
				N3	-0.3610	0.2476	-0.1232
				N4	-0.4723	-0.2830	0.1926
				N5	-0.3208	0.0472	-0.1640
				N6	-0.4030	-0.0747	0.27922

				N7	0.3156	0.0176	0.2418
				N8	0.3708	-0.0938	-0.2669
				N9	-0.1888	0.3196	0.4152
				N10	-0.2481	-0.2927	-0.3143
				N11	0.3230	0.2774	-0.2000
				N12	0.1951	-0.3892	0.1076
Li_6WN_{14}	40	R-3	a = 6.74	Li1	-0.1492	0.2908	0.0002
		(148)	b = 6.74	W1	0.0000	0.0000	0.0000
			c = 11.26	N1	0.1835	-0.0474	0.1209
			α= 90.00	N2	-0.2464	-0.1965	0.2247
			β= 90.00	N3	0.0000	0.0000	0.4487
			γ= 120.00				
Li_6WN_{16}	120	P-1	a = 6.74	Li1	0.0869	0.3224	-0.1652
		(2)	b = 6.74	Li2	-0.2272	0.4604	0.4471
			c = 11.26	Li3	-0.1781	0.1057	0.3373
			α= 90.00	W1	0.5000	0.0000	0.0000
			β= 90.00	N1	0.4117	-0.4520	-0.1837
			γ= 120.00	N2	-0.1493	0.1120	-0.3157
				N3	-0.4847	-0.1171	0.3130
				N4	0.2334	0.4509	0.1851
				N5	-0.1346	-0.2532	-0.1108
				N6	0.4144	0.2457	-0.4696
				N7	-0.0493	-0.2499	0.4657
				N8	-0.2402	0.2557	0.1047
Li_6WN_{18}	120	P4/m	a = 6.30	Li1	-0.1803	0.2252	0.0000
		(83)	b = 6.30	Li2	0.0000	0.5000	0.0000

			c = 3.56	W1	0.5000	0.5000	0.0000
			α= 90.00	N1	0.2950	-0.0470	0.3410
			β= 90.00	N2	0.0000	0.0000	-0.1641
			γ= 90.00	N3	0.2617	-0.4225	-0.3348
Li_6WN_{22}	120	P-1	a = 5.66	Li1	-0.3958	0.0332	-0.0944
		(2)	b = 6.30	Li2	-0.0292	0.3544	0.0386
			c = 5.37	Li3	-0.0856	0.1192	-0.4276
			α= 72.00	W1	0.5000	0.5000	0.5000
			β= 112.57	N1	0.1944	0.1280	0.4604
			γ= 80.34	N2	0.4325	-0.1991	-0.1518
				N3	-0.1111	-0.4421	0.2156
				N4	-0.2743	0.4518	0.2742
				N5	0.2793	0.2636	-0.4089
				N6	-0.4262	-0.2727	-0.2709
				N7	0.2813	-0.3178	-0.1375
				N8	-0.1426	-0.2599	0.2605
				N9	0.3103	0.1112	0.3078
				N10	-0.2266	0.2420	-0.2181
				N11	0.0723	-0.0758	-0.0213
Li_3WN_3-I	120	$Pmn2_1$	a = 2.64	Li1	0.0000	-0.1245	0.4923
		(31)	b = 6.10	Li2	0.0000	0.1217	0.2414
			c = 4.47	Li3	0.0000	0.1479	-0.3335
			α= 90.00	W1	0.0000	0.4998	0.2964
			β= 90.00	N1	0.0000	0.3056	-0.0361
			γ= 90.00	N2	0.0000	-0.0653	-0.0519
				N3	0.0000	-0.2905	-0.0416

Li_3WN_3-II	120	P1	a = 4.73	Li1	-0.3947	0.1884	0.4621
		(1)	b = 8.97	Li2	0.4324	-0.2586	-0.3545
			c = 4.74	Li3	0.0469	-0.1920	0.0193
			α= 95.15	Li4	0.2416	0.1883	0.1499
			β= 60.06	Li5	-0.1305	0.3100	-0.4605
			γ= 85.11	Li6	0.0807	-0.2586	0.3490
				Li7	-0.2944	-0.2593	-0.0030
				Li8	0.2391	0.3108	-0.1495
				Li9	-0.4504	0.3100	0.1701
				Li10	-0.0702	0.1885	-0.1744
				Li11	-0.0143	0.0083	0.0857
				Li12	0.4907	-0.4939	-0.0813
				W1	0.3279	-0.0199	0.4099
				W2	-0.3386	-0.0199	-0.2568
				W3	0.1497	-0.4836	-0.4120
				W4	-0.1844	-0.4831	0.2563
				N1	0.3623	-0.1340	0.0386
				N2	-0.0500	0.1114	0.4628
				N3	0.2936	0.1117	-0.2215
				N4	0.0325	-0.1354	-0.2952
				N5	0.1303	-0.3754	-0.0419
				N6	-0.4704	0.3845	-0.4659
				N7	0.1847	0.3846	0.2213
				N8	0.4456	-0.3700	0.2888
				N9	-0.1301	0.3847	-0.1209
				N10	-0.2254	-0.3701	-0.3684

				N11 N12	-0.3901 -0.3012	0.1113 -0.1354	0.1191 0.3715
$LiWN_3$	80	Pmmn (59)	a = 3.59 b = 2.77 c = 6.79 α= 90.00 β= 90.00 γ= 90.00	Li1 W1 N1 N2	0.2500 0.2500 0.2500 -0.4397	0.2500 0.7500 0.2500 0.2500	0.0290 -0.3298 0.4574 -0.1814